



National Library
of Canada

Acquisitions and
Bibliographic Services Branch

395 Wellington Street
Ottawa, Ontario
K1A 0N4

Bibliothèque nationale
du Canada

Direction des acquisitions et
des services bibliographiques

395, rue Wellington
Ottawa (Ontario)
K1A 0N4

Your file *Votre référence*

Our file *Notre référence*

NOTICE

The quality of this microform is heavily dependent upon the quality of the original thesis submitted for microfilming. Every effort has been made to ensure the highest quality of reproduction possible.

If pages are missing, contact the university which granted the degree.

Some pages may have indistinct print especially if the original pages were typed with a poor typewriter ribbon or if the university sent us an inferior photocopy.

Reproduction in full or in part of this microform is governed by the Canadian Copyright Act, R.S.C. 1970, c. C-30, and subsequent amendments.

AVIS

La qualité de cette microforme dépend grandement de la qualité de la thèse soumise au microfilmage. Nous avons tout fait pour assurer une qualité supérieure de reproduction.

S'il manque des pages, veuillez communiquer avec l'université qui a conféré le grade.

La qualité d'impression de certaines pages peut laisser à désirer, surtout si les pages originales ont été dactylographiées à l'aide d'un ruban usé ou si l'université nous a fait parvenir une photocopie de qualité inférieure.

La reproduction, même partielle, de cette microforme est soumise à la Loi canadienne sur le droit d'auteur, SRC 1970, c. C-30, et ses amendements subséquents.

THERMAL PROPERTIES OF SELECTED CLATHRATES

by

Dariusz Michalski

A thesis

Submitted in partial fulfilment of the requirements

for the degree of Doctor of Philosophy

at

Department of Chemistry

Dalhousie University

Halifax, Nova Scotia

January, 1995

© Copyright by Dariusz Michalski, 1995



National Library
of Canada

Bibliothèque nationale
du Canada

Acquisitions and
Bibliographic Services Branch

Direction des acquisitions et
des services bibliographiques

395 Wellington Street
Ottawa, Ontario
K1A 0N4

395, rue Wellington
Ottawa (Ontario)
K1A 0N4

Your file *Votre référence*

Our file *Notre référence*

THE AUTHOR HAS GRANTED AN
IRREVOCABLE NON-EXCLUSIVE
LICENCE ALLOWING THE NATIONAL
LIBRARY OF CANADA TO
REPRODUCE, LOAN, DISTRIBUTE OR
SELL COPIES OF HIS/HER THESIS BY
ANY MEANS AND IN ANY FORM OR
FORMAT, MAKING THIS THESIS
AVAILABLE TO INTERESTED
PERSONS.

L'AUTEUR A ACCORDE UNE LICENCE
IRREVOCABLE ET NON EXCLUSIVE
PERMETTANT A LA BIBLIOTHEQUE
NATIONALE DU CANADA DE
REPRODUIRE, PRETER, DISTRIBUER
OU VENDRE DES COPIES DE SA
THESE DE QUELQUE MANIERE ET
SOUS QUELQUE FORME QUE CE SOIT
POUR METTRE DES EXEMPLAIRES DE
CETTE THESE A LA DISPOSITION DES
PERSONNE INTERESSEES.

THE AUTHOR RETAINS OWNERSHIP
OF THE COPYRIGHT IN HIS/HER
THESIS. NEITHER THE THESIS NOR
SUBSTANTIAL EXTRACTS FROM IT
MAY BE PRINTED OR OTHERWISE
REPRODUCED WITHOUT HIS/HER
PERMISSION.

L'AUTEUR CONSERVE LA PROPRIETE
DU DROIT D'AUTEUR QUI PROTEGE
SA THESE. NI LA THESE NI DES
EXTRAITS SUBSTANTIELS DE CELLE-
CI NE DOIVENT ETRE IMPRIMES OU
AUTREMENT REPRODUITS SANS SON
AUTORISATION.

ISBN 0-612-05218-4

Canada

DARIUSZ MICHALSKI

Name

Dissertation Abstracts International is arranged by broad, general subject categories. Please select the one subject which most nearly describes the content of your dissertation. Enter the corresponding four-digit code in the spaces provided.

PHYSICAL CHEMISTRY

SUBJECT TERM

0494

U·M·I

SUBJECT CODE

Subject Categories

THE HUMANITIES AND SOCIAL SCIENCES

COMMUNICATIONS AND THE ARTS

Architecture 0729
 Art History 0377
 Cinema 0900
 Dance 0378
 Fine Arts 0357
 Information Science 0723
 Journalism 0391
 Library Science 0399
 Mass Communications 0708
 Music 0413
 Speech Communication 0459
 Theater 0465

EDUCATION

General 0515
 Administration 0514
 Adult and Continuing 0516
 Agricultural 0517
 Art 0273
 Bilingual and Multicultural 0282
 Business 0688
 Community College 0275
 Curriculum and Instruction 0727
 Early Childhood 0518
 Elementary 0524
 Finance 0277
 Guidance and Counseling 0519
 Health 0680
 Higher 0745
 History of 0520
 Home Economics 0278
 Industrial 0521
 Language and Literature 0279
 Mathematics 0280
 Music 0522
 Philosophy of 0998
 Physical 0523

Psychology 0525
 Reading 0535
 Religious 0527
 Sciences 0714
 Secondary 0533
 Social Sciences 0534
 Sociology of 0340
 Special 0529
 Teacher Training 0530
 Technology 0710
 Tests and Measurements 0288
 Vocational 0747

LANGUAGE, LITERATURE AND LINGUISTICS

Language
 General 0679
 Ancient 0289
 Linguistics 0290
 Modern 0291

Literature
 General 0401
 Classical 0294
 Comparative 0295
 Medieval 0297
 Modern 0298
 African 0316
 American 0591
 Asian 0305
 Canadian (English) 0352
 Canadian (French) 0355
 English 0593
 Germanic 0311
 Latin American 0312
 Middle Eastern 0315
 Romance 0313
 Slavic and East European 0314

PHILOSOPHY, RELIGION AND THEOLOGY

Philosophy 0422
 Religion
 General 0318
 Biblical Studies 0321
 Clergy 0319
 History of 0320
 Philosophy of 0322
 Theology 0469

SOCIAL SCIENCES

American Studies 0323
 Anthropology
 Archaeology 0324
 Cultural 0326
 Physical 0327

Business Administration
 General 0310
 Accounting 0272
 Banking 0770
 Management 0454
 Marketing 0338
 Canadian Studies 0385

Economics
 General 0501
 Agricultural 0503
 Commerce-Business 0505
 Finance 0508
 History 0509
 Labor 0510
 Theory 0511
 Folklore 0358
 Geography 0366
 Gerontology 0351
 History
 General 0778

Ancient 0579
 Medieval 0581
 Modern 0582
 Black 0328
 African 0331
 Asia, Australia and Oceania 0332
 Canadian 0334
 European 0335
 Latin American 0336
 Middle Eastern 0333
 United States 0337
 History of Science 0585
 Law 0398
 Political Science
 General 0615
 International Law and Relations 0616
 Public Administration 0617
 Recreation 0814
 Social Work 0452

Sociology
 General 0626
 Criminology and Penology 0627
 Demography 0938
 Ethnic and Racial Studies 0631
 Individual and Family Studies 0628
 Industrial and Labor Relations 0629
 Public and Social Welfare 0630
 Social Structure and Development 0700
 Theory and Methods 0344
 Transportation 0709
 Urban and Regional Planning 0999
 Women's Studies 0453

THE SCIENCES AND ENGINEERING

BIOLOGICAL SCIENCES

Agriculture
 General 0473
 Agronomy 0285
 Animal Culture and Nutrition 0475
 Animal Pathology 0476
 Food Science and Technology 0359
 Forestry and Wildlife 0478
 Plant Culture 0479
 Plant Pathology 0480
 Plant Physiology 0817
 Range Management 0777
 Wood Technology 0746

Biology
 General 0306
 Anatomy 0287
 Biostatistics 0308
 Botany 0309
 Cell 0379
 Ecology 0329
 Entomology 0353
 Genetics 0369
 Limnology 0793
 Microbiology 0410
 Molecular 0307
 Neuroscience 0317
 Oceanography 0416
 Physiology 0433
 Radiation 0821
 Veterinary Science 0778
 Zoology 0472

Biophysics
 General 0786
 Medical 0760

EARTH SCIENCES
 Biogeochemistry 0425
 Geochemistry 0996

Geodesy 0370
 Geology 0372
 Geophysics 0373
 Hydrology 0388
 Mineralogy 0411
 Paleobotany 0345
 Paleoecology 0426
 Paleontology 0418
 Paleozoology 0985
 Palynology 0427
 Physical Geography 0368
 Physical Oceanography 0415

HEALTH AND ENVIRONMENTAL SCIENCES

Environmental Sciences 0768
 Health Sciences
 General 0566
 Audiology 0300
 Chemotherapy 0992
 Dentistry 0567
 Education 0350
 Hospital Management 0769
 Human Development 0758
 Immunology 0982
 Medicine and Surgery 0564
 Mental Health 0347
 Nursing 0569
 Nutrition 0570
 Obstetrics and Gynecology 0380
 Occupational Health and Therapy 0354
 Ophthalmology 0361
 Pathology 0571
 Pharmacology 0419
 Pharmacy 0572
 Physical Therapy 0382
 Public Health 0573
 Radiology 0574
 Recreation 0575

Speech Pathology 0460
 Toxicology 0383
 Home Economics 0386

PHYSICAL SCIENCES

Pure Sciences
 Chemistry
 General 0485
 Agricultural 0749
 Analytical 0486
 Biochemistry 0487
 Inorganic 0488
 Nuclear 0738
 Organic 0490
 Pharmaceutical 0491
 Physical 0494
 Polymer 0495
 Radiation 0754
 Mathematics 0405

Physics
 General 0605
 Acoustics 0986
 Astronomy and Astrophysics 0606
 Atmospheric Science 0608
 Atomic 0748
 Electronics and Electricity 0607
 Elementary Particles and High Energy 0798
 Fluid and Plasma 0759
 Molecular 0609
 Nuclear 0610
 Optics 0752
 Radiation 0756
 Solid State 0611
 Statistics 0463

Applied Sciences
 Applied Mechanics 0346
 Computer Science 0984

Engineering
 General 0537
 Aerospace 0538
 Agricultural 0539
 Automotive 0540
 Biomedical 0541
 Chemical 0542
 Civil 0543
 Electronics and Electrical 0544
 Heat and Thermodynamics 0348
 Hydraulic 0545
 Industrial 0546
 Marine 0547
 Materials Science 0794
 Mechanical 0548
 Metallurgy 0743
 Mining 0551
 Nuclear 0552
 Packaging 0549
 Petroleum 0765
 Sanitary and Municipal 0554
 System Science 0790
 Geotechnology 0428
 Operations Research 0796
 Plastics Technology 0795
 Textile Technology 0994

PSYCHOLOGY

General 0621
 Behavioral 0384
 Clinical 0622
 Developmental 0620
 Experimental 0623
 Industrial 0624
 Personality 0625
 Physiological 0989
 Psychobiology 0349
 Psychometrics 0632
 Social 0451



*Dedicated to my wife
and my parents*

TABLE OF CONTENTS

Figure Captions	x
List of Tables	xiv
Abstract	xv
List of Symbols and Abbreviations	xvi
Acknowledgments	xxii
Chapter 1	
General Preamble	1
Chapter 2	
Thermal Properties - Basic Résumé	12
2.1 Introduction	12
2.2 Models of Heat Capacity	19
2.3 Essential Physics of Phonon Motion and Thermal Conductivity	23

Chapter 3

Inclusion Compounds Investigated	28
3.1 Introduction	28
3.2 Preparation and Crystal Growth	35
3.2.1 Dianin's Compound and its CCl_4 Clathrate	35
3.2.2 HPTB	35
3.2.2 HPTB- CBr_4	37
3.3 Crystal Structure of HPTB and its CBr_4 Clathrate	40
3.3.1 HPTB	40
3.2.2 HPTB- CBr_4	40

Chapter 4

Brillouin Scattering Experiment	46
4.1 Introduction	46
4.2 Résumé of the Experimental Method	51
4.3 Experimental Procedure	56
4.4 Results and Discussion	59
4.4.1 Experimental Findings	59
4.4.2 Derived Parameters and Other Systems	63

Chapter 5

Thermal Expansion and Related Properties	68
--	----

5.1	Introduction	68
5.2	Experimental Procedure	71
5.3	Results and Discussion	72
5.3.1	Experimental Findings	72
5.3.2	Temperature Evolution of Unit Cell Parameters	72
5.3.3	Other Inclusion Lattice Systems	79
5.3.4	The Role of the Guest in Thermal Expansion	79
5.3.5	Volume Thermal Expansion of HPTB Systems	81
5.3.6	Grüneisen Function of HPTB Systems	81
5.3.7	Grüneisen Function of CBr ₄	86
5.3.8	Concluding Remarks on the Grüneisen Parameter	88
Chapter 6		
	Heat Capacity Determinations	90
6.1	Introduction	90
6.2	Experimental Setup	94
6.3	Experimental Procedure	99
6.4	Results and Discussion	101
6.4.1	Experimental Findings	101
6.4.2	Heat Capacity of CBr ₄ Guest in HPTB-CBr ₄	101
6.4.3	Isochoric Heat Capacity	109
6.4.5	Characteristic Temperatures	112

Chapter 7

Thermal Conduction	119
7.1 Formal Theory of Thermal Conductivity	119
7.2 Résumé of the Experimental Method	124
7.3 Experimental Procedure	127
7.3.1 Experimental Setup	127
7.3.2 Sample Preparation	131
7.4 Results and Discussion	134
7.4.1 The CCl_4 clathrate of Dianin's compound	134
7.4.1.1 Experimental Findings	134
7.4.1.2 Glassy-like Behaviour	137
7.4.1.3 Mean Free Path	138
7.4.1.4 Minimum Thermal Conductivity	141
7.4.1.5 Resonance Scattering Model	142
7.4.1.6 Role of the Guest	148
7.4.2 The CBT_4 Clathrate of HPTB	151
7.4.2.1 Experimental Findings	151
7.4.2.2 Glassy-like Behaviour	151
7.4.2.3 Slack's Minimum Thermal Conductivity	155
7.4.2.4 Einstein Model	157
7.4.2.5 Cahill-Pohl Model	157
7.4.2.6 Resonant Scattering Model	159

7.4.3 Conclusions	164
Chapter 8	
Summary	167
Appendix	170
References	181

FIGURE CAPTIONS

Figure 1.1	The temperature profiles of the thermal conductivity for a typical crystal and glass.	8
Figure 2.1	Two-dimensional representation of three-phonon processes.	26
Figure 3.1	Molecular structure of Dianin's compound, 1.	29
Figure 3.2	Close structural analogy between (a) a hydrogen-bonded hexamer supramolecular unit, <i>e.g.</i> in Dianin's systems and (b) a typical hexasubstituted benzene analogue, <i>e.g.</i> hexakisphenylthiobenzene.	30
Figure 3.3	The crystal structure of the CCl ₄ clathrate of Dianin's compound.	32
Figure 3.4	Molecular structure of hexakisphenylthiobenzene, 2.	34
Figure 3.5	A DSC scan of (a) HPTB and (b) HPTB-CBr ₄ measured on heating at 5 K min ⁻¹	38
Figure 3.6	¹ H NMR spectrum of HPTB in chloroform.	39
Figure 3.7	An ORTEP drawing of an HPTB molecule in pure HPTB.	42
Figure 3.8	An illustration of the CBr ₄ clathrate of HPTB showing the host-guest packing as projected onto the <i>ac</i> plane.	43
Figure 4.1	The Cartesian coordinate system in which the tensor is written . . .	49
Figure 4.2	Representative 2-h Brillouin spectrum of [0.470, 0.882, -0.039] phonons in the CBr ₄ clathrate of HPTB.	52

Figure 4.3	A schematic diagram of the experimental setup for the Brillouin scattering experiment.	57
Figure 4.4	Sound velocities in the xy-plane for (a) the CBr ₄ clathrate of HPTB and (b) the ethanol clathrate of Dianin's compound.	62
Figure 5.1	(a) HPTB-CBr ₄ <i>a</i> -axis lattice parameter as a function of temperature. (b) The thermal expansion coefficient along this axis as a function of temperature.	74
Figure 5.2	(a) HPTB-CBr ₄ <i>c</i> -axis lattice parameter as a function of temperature. (b) The thermal expansion coefficient along this axis as a function of temperature.	75
Figure 5.3	(a) HPTB-CBr ₄ unit cell volume as a function of temperature. (b) The volume thermal expansion coefficient as a function of temperature.	76
Figure 5.4	HPTB: (a) <i>a</i> -axis, (b) <i>b</i> -axis and (c) <i>c</i> -axis as a function of temperature.	77
Figure 5.5	(a) HPTB unit cell volume as a function of temperature. (b) The volume thermal expansion coefficient as a function of temperature.. . . .	78
Figure 5.6	Temperature dependence of the overall Grüneisen parameter, γ_v , for pure HPTB.	83
Figure 5.7	Temperature dependence of the overall Grüneisen parameter, γ_v , for HPTB-CBr ₄	84

Figure 5.8	Temperature dependence of the Grüneisen parameters, γ_a and γ_c , for HPTB-CBr ₄	85
Figure 5.9	Temperature dependence of the overall Grüneisen parameter, γ_V , for pure CBr ₄	87
Figure 6.1	Schematic diagram of the adiabatic calorimeter.	92
Figure 6.2	A schematic diagram of the computer system controlling the automated adiabatic calorimeter.	95
Figure 6.3	The sample container and heater/thermometer assembly of the calorimetric vessel.	97
Figure 6.4	Experimental molar heat capacity of CBr ₄	102
Figure 6.5	Experimental heat capacities of HPTB and HPTB-CBr ₄ with the latter expressed per mole of HPTB.	104
Figure 6.6	The molar heat capacity of the CBr ₄ molecule	108
Figure 6.7	Molar isochoric heat capacity of pure CBr ₄	110
Figure 6.8	Molar isochoric heat capacity of HPTB-CBr ₄	111
Figure 6.9	The Debye temperature for pure CBr ₄ as a function of temperature.	115
Figure 6.10	The Debye temperature for pure HPTB as a function of temperature.	116
Figure 6.11	The Debye temperatures for HPTB-CBr ₄ as functions of temperature.	117

Figure 7.1	Schematic illustration of a typical temperature profile of the thermal conductivity for an insulating crystal.	122
Figure 7.2	A typical plot for Dianin- CCl_4 of the scaled rate of heating.	126
Figure 7.3	Plan of the thermal conductivity apparatus.	128
Figure 7.4	The thermal conductivity of Dianin- CCl_4 as determined in this experiment.	135
Figure 7.5	The scaled thermal conductivity for Dianin- CCl_4 and HPTB- CBr_4 , and other materials exhibiting similar types of glass-like thermal behaviour.	139
Figure 7.6	Phonon mean free paths as functions of temperature for Dianin's systems.	140
Figure 7.7	The experimental thermal conductivity of the CCl_4 clathrate of Dianin's compound and the least-squares fit to the resonant-scattering model as described in the text.	147
Figure 7.8	The experimental thermal conductivity of the CBr_4 clathrate of HPTB.	152
Figure 7.9	The mean free path of phonons in the CBr_4 clathrate of HPTB. . .	156
Figure 7.10	The experimental thermal conductivity of the CBr_4 clathrate of HPTB and the Einstein and Cahill-Pohl models of the thermal conductivity.	158
Figure 7.11	The experimental thermal conductivity of the CBr_4 clathrate of HPTB and the least-square fit to the resonant-scattering model. . .	161

LIST OF TABLES

Table 3.1	Crystallographic properties of HPTB and HPTB-CBr ₄ at 22°C.	41
Table 4.1	The seven independent components of the stiffness (c_{ij}) and compliance (s_{ij}) matrices for the CBr ₄ clathrate of HPTB	60
Table 6.1	Smoothed values of C_p for CBr ₄	103
Table 6.2	Smoothed values of C_p for HPTB.	105
Table 6.3	Smoothed values of C_p for HPTB-CBr ₄ , per mole HPTB.	106
Table 7.1	The thermal conductivity of the CCl ₄ clathrate of Dianin's compound.	136
Table 7.2	The thermal conductivity of the CBr ₄ clathrate of HPTB.	153
Table A1	Heat capacity of CBr ₄ as determined in the experiment.	170
Table A2	Heat capacity of HPTB as determined in the experiment.	171
Table A3	Heat capacity of HPTB-CBr ₄ as determined in the experiment.	175
Table A4	The smoothed values of C_v for CBr ₄	177
Table A5	The smoothed values of C_v for HPTB-CBr ₄	178
Table A6	Positional parameters and B(eq) of nonhydrogen atoms for HPTB.	179
Table A7	Positional parameters and B(eq) of nonhydrogen atoms for HPTB-CBr ₄	180

ABSTRACT

Clathrates are lattice inclusion compounds in which one type of molecule forms a framework, called a host lattice, with lacunae in which the other kinds of molecules, called guests, reside. Clathrates are crystals, but long-range structural order does not seem to be sufficient to provide typical thermal behaviour. Their thermal conductivity is low and its temperature profile is unusual compared to other crystals. The origin of that unusual behaviour is the main subject of this research.

A new group of clathrates was synthesized in the mid-1970's. The idea for their structure came from the dimensional and geometrical similarity of the hydrogen-bonded hexamer unit, as in Dianin's compound and related systems, with hexa-substituted benzene. This thesis concerns the study of thermal and related properties of systems based on hexakisphenylthiobenzene (HPTB), the archetypal compound in this series and the thermal conductivity of the CCl_4 clathrate of Dianin's compound, which is an example of its structural model. Since thermal and mechanical properties are determined by intermolecular forces, these systems afforded an opportunity to investigate the intermolecular interaction between guest and host molecules, the dynamics of molecular clusters and its effect on physical properties, and the role of concentration and type of guest species on thermal behaviour.

Crystal structure (X-ray diffraction), thermal expansion (neutron powder diffraction), heat capacity (adiabatic calorimetry), elastic properties (Brillouin scattering) and thermal conductivity (steady-state method) were determined. Pertinent parameters were derived to shed light on the anharmonicity of molecular interactions and dynamics of the crystal lattice. Thermal behaviour was modelled. The resonant-scattering of acoustic phonons from localized modes brought about by dynamical disorder of the crystalline structure was identified as the primary source of the highly efficient thermal resistant mechanism.

In addition the heat capacity of pure CBr_4 was measured and analyzed. This was required to delineate thermal effects in the investigation of the CBr_4 clathrate of HPTB.

LIST OF SYMBOLS AND ABBREVIATIONS

κ	thermal conductivity
C	heat capacity
l	mean free path of a particle
ρ	density
v	velocity
Q	heat
T	temperature
S	entropy
U	internal energy
w	work done by the crystal
V	volume
A	Helmholtz energy
G	Gibbs energy
H	enthalpy
P	pressure
C_p	isobaric heat capacity
C_v	isochoric heat capacity
α_v	volume thermal expansion coefficient
β	compressibility
Φ	potential energy of the crystal lattice
M_j	mass of the j -th atom

$u_{j,\mu}$	μ -th Cartesian component of the displacement of the j -th atom in the i -th unit cell
n	number of atoms in the unit cell
N	number of unit cells in the crystal
\underline{k}	wave vector
ω	angular frequency
k	length of the wave vector
h	Planck's constant
$N_j(\underline{k})$	Bose-Einstein distribution function
\hbar	Planck's constant divided by 2π
k_B	Boltzmann's constant
n_a	number of separate atoms in the unit cell for the external mode formalism of lattice dynamics
n_g	number of separate molecular clusters in the unit cell for the external mode formalism of lattice dynamics
Z	canonical partition function
$g(\omega)$	phonon density of states
ω_E	Einstein frequency
δ	Dirac delta function
θ_E	Einstein temperature
ω_D	Debye frequency
$V_{u'}$	volume of the unit cell

θ_D	Debye temperature
\mathfrak{H}	total heat current
$n_j(\underline{k})$	phonon distribution
∇	Nabla operator
\underline{G}	reciprocal lattice vector
a_{kj}^+	creator operator
a_{kj}	annihilator operator
P_j	crystal quasimomentum for the j -th dispersion curve
\mathcal{N}	displaced phonon distribution
τ	relaxation time
\underline{r}	position vector
t	time
$u(\underline{r}, t)$	particle displacement field
\underline{f}	restoring force
$\underline{\epsilon}$	strain tensor
ϵ_{ij}	component of the strain tensor
$\underline{\sigma}$	stress tensor
σ_{ij}	component of the stress tensor
s_{ijkl}	component of the compliance tensor
c_{ijkl}	component of the stiffness tensor
s_{ij}	component of the compliance matrix
c_{ij}	component of the stiffness matrix

q_n	direction cosine of wave propagation
Π	polarization vector of sound wave
δ_{ij}	Kronecker delta
D_{ij}	component of the dynamical matrix of the lattice motion
\underline{k}_i	wave vector of the incident light
ω_i	angular frequency of the incident light
\underline{k}_s	wave vector of the scattered light
ω_s	angular frequency of the scattered light
\underline{k}_p	wave vector of the phonon involved in scattering of light
ω_p	angular frequency of the phonon involved in scattering of light
v_g	group velocity
c	velocity of light in vacuum
$\Delta\nu$	Brillouin shift
n_i	refractive index of the incident light
n_s	refractive index of the scattered light
θ	scattering angle
v_{exp}	experimental sound velocity
σ_i	standard deviation of the i -th experimental value
B_s	adiabatic bulk modulus
β_1	compressibility along x axis
β_2	compressibility along y axis
ϵ_{ki}	energy of a single mode

γ	Grüneisen parameter
$C_{V(ki)}$	isochoric single mode heat capacity
γ_{ki}	mode Grüneisen parameter
α_λ	component of the thermal expansion tensor
γ_μ	component of the Grüneisen parameter matrix
C_{exp}	experimental heat capacity
C_σ	heat capacity at constant stress
C_ϵ	heat capacity at constant strain
R	gas constant
λ	light wavelength
λ_d	thermal diffusivity
\tilde{A}	cross-sectional area of the crystal sample
d	distance between thermocouple junctions
κ_{CP}	thermal conductivity in Cahill-Pohl model
n_d	atomic density number
τ_N	relaxation time due to N-processes
τ_U	relaxation time due to Umklapp processes
τ_B	relaxation time due to boundary scattering
τ_S	relaxation time due to resonant scattering
B	experimental parameter in formula for Umklapp scattering
α	experimental parameter in formula for Umklapp scattering
\tilde{d}	diameter of the sample

- G concentration of the resonant scatterer
- D coefficient related to the strength of the coupling
- ω_0 angular frequency of vibrations involved in resonant scattering
- $\kappa_{Smin\infty}$ high temperature limit of the thermal conductivity in Slack's model
- Ω atomic volume
- κ_{Eins} thermal conductivity in Einstein model

ACKNOWLEDGMENTS

I would like to thank Prof. Mary Anne White for the opportunity to undertake this project as well as her assistance and attention to details throughout the past years.

I would like to acknowledge the Faculty of Graduate Studies, Dalhousie University and the Natural Sciences and Engineering Research of Canada for their provision of funding during my graduate work.

I would like to thank the Killam Trustees for bestowing upon me the title of Honourary Killam Scholar.

I would like to acknowledge M. Zakrzewski for chemical synthesis of Dianin's compound, Prof. S. Grossert and K. Wright for their assistance in preparation of HPTB, Prof. T. S. Cameron and P. Bakshi for their assistance and expertise in crystallographic related matters and Dr. R. G. Ross for useful interaction concerning thermal conductivity measurements.

I would like to thank Prof. H. Kiefte of Memorial University, where I carried out the Brillouin scattering experiment, for his hospitality, assistance and interest in my work. I am also indebted to Dr. B. Mróz for his experimental expertise in this field.

I would like to acknowledge AECL Research, Chalk River Laboratories for the use of their facility. I would like to thank Dr. B. Powell for arranging my sojourn at Chalk River Laboratory, and Dr. I. Swainson for his assistance during the experiment.

At last but absolutely not at least I would like to thank Bozena, Bogusia, Greg and Paul for their friendship which made my life in Halifax more interesting.

CHAPTER 1

GENERAL PREAMBLE

Beyond chemistry focused on materials with strong bonds between the various atoms comprising the substance lies supramolecular chemistry centred on complexes consisting of two or more chemical entities associated through intermolecular interaction.^{1,2} This interaction of molecular moieties, although anisotropic, is neither as orientationally determined nor as energetic as that found within molecules.³ An upsurge of keen interest in inclusion compounds and its sub-group clathrates^{4,5,6,7} is due to recent emphasis on supramolecular systems that amended our paradigm of chemistry to include organization, composition and geometry of the molecular assembly.⁸ The way these three mainly structural features interplay to define molecular architecture can be delineated as molecular recognition.⁹ The less universal concept of crystal packing was originally conceived and applied to molecular crystals.¹⁰

The generic term, *inclusion compound*, refers to a wide scope of systems in which one type of species (the "guest") is spatially confined in non-rigorously defined cavities distributed within another species (the "host").¹¹ The host-guest interaction criterion as well as the topology classification distinguishes *clathrates*.^{5,12} These are aggregates in which the guest molecules are virtually trapped, held by steric barriers created by the architecture of a crystalline host framework. The usual intermolecular

interaction caused by van der Waals forces between the guest and host molecules is weak in comparison with regular chemical bonding.⁵ Such interactions can be practically neglected to simplify the physical picture of the encaged species which is that of two non-interacting subsystems (guests and hosts).^{13,14,15} Nevertheless, recent molecular dynamics calculations have shown the significant effect of these interactions on the physical properties of some clathrates.^{16,17,18}

The systematic development of knowledge about these systems, which underlies the understanding of supramolecular complexes, experienced a long period of dormancy^{4,6} followed by a dramatic resurgence in the latter part of the 1940's.^{12,19,20} The lack of appropriate research methods and the lack of the cognizance of this unusual type of association between chemical species initially hindered the progress. For more than 100 years, clathrates, very often serendipitously found, were only laboratory curiosities on the fringe of academic interest.^{6,21} Recently this has changed diametrically because of the advancement in understanding of their make-up and energetic composition as well as the recognition of their occurrence and possible applications.

The first inclusion compounds were observed by Kronstedt in 1776²² (allegedly a zeolite) and Priestley in 1778²³ (allegedly a clathrate hydrate). Davy in 1811 obtained the chlorine hydrate by cooling an aqueous solution saturated with chlorine gas.²⁴ Twelve years later, Faraday failed in his attempt to propose a formula for this system.²⁵ The synthesis of other clathrate systems followed, *e.g.* quinol clathrate had been obtained in 1849.²⁶ It had not been fully understood how these

crystals were composed until 1886, when Mylius suggested an absence of any ordinary chemical combination between host and guest molecules.²⁷ Finally, the advent of X-ray crystallography revealed the non-conventional architecture of these materials and provided required impetus for further study. Palin and Powell expounded the structural conundrum of the SO₂-hydroquinone system in 1947 and it was Powell who coined a new term "clathrate" for the molecular compound in which one species forms voids in a lattice where the other one sits.^{12,19}

The host-guest relationship, complementary in nature, is a crucial feature of any inclusion system and may be described as steric compatibility. It is determined directly by the shape, the size, and the character of the guest molecule and the lacunae formed by the molecules of the host lattice^{5,7}, and indirectly by the host molecules themselves, *e.g.* the guest species may possess a modified non-typical conformation,²⁸ their motional freedom may differ from that in the liquid and in the solid state,²⁹ and they can also modify the shape of the cavity²¹. The existence of many clathrates is due to the presence of guest molecules in voids of the host lattice. *Clathrands*, *i.e.* unsolvated clathrates, usually do not exist due to the instability of an empty isostructural host framework.⁶

The architecture of inclusion compounds allows for the study and utilization of the effects of the molecular confinement on behaviour of individual guest molecules, their small clusters, and even their whole assembly.²⁸ The technological application of these systems is versatile and ranges from chemical analysis to the pharmaceutical industry,^{4,30} *e.g.* they can be used as model systems in molecular recognition, *i.e.* in a

separation of mixtures, isomers or enantiomers,^{31,32} or in the molecular encapsulation of certain drugs to improve the rate and extent of their absorption as well as their lability.³³ The particular geometry of the cavities can provide a novel environment²⁹ for chemical reactions which can result in new products that are not obtainable from other phases. The structure of inclusion compounds can also be used to control physical properties, *e.g.* thiourea with certain organometallic guests is capable of second-harmonic generation.³⁴

The most well-known clathrates are naturally occurring hydrates which are crystalline host-guest systems based on a framework composed of water molecules.^{35,36,37,38,39,40} In the 1930's, gas hydrates caused technological problems blocking gas pipelines at temperatures higher than one would anticipate for normal ice formation.³⁶ Gas hydrates found in the permafrost region and in the suboceanic environment can be used as a potential source of energy.^{37,40} They may also contribute to the greenhouse effect by releasing methane into the atmosphere.⁴¹ It has also been suggested that clathrate hydrates may be found in comets and Saturn's satellite Titan.³⁶ Other naturally occurring inclusion compounds are zeolites which are based on the aluminosilicate framework. They can be used as absorbents, catalysts, storage media for nuclear waste and semiconductors.

Yet at present, most of the supramolecular systems of interest are the products of laboratory synthesis. Earlier, preparative chemists paid little attention either to an assembly of synthesized molecules or to the crystalline form these molecules would adopt in the solid state. New interest encompasses geometry, *i.e.* the positional

aspect of an assembly, and topology, *i.e.* the pattern of connectivity between different chemical species.⁸ This neglected facet of how molecular geometry controls crystalline morphology is one of the dominant structural considerations in supramolecular complexes and especially in the lattice inclusion compounds.^{11,42,43,44}

Investigation of thermal properties of any material is an intrinsic part of the materials's characterization. Specific heat is one of the basic properties of the solid state.^{45,46,47,48,49} Its dependence on temperature makes this function so useful. It allows one to gain insight into microscopic phenomena on the molecular or even on the atomic level from the macroscopic measurement of a bulk property.^{50,51} Heat capacity can provide information about possible phase transitions in clathrates and their thermodynamic nature. Concomitant to that may be the determination of the motion of the guest molecules in the cages⁵² (*e.g.* type and character of the motion^{53,54}) as well as the guest contribution to the overall thermal properties of the system.^{55,56} Heat capacity data can also be used to test various intermolecular potential functions used in computations and computer simulations for host-host and host-guest interactions.⁵⁷

Thermal expansion measurements aid in the understanding of the anharmonicity of a crystal lattice and other relevant physical properties.⁵⁸ The driving force for thermal expansivity is brought about by a strain-dependent entropy that creates the elastic response of the solid phase. It is a bulk property that does not have an atomic or molecular counterpart like, *e.g.* polarizability. Knowledge of the thermal expansion coefficients is essential, *e.g.* for the conversion of the most often

experimentally determined isobaric heat capacity to the theoretically useful isochoric heat capacity.⁵⁹ The latter, on the premise of quasiharmonic theory, can be used for the analysis of volume-dependent crystal properties.^{60,61}

Thermal conductivity is another principal property of a solid phase.⁶² Ideally, the characteristic features of the temperature profile of the thermal conductivity coefficient of dielectric materials can be ascribed to the structure as well as to the extent of order (and/or disorder) within the material.^{62,63,64,65} Two extreme examples of the topological regularity in a solid are simple well-ordered crystals and amorphous materials. Each has its own characteristic temperature evolution of the thermal conductivity. The starting point for the phenomenological analysis of the thermal conductivity coefficient, κ , is the concept of the phonon gas and the Debye expression⁶⁶

$$\kappa = \frac{1}{3} C \rho v l \quad (1.1)$$

where C , the specific heat capacity (*i.e.* per unit mass) and l , the average phonon mean free path are the only significantly temperature-dependent components of the equation; ρ is the density and v is the sound velocity. For simple crystals, the temperature derivative, $\partial\kappa/\partial T$, changes sign from positive to negative with increasing temperature yielding a pronounced maximum, whereas for amorphous materials it remains positive all along the temperature axis with a small exception between approximately 1 and 10 K where the derivative is *ca.* zero. This plateau seems to be

a generic feature of all amorphous materials that have been measured to date.^{67,68}

Typical crystalline and amorphous thermal conductivity behaviour can, to a first approximation, be inferred from equation (1.1) by taking into consideration temperature dependence of C and l (Figure 1.1). The more detailed description of the temperature evolution of the thermal conductivity includes three characteristic temperature regions in which κ behaves differently albeit distinctively. At low temperatures $\kappa \sim T^3$ for crystals and $\kappa \sim T^\eta$ with $\eta=1.9\pm 0.1$ for amorphous materials. At intermediate temperatures κ assumes the maximum value for crystals and a plateau for amorphous materials. At high temperatures $\kappa \sim T^{-1}$ for crystals and $\kappa \sim T$ for amorphous materials. The temperature profile of κ seems to be well understood for simple (*e.g.* monatomic) crystalline materials. The understanding is not so complete for glasses for which the only definitely identified mechanism of heat conduction is that below 1 K and it is governed by inelastic phonon scattering from two-level systems. The plateau is a consequence of a sudden decrease in the phonon mean free path, the origin of which is still the subject of debate despite attempts to describe κ over a wide temperature range.^{68,69,70,71,72} The character of the temperature-dependence of κ for all amorphous materials is strikingly similar and relatively independent of the chemical composition of the conducting medium. This suggests considerable universality of heat flow phenomena in glasses.

On the other hand there are some crystalline materials, *e.g.* "dirty" ferroelectrics⁷³, the $\text{Ar}_{1-x}(\text{N}_2)_x$ quadrupole glass⁷⁴, the Li_3N superionic conductor⁷⁵ which do not lend themselves to straightforward interpretation of the temperature

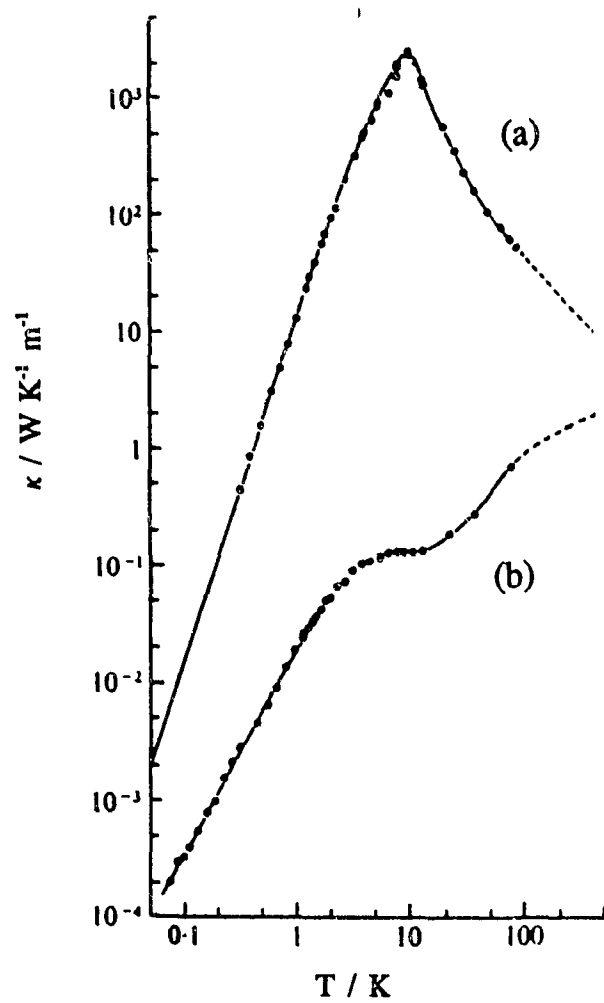


Figure 1.1 The temperature profiles of the thermal conductivity for a typical crystal and glass: (a) crystalline (quartz) SiO_2 ; (b) amorphous SiO_2 . Data are from ref. 64.

evolution of κ in terms of their morphology. They have very low values of κ and a positive derivative of κ with respect to the temperature. Therefore there must be a highly efficient thermal-resistance mechanism in these materials that impedes the thermal energy flux in the relevant temperature regions.

Clathrates are well-defined crystals, but long-range structural order does not appear sufficient to provide a "typical" crystalline behaviour of the thermal conductivity. On the contrary, the thermal resistance mechanism is so effective that κ is rather glass-like. The first reported thermal conductivity measurements of inclusion compounds were carried out on clathrate hydrates.^{76,77} Many physical properties of clathrate hydrates and their close analog, ice Ih, are similar due to the abundance of water molecules and the similarity of the intermolecular bonds. Yet, the thermal expansion^{78,79} and the thermal conductivity^{77,80} for the clathrate hydrates both differ from ice Ih. The temperature profile of κ of clathrate hydrates attracted immediate attention due to its similarities to the thermal properties of glassy materials — its low value of κ and positive $\partial\kappa/\partial T$, in contrast with a negative value of this derivative for ice Ih in the corresponding temperature region. Moreover, measurements of κ of various clathrate hydrates have indicated a certain degree of universal thermal behaviour of these systems in that κ appears to have only a slight dependence on the crystal structure (*i.e.* type I or II) or on the type of guest species (either an atom or a molecule) in clathrate hydrates.^{81,82,83,84,85} The role of guest molecules was further explored through the investigation of thermal conductivity of the ethanol clathrate and the clathrand of Dianin's compound⁸⁶ (unsolvated clathrate hydrate does not exist).

The temperature evolution of κ of these systems falls into the same pattern. The most interesting finding was that the thermal conductivity of the clathrand was qualitatively similar to that of the clathrate.

The only additional report of thermal conductivity of an inclusion compound appears to be the channel compound formed by hexadecane included in urea.⁸⁷ The thermal conductivity of this material was found to have a temperature-dependence intermediate between that of a normal crystalline material ($(\partial\kappa/\partial T) < 0$) and the clathrates described above ($(\partial\kappa/\partial T) > 0$); this intermediate behaviour was ascribed to weaker guest-host coupling in that material than in the clathrate hydrates.

Investigation of thermal conductivity aims at the identification of the prospective topological and/or dynamical causes of such low conduction. It is of fundamental interest to single out and elucidate the importance of individual heat-carrying and/or heat-resistant processes in complex structures. This information would be also applicable to related systems and/or to materials with similar thermal characteristics.

The knowledge of elastic behaviour complements the aforementioned investigations. It reflects directly the intermolecular interactions which determine the force constants between molecular groups and therefore phonon dynamics. Elastic constants are practically determined by measurements of sound velocities along known crystallographic directions. They are essential in the understanding of the relevant thermodynamic quantities. The stability of a crystal lattice can be said to be prescribed by the components of the elastic compliance tensor that represent the

second derivatives of the pertinent state functions with respect to the strain tensor components.

A new group of clathrates was synthesized in the mid-1970's. The idea of their structure came from the similarity of the hydrogen-bonded hexamer unit (*e.g.* as in Dianin's compound) with hexa-substituted benzene.^{88,89} It was one of the first instances of the premeditated design of cavities. The main focus of this thesis is on thermal and related properties of this family of inclusion compounds.

Since thermal and mechanical properties are determined by intermolecular forces, these model systems afford an opportunity to probe the intermolecular interaction between guest and host molecules and also to shed light on the dynamics of molecular moieties and its effect on physical properties, as well as the role of the concentration and type of guest species on thermal behaviour.

To this end, the foredescribed properties have been investigated. This thesis concerns mainly the study of thermal properties of the hexakisphenylthiobenzene (HPTB for short) system, the archetypal compound in this series. The thermal conductivity of the carbon tetrachloride clathrate of Dianin's compound, which is an example of its structural matrix, also has been investigated.

THERMAL PROPERTIES - BASIC RÉSUMÉ

2.1 INTRODUCTION

The theoretical fundamentals of the thermal properties of the solid state are based on thermodynamics which deal with specific macroscopic properties where temperature is a crucial variable. The natural connection with a molecular level of understanding of these properties is introduced by statistical thermodynamics. The principal equation which includes the first and second law of thermodynamics can be written in differential form as⁵⁹

$$TdS(=dQ)=dU+dw \quad (2.1)$$

where Q is the energy absorbed by the crystal in the form of the heat, T is the absolute temperature, S is the entropy, U is the internal energy and w is the work done by the crystal. It seems natural to regard the internal energy U as a function of the volume, V , and the entropy ($U=U(S, V)$). Other thermodynamic state functions like the Helmholtz energy $A(P, T)$, the Gibbs energy, $G(T, V)$ or the enthalpy, $H(P, V)$, can be introduced employing Legendre transforms.⁹⁰ Certain thermodynamic variables are not independent, *e.g.* the relationship between volume, temperature and pressure (P), at equilibrium can be written formally as

$$f(P, V, T) = 0 \quad (2.2)$$

which constitutes the equation of state.

Thermal properties of a crystal are described by the heat capacity, C , the thermodynamic function which measures the changes of the crystal temperature ascribed to heat input, *i.e.*

$$C = \frac{dQ}{dT} = \frac{TdS}{dT} \quad (2.3)$$

Since dQ is inexact, the heat capacity depends on the path of the process and an appropriate constraint is always attached to that function. The most commonly used constraints are constant pressure and constant volume. The relation between the isobaric heat capacity, C_p , and isochoric heat capacity, C_v , for isotropic materials is given by the expression⁵⁹

$$C_p = C_v + TV \frac{\alpha_v^2}{\beta} \quad (2.4)$$

where $\alpha_v = (\partial \ln V / \partial T)_p$ is the volume thermal expansion coefficient and $\beta = -(\partial \ln V / \partial P)_T$ is the isothermal compressibility. The first law of thermodynamics relates the isochoric heat capacity, C_v , to the internal energy of the solid state and hence C_v can provide information about dynamics of species which form the lattice. Crystals are obviously anisotropic materials. Certain functions must be modified in order to

incorporate the symmetry of the structure and thus to exhibit the real nature of the lattice behaviour, *e.g.* the appropriate constraints for the heat capacity function are the constant strain and constant stress.

The internal energy, U , of the crystal which is a finite array of identical building blocks of atoms consists of the potential energy of the interacting atoms, Φ , (assumed to be an analytic function; *vide infra*) and the kinetic energy of the motion of these atoms, *i.e.*^{59,91,92,93}

$$U = \Phi + \frac{1}{2} \sum_{i,j,\mu} M_j \left(\frac{\partial u_{i,j,\mu}}{\partial t} \right)^2 \quad (2.5)$$

where the kinetic energy is the sum taken over all unit cells denoted by i and over all atoms in these unit cells denoted by j (M_j is the mass of the j -th atom, $u_{i,j,\mu}$ is the displacement of the j -th atom in the i -th unit cell; μ is the Cartesian coordinate, t is time). Since the second term is relatively small in comparison to the first the potential energy can be regarded as an approximation of the internal energy (or the Helmholtz energy, A , especially at low temperatures).

The difference in the time scales of the motions of the nuclei and electrons allows for a practical assumption known as the adiabatic approximation in which the motions of nucleus and the electrons are decoupled, *i.e.* electrons can be regarded to be in the lowest energy state even if the atoms are in motion.^{92,93,94}

In principle, crystallographic positions of atoms are their equilibrium positions about which the atoms vibrate. The instantaneous displacements of the atoms are

assumed to be small in comparison to distances between them. Therefore the potential energy (analytic function) can be expanded in the Taylor's series in powers of the atomic displacements around the equilibrium positions, *i.e.*⁹³

$$\Phi = \Phi_0 + \sum_{i,\alpha} \left(\frac{\partial \Phi}{\partial u_{i,\alpha}} \right)_0 u_{i,\alpha} + \frac{1}{2} \sum_{i,\alpha; j,\beta} \left(\frac{\partial^2 \Phi}{\partial u_{i,\alpha} \partial u_{j,\beta}} \right)_0 u_{i,\alpha} u_{j,\beta} + \dots \quad (2.6)$$

The first term is constant and is irrelevant to dynamical considerations; the second one vanishes since the crystal is at equilibrium that corresponds to the minimum of the potential energy, and the first important term in this expansion is of 2nd order in the displacements. Harmonic theory of the crystal lattice considers only these 2nd order terms.⁹³ However there are some properties that, in principle, can be explained only when higher terms are considered. Therefore anharmonic theory takes into account higher terms (third and fourth and/or onwards). Anharmonicity, considered as a weak effect, can also be dealt with by theories based on the harmonic approximation.⁹³ The most popular is quasiharmonic theory. The Helmholtz energy must be determined first and the positions are treated as free parameters. Once again only the 2nd order terms are included in the expression for the total energy but the relevant expansion is taken not around the minimum of the potential energy but the minimum of the Helmholtz energy.⁹⁵

There are $3nN$ equations of motion in the harmonic approximation obtained using the Lagrange equations, where n is the number of atoms in the unit cell and N is the number of unit cells in the crystal. On the basis of the crystal symmetry these equations can be simplified, written by means of the dynamical matrix, and their number decreased to $3n$. Thus for each value of the wave vector \underline{k} there are $3n$ values of the frequency, ω , referred to as normal modes. The polarization of the normal modes is purely longitudinal or transverse only in certain directions determined by the symmetry. In the general case the polarization is quasi-longitudinal and quasi-transverse. The behaviour of dispersion (*i.e.* the dependence of the frequency on the wave vector \underline{k} when the equations of motion are solved for parallel \underline{k}) for three of $3n$ branches, called acoustic, is that $\omega \propto k$ ($k = |\underline{k}|$) when $k \rightarrow 0$. For the remaining branches, called optic, $\omega \neq 0$ when $k \rightarrow 0$.

The above conforms to the phenomenological approach to the lattice dynamics in which the forces between atoms are assumed to be known. These forces are described by the force constants that are the second derivatives of the interatomic potentials with respect to the atom displacements. Thus, any atom displacement can be regarded as a collection of the eigenvectors of the dynamical matrix and the energy of the lattice can be expressed as a sum of the energy of the decoupled harmonic oscillators.

Quantum treatment of lattice dynamics in the harmonic approximation considers the relevant Hamiltonian that is similarly simplified by subsection to the pertinent orthogonal transformation that diagonalizes the quadratic form of the

potential energy and introduces normal coordinates and quantized normal modes. This so-called second quantization employs creation and annihilation operators that yield the concept of the phonon which is the quasiparticle with energy $\hbar\omega$ and quasimomentum $\hbar\mathbf{k}$ with statistics given by the Bose-Einstein distribution function⁹⁰ ($N_j(\mathbf{k}) = (\exp(\hbar\omega_j(\mathbf{k})/k_B T) - 1)^{-1}$); $\hbar = h/2\pi$ where h is the Planck constant and k_B is the Boltzmann constant. Thus the normal modes are quantized like a harmonic oscillator and the internal energy of the crystal can be expressed as⁹⁰

$$U = \sum_{\mathbf{k}j} \hbar\omega_j(\mathbf{k}) \left(\frac{1}{e^{\hbar\omega_j(\mathbf{k})/k_B T} - 1} + 1/2 \right) \quad (2.7)$$

where the sum is over values of \mathbf{k} from the first Brillouin zone and over all branches of phonon dispersion denoted by j .

This general harmonic approach to lattice dynamics can be appropriately modified if applied to complex crystals which are distinguished on the basis of their structural features that significantly influence their physical properties.^{95,96} Well-bound molecules or polyatomic clusters commonly called molecular groups are easily discernible in molecular crystals and in certain ionic crystals.^{97,98} Since the valence force field is much stronger than the crystal field these crystals retain certain properties characteristic for other states of condensation of the comprising species, *e.g.* the frequencies of vibrations within a molecular group depend relatively little on the state of condensation and molecular groups form a lattice without any substantial modification of their internal geometry. This is the premise of the rigid molecule

approximation that assumes that these groups can be treated as separate blocks. That, in turn, allows for decoupling the internal motion of atoms within the molecular group (internal modes) from the motion of these groups as the distinctive units (external modes). The frequencies of the latter are generally much lower than that of the internal modes due to much weaker forces involved in binding.⁹⁷ Since the molecular groups are three-dimensional, in addition to translational vibration they also can exhibit rotational motion. The validity of the harmonic approximation holds if the rotations are limited only to small amplitudes, which allows one to treat these small rotations (librations) as vectors. Thus, in the general case, the following is the physical picture of the lattice dynamics of a complex crystal with n atoms in the unit cell that can be partitioned into n_a single atoms and n_g well-bound non-linear molecular groups. There are $3n_a + 6n_g$ external branches (equal to the number of degrees of freedom of the different components per unit cell) and $3n - (3n_a + 6n_g)$ internal branches of the phonon dispersion. Three of the external branches are acoustic; the remainder are optic.

2.2 MODELS OF HEAT CAPACITY

The Helmholtz energy, A , describing the macroscopic state of the crystal is related to the energetic behaviour of the lattice at the microscopic level through the canonical partition function Z (*i.e.* $A = -k_B T \ln Z$).⁹⁰ The previously described treatment of the lattice dynamics that gave a collection of the normal modes or phonons provides the necessary information (equation (2.7)) for energetic states of the lattice to employ this relation ($Z = \sum \exp(-U/k_B T)$) where the sum is taken over all possible choices of U given by equation (2.7). On the other hand, from the thermodynamic definition of A and the pertinent Maxwell relation the internal energy of the lattice is expressed by⁹⁰

$$U = A - T(\partial A / \partial T)_V . \quad (2.8)$$

Hence, from the Helmholtz energy expressed through the canonical partition function on the basis of the equations (2.3), (2.7) and (2.8), the isochoric heat capacity is given by

$$C_V = \sum_{kj} k_B (\hbar \omega_j(\underline{k}) / 2k_B T)^2 / \sinh^2(\hbar \omega_j(\underline{k}) / 2k_B T) \quad (2.9)$$

with the sum as in equation (2.7). In order to introduce the Einstein and Debye models of heat capacity it is instructive to replace the sum over \underline{k} in eq.(2.9) by integrals over the frequency using the state density function $g(\omega)$, where $g(\omega)d\omega$ is the total number of modes with frequencies between ω and $\omega + d\omega$, normalized by⁹³

$$\int g(\omega)d\omega = 3nN \quad (2.10)$$

where n is the number of the atoms in the unit cell and N is the number of unit cells in the crystal.

In the Einstein approximation, the density of states is given by⁹³

$$g(\omega) = 3nN\delta(\omega - \omega_E) \quad (2.11)$$

with the Einstein frequency ω_E chosen to give the best agreement with experimental findings; δ is the Dirac delta function. This model accurately describes the heat capacity related to the optic modes. At low temperatures the heat capacity, C_V , varies as⁹³

$$\lim_{T \rightarrow 0} C_V = 3nNk_B \left(\frac{\theta_E}{T} \right)^2 e^{-\theta_E/T} \quad (2.12)$$

where θ_E is the Einstein temperature corresponding to ω_E ($k_B\theta_E = \hbar\omega_E$). At high temperatures C_V approaches the value stated by the Petit-Dulong law, *i.e.* $3nNk_B$, but the low-temperature dependence differs in character from experimental values.

The Debye model takes a similar approach, only the frequency is not confined to a single value but varies linearly with wave number, *i.e.* $\omega = kv$ where v is the average velocity of sound in the crystal. Whereas the motion of atoms was treated as the motion of isolated oscillators in the Einstein model, the Debye model considers collectively propagating waves in the crystal as a continuous, not discrete, medium.

In order to maintain the reality of the Debye approximation the angular frequency is cut off at an upper value called the Debye frequency, ω_D . The non-zero density of states is given by⁹³

$$g(\omega) = \frac{3}{2\pi^2} V \frac{\omega^2}{v^3} \quad (2.13)$$

for values of $\omega \leq \omega_D$, where V is the volume of the crystal. The value of ω_D obtained from the normalization condition (Eq.(2.10)) is given by⁹³

$$\omega_D = (6n\pi^2 v^3 / V_{unit})^{1/3} \quad (2.14)$$

where n is the number of atoms in the unit cell and V_{unit} is the volume of the unit cell.

Since the Debye model describes the heat capacity related to the acoustic modes

which dominate in simple solids it is more realistic than the Einstein approximation.

The heat capacity, C_V , is given by⁹³

$$C_V = 9nNk_B \left(\frac{T}{\theta_D} \right)^3 \int_0^{\theta_D/T} \frac{x^4 e^x}{(e^x - 1)^2} dx \quad (2.15)$$

where θ_D is the Debye temperature corresponding to the cut-off frequency ω_D

($k_B \theta_D = \hbar \omega_D$). At high temperatures C_V approaches the classical value of $3nNk_B$; at low temperatures it predicts the behaviour known as the Debye T^3 law, *i.e.*⁹³

$$\lim_{T \rightarrow 0} C_V = \frac{12\pi^4}{5} nNk_B \left(\frac{T}{\theta_D} \right)^3 . \quad (2.16)$$

The Einstein and the Debye temperatures demarcate the low-temperature region from high temperatures, *i.e.* the applicability of the quantum or classical statistics, respectively.

2.3 ESSENTIAL PHYSICS OF PHONON MOTION AND THERMAL CONDUCTIVITY

Harmonic theory resolves the dynamics of the crystal lattice into travelling plane waves, *i.e.* normal modes. There is no mechanism of energy exchange between these waves. Hence, at equilibrium the heat flux must vanish since there is the same number of waves travelling in either direction. If equilibrium is disturbed, then such a *status quo* is sustained because of the absence of energy exchange mechanism (even if the cause of the disturbance is removed). The equivalent but clearer picture uses phonons. In order to visualize these quanta of energy as quasiparticles the phonons are localized within the region $\Delta x \sim 1/\Delta k$ by taking the superposition of states smeared over Δk (*i.e.* wavepacket). The energy flow, \mathfrak{H} , can be expressed as⁶²

$$\mathfrak{H} = \sum_{\underline{k}j} n_j(\underline{k}) \hbar \omega_j(\underline{k}) \nabla_{\underline{k}} \omega_j(\underline{k}) \quad (2.17)$$

where $n_j(\underline{k})$ is the phonon distribution. At equilibrium $\omega(\underline{k}) = \omega(-\underline{k})$, $n_j(\underline{k}) = N(\underline{k})$ and $n_j(-\underline{k}) = N(-\underline{k})$, and $\mathfrak{H} = 0$. Away from equilibrium, the asymmetry of the distribution $n_j(\underline{k})$ maintains perpetual heat flow. On the other hand, the macroscopic expression for lattice thermal conductivity, with a steady state rate of heat flux established, is

$$\mathfrak{H} = -\kappa \nabla T \quad (2.18)$$

where κ is the thermal conductivity coefficient and ∇T is the temperature gradient

along the crystal. Thus the harmonic crystal has infinite thermal conductivity and in order to explain the observed finite κ the higher order terms in the potential energy expansion must be considered. A first approximation takes into account the cubic term⁹⁴

$$\Phi_3 = \frac{1}{3!} \sum_{i,i',i''} \sum_{\alpha\beta\gamma} \left(\frac{\partial^3 \Phi}{\partial u_{i,\alpha} \partial u_{i',\beta} \partial u_{i'',\gamma}} \right)_0 u_{i,\alpha} u_{i',\beta} u_{i'',\gamma} . \quad (2.19)$$

Thus the Hamiltonian, after second quantization, includes the component that acts on the three-phonon state. This component, which imposes the quasimomentum conservation (*i.e.* $\underline{k} + \underline{k}' + \underline{k}'' = \underline{G}$ where \underline{k} 's are wavevectors and \underline{G} is a reciprocal lattice vector), depends on the following operator⁹⁴

$$(a_{kj}^+ - a_{-kj}) (a_{k'j'}^+ - a_{-k'j'}) (a_{k''j''}^+ - a_{-k''j''}) \quad (2.20)$$

where a_{kj}^+ and a_{-kj} are the relevant creator and annihilator operators. This, in turn, defines the three phonon processes taking place in the crystal. Provided that energy is conserved these processes determine two classes of allowed events which can be described in the language of appropriate conservation laws as follows;

A-event; annihilation of two phonons and creation of a third phonon:

$$\omega(\underline{k}j) + \omega(\underline{k}'j') = \omega(\underline{k}''j'') ; \quad \underline{k} + \underline{k}' = \underline{k}'' + \underline{G} \quad (2.21)$$

B-event: annihilation of one phonon and creation of two phonons:

$$\omega(kj) = \omega(k'j') + \omega(k''j'') ; \quad k + \underline{G} = k' + k'' . \quad (2.22)$$

When $\underline{G}=0$ this is a so-called normal process (N-process), otherwise, *i.e.* if $\underline{G} \neq 0$ this is an Umklapp process (U-process). The difference between these two is shown in Figure 2.1. The resultant phonon in an N-process falls within the first Brillouin zone and the direction of the energy flux remains unchanged. The converse situation exists for an U-process, *i.e.* the outgoing phonon is different from the sum of the incoming phonons and the energy flow is diverted. U-processes are of paramount importance for thermal conductivity. Only the low-energy modes are excited at low temperatures and then $\omega = k\nu$ where ν is the group velocity. If this is the case, the heat flux can be written in terms of the crystal quasimomentum ($P_j = \sum_{\underline{k}} n_j(\underline{k}) \hbar \underline{k}$) as⁶²

$$\mathcal{H} = \sum_j P_j \nu^2 . \quad (2.23)$$

Then if only N-processes are present, for which $P = \sum_j P_j$ is constant, collisions cannot lead to the equilibrium value of $P=0$ and the heat flux persists even without the temperature gradient, giving infinite thermal conductivity. Yet Normal processes indirectly contribute to thermal resistance. They change the phonon distribution and thus they are able to facilitate other thermal resistant mechanisms. N-processes tend to the displaced distribution, N^p , given by⁶²

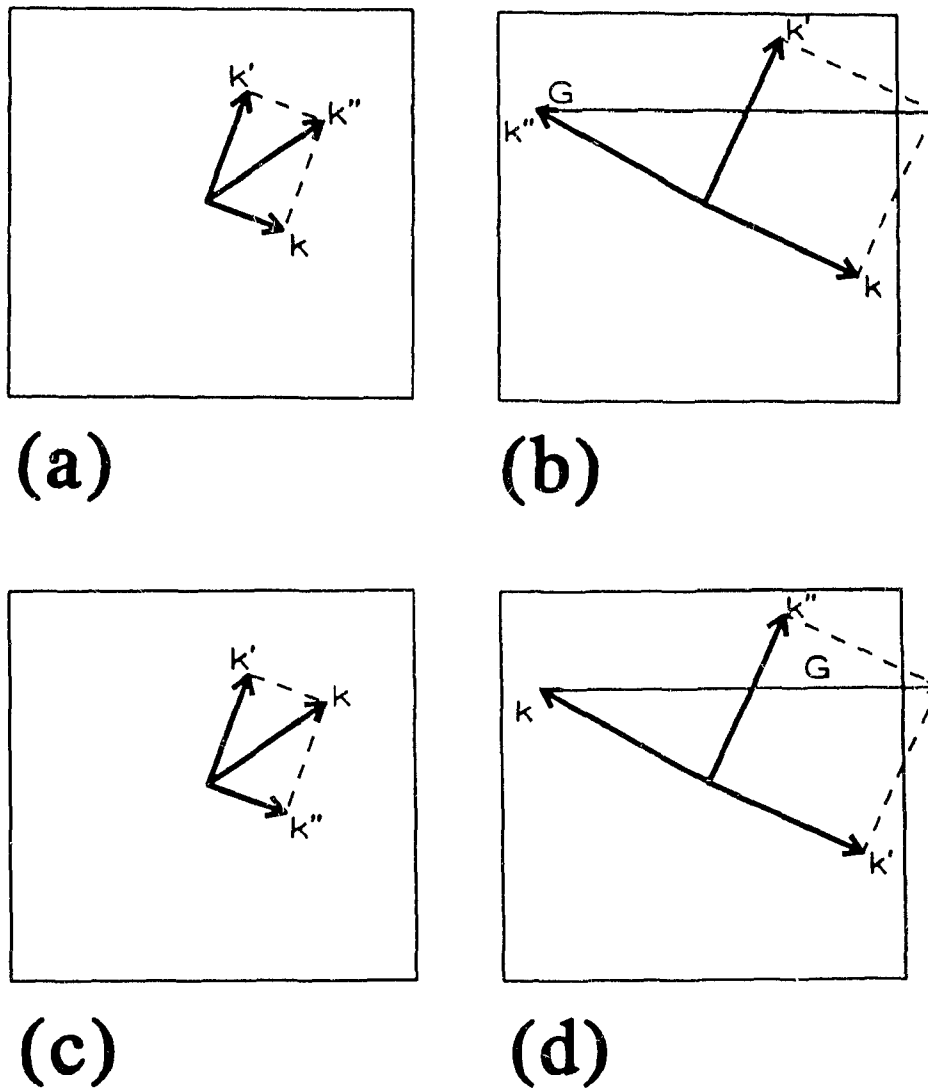


Figure 2.1 Two-dimensional representation of three-phonon processes: (a) A-event, N-process; (b) A-event, U-process; (c) B-event, N-process; (d) B-event, U-process.

$$N' = \frac{1}{e^{(\hbar\omega - q^* u_{ax})/k_B T} - 1} \quad (2.24)$$

where u_{ax} reflects the asymmetry of the distribution.

The U-processes lead to the change of the crystal quasimomentum and they are directly responsible for thermal resistance. If one considers the A-event U-processes in the low temperature region the probability of such processes is tantamount to the factor $N_j(k)N_{j'}(k') \sim \exp(-\hbar\omega_j(k)/k_B T)\exp(-\hbar\omega_{j'}(k')/k_B T)$ and because $\hbar\omega_{j'}(k') > k_B\theta_D$ for the Debye crystal the rate of U-processes, τ^{-1} , is given by

$$\tau^{-1} \approx e^{-\frac{\theta_D}{\alpha T}} \quad (2.25)$$

where $\alpha > 1$ is an experimental parameter. Other temperature dependences of these processes can be incorporated into the expression in the form of a preexponential factor, T^η , with η as an experimental parameter.⁶²

INCLUSION COMPOUNDS INVESTIGATED

3.1 INTRODUCTION

The systematic development of knowledge of clathrates had begun with the solution of the hydroquinone structure. Hydroquinone, phenol 4-(3,4-dihydro-2,2,4-trimethyl-2H-1-benzopyran-4-yl)phenol, **1**, (Dianin's compound; shown in Figure 3.1) and related systems have a common structural feature which is of paramount geometrical importance in their ability to create a crystal lattice with well-defined cavities. All of these molecules have hydroxyl groups which link them together in hexamers. These hexamers become basic building units of the host framework of the clathrate. The host molecules in the hexamer are alternatively pointing up and down which gives the supramolecular unit trigonal symmetry. A schematic of the basic building block of these systems is shown in Figure 3.2. Two hexamers of the host molecules, bound by van der Waals interactions, are stacked on each other making a cavity where a guest molecule can reside. Dianin's compound is, perhaps, the most interesting since it can also yield the clathrand. Since a thermal conductivity investigation of the CCl_4 clathrate of Dianin's compound is part of the research described in this thesis, it is instructive to digress a bit on this system.

The clathrand and all clathrates of Dianin's compound appear to crystallize in the same trigonal $\bar{R}3$ space group with only a slight variation of unit cell dimensions

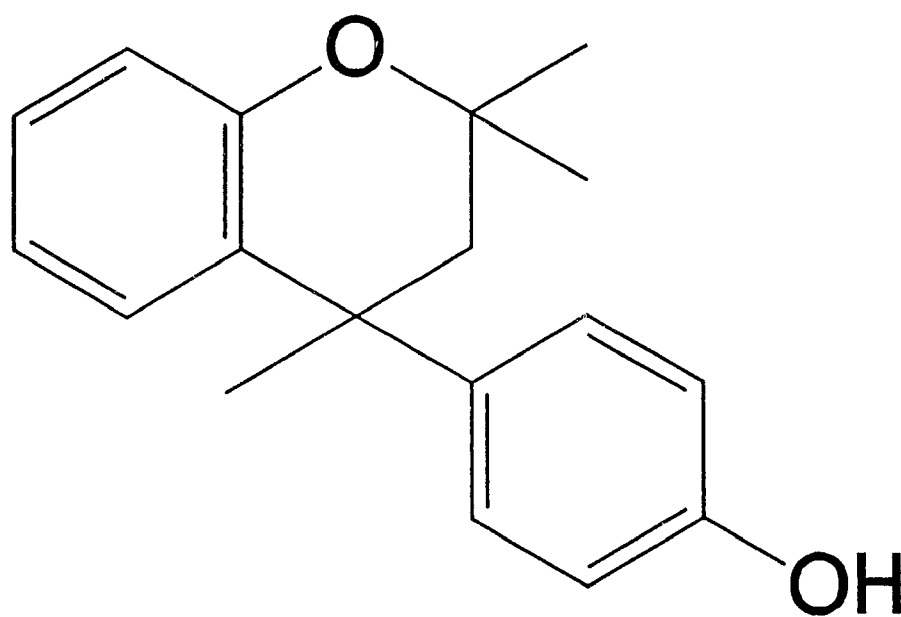


Figure 3.1 Molecular structure of Dianin's compound, 1.

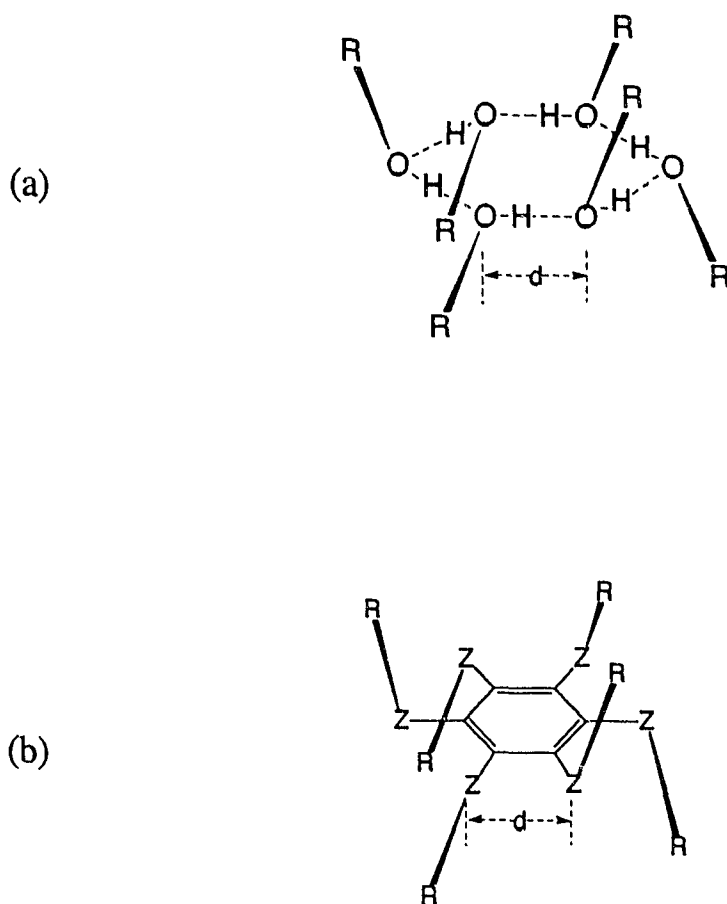


Figure 3.2 Close structural analogy between (a) a hydrogen-bonded hexamer supramolecular unit, *e.g.* in Dianin's systems and (b) a typical hexasubstituted benzene analogue, *e.g.* hexakisphenylthiobenzene. The geometric as well as dimensional (distances denoted by *d*) resemblance is conspicuous.

that depends on the type of enclathrated species. They all have geometries based on the forementioned hexamer supramolecular unit made up of six host molecules linked with hydrogen bonds through the phenolic hydroxyl groups. The oxygen atoms form a distorted hexagon with alternate Dianin molecules lying above and below the plane of the hexagon. The exceptional stability of the host structure is ascribed to hydrogen bonding and the shape of the host molecule. The cavity (volume of *ca.* 120 Å³) has an hour-glass shape with three-fold symmetry and a centre of inversion (the cavity in the case of the CCl₄ clathrate is shown in Figure 3.3). It can incarcerate one or two small guest molecules. There are 18 Dianin's molecules in the unit cell. The unit cell dimensions of the clathrand are : $a=26.94$ Å and $c=10.94$ Å.¹¹ Dianin-CCl₄ conforms to the structure of the clathrand as described. The dimensions of the hexagonal unit cell of the CCl₄ clathrate of Dianin's compound at room temperature are⁹⁹ $a=27.134\pm 0.008$ Å and $c=10.933\pm 0.002$ Å. There is one two-fold statically disordered CCl₄ molecule per cage. The CCl₄ guests are aligned along the crystallographic *c*-axis such that one C-Cl bond lies along this axis, with two possible molecular orientations. Both orientations are present in a 1:1 ratio but it is not known whether there is any correlation in the orientations of neighbouring CCl₄ molecules. At room temperature the mean displacement of the centre of gravity of the CCl₄ molecule is of the order of 0.4 Å with a mean librational angle of 14°.⁹⁹

The idea of this hexagonal arrangement, through hydrogen bonds of OH groups of six host molecules was the basis for the proposal and realization of a

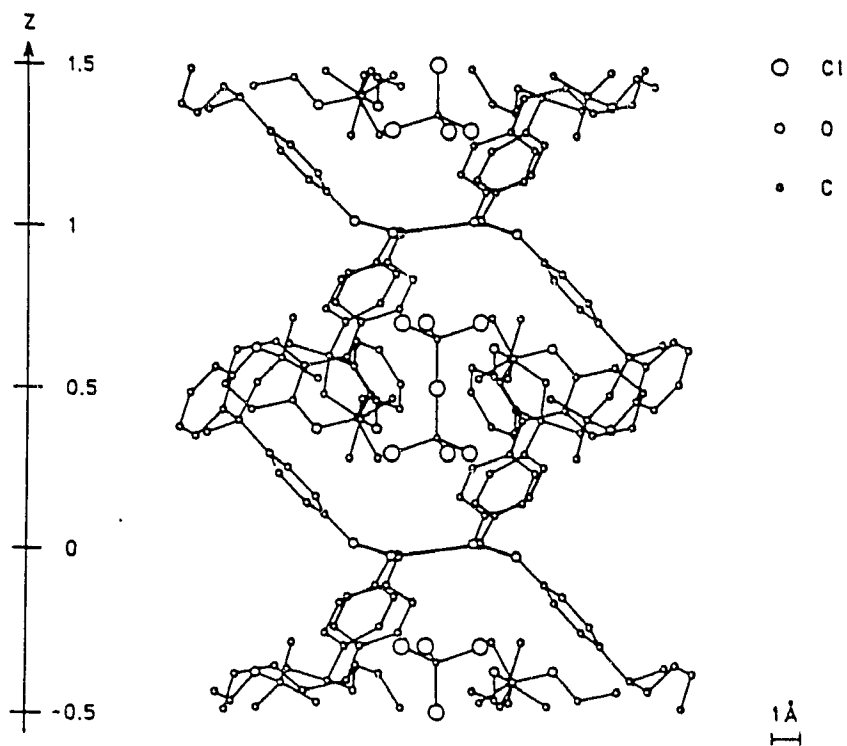


Figure 3.3 The crystal structure of the CCl_4 clathrate of Dianin's compound. Both positions of the CCl_4 guest molecules are shown but only one position is occupied in each cage.⁹⁹

strategy for the design of new lattice inclusion compounds.^{88,89} The hexagonal arrangements present a close analogy to the hexa-substituted benzene ring. The resemblance between the hexamer and its hexa-host analogue can be seen in terms of geometric aspects as well as in dimensions. This is depicted in Figure 3.2.

Hexakisphenylthiobenzene, **2**, is the archetypal compound for these systems engineered specifically on the premise of the above described similarity. The molecule is highly symmetrical in the solid state (Figure 3.4; *vide infra*); phenyl groups are situated alternatively above and below the plane of the central phenyl ring. No inclusion behaviour of HPTB had been found after recrystallization from chloroform, trichlorofluoromethane or pentachloroethane.^{88,89} It was reported that recrystallization of HPTB from the solvents CCl_4 , CBrCl_3 , CH_3CCl_3 and CCl_3SCl yielded clathrates of HPTB with the mole host-guest ratio 1:2, 1:1, 1:2, and 1:2 respectively.^{88,89} The first three of these systems were prepared and initially studied but since the guest escaped when left in air they were deemed inappropriate for the planned study. Instead, a new clathrate system was prepared from the solution of chloroform with an excess of CBr_4 . This yielded the CBr_4 clathrate of HPTB.

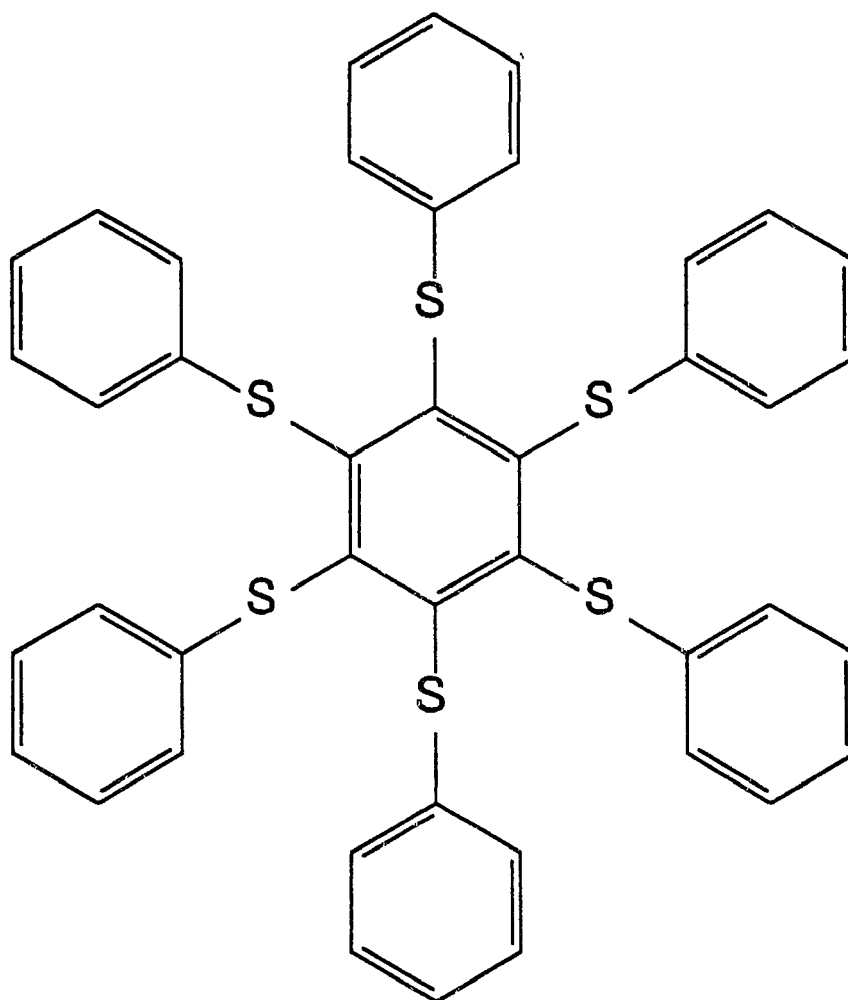


Figure 3.4 Molecular structure of hexakisphenylthiobenzene, 2.

3.2 PREPARATION AND CRYSTAL GROWTH

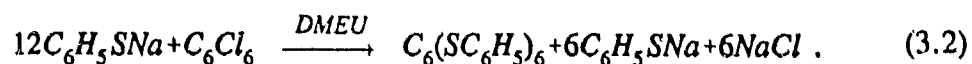
3.2.1 DIANIN'S COMPOUND AND ITS CCl₄ CLATHRATE

Dianin's compound was prepared by M. Zakrzewski using a literature route.¹⁰⁰ Single crystals of Dianin-CCl₄ were grown here from a solution of Dianin's compound dissolved in CCl₄/decanol (3:2 volume ratio). Decanol is too large to be caught in the hexamer cages of Dianin's compound¹⁰¹ and it was used to lower the density of the solution to suspend the crystals. Crystals were grown by repeated cycling of the temperature of the solution between 30°C and 45°C with periodic addition of powdered CCl₄ clathrate of Dianin's compound, taking advantage of the increased solubility at higher temperatures, and, on cooling, preferential precipitation on the faces of the crystal(s). Sporadically CCl₄ was also added to the vial. The crystal density, determined at room temperature by density matching with aqueous KI solutions for which the density was found using a calibrated pycnometer, was $\rho = 1.263 \pm 0.005 \text{ g cm}^{-3}$, which gives a host-guest ratio of $5.94 \pm 0.05 : 1$ (ideal value of 6 : 1).

3.2.2 HPTB

The preparation of hexakisphenylthiobenzene, abbreviated HPTB, was based on two reactions carried out in a nitrogen atmosphere:^{88,89,102}





First, 13.5 g of sodium hydride (Aldrich) was put into a 500 mL three-necked round-bottom reaction flask. Ligroin (Aldrich) was introduced into the same flask in an amount sufficient to cover the NaH by 5 mm. The flask was swirled and left to let the NaH settle to the bottom. The ligroin was decanted by means of a pipette. This was done twice in order to wash the NaH. The reaction flask was connected to a nitrogen gas line and a flow of gas was commenced. The nitrogen was not pumped directly to the reaction flask: a paraffin oil trap was used to maintain a relatively constant pressure. 62.5 mL of 1,2-dimethyl-2-imidazolidinone (Aldrich; DMEU for short) was introduced into the flask as a solvent. DMEU was used instead of the carcinogenic hexamethylphosphoric triamide (HMPA) that originally had been used in this reaction.⁸⁹ Stirring was started using a magnetic stirrer. 35.7 mL of thiophenol, C₆H₅SH, (Ph-SH here for short; crude Ph-SH (Aldrich) had been vacuum distilled) and 14.3 mL of DMEU were introduced into another round-bottom flask. That solution was added to the reaction flask by means of a syringe. This was done slowly and with care because the addition of the Ph-SH solution produced hydrogen in a violent reaction. 60 mL of DMEU was added to the next round-bottom flask containing 8.7 g of hexachlorobenzene, C₆Cl₆, (Aldrich). 50 mL of that solution was added slowly to the reaction flask. The reaction was left stirring for six days to allow the reaction to be completed. To prevent rapid temperature fluctuations during the reaction, the flask was put into a water bath maintained at 19°C. The final product,

HPTB, was recovered using suction filtration and left to dry in air. It was a fine yellow powder. The yield of the reaction was 80%.

Slow evaporation was employed to obtain HPTB crystals. Chloroform was used as the solvent. The crystals were transparent and yellow.

Differential scanning calorimetric measurements were used to determine melting point of HPTB crystals (using a Perkin-Elmer DSC-1¹⁰³ set up at heating rates of 5 and 10 K/min.) which was found to be 180°C. The samples were composed of small crystals and their masses were 0.0025-0.0085 g. A typical DSC plot is shown in Figure 3.5. The ¹H NMR spectrum of HPTB in chloroform is shown in Figure 3.6.

3.2.2 HPTB-CBr₄

Crystals of the CBr₄ clathrate of HPTB were grown from a solution of HPTB in chloroform with excess CBr₄ (3:1, CBr₄ to HPTB mole ratio) by slow evaporation. They were yellow (with orange hue) and transparent. Differential scanning calorimetric measurements were used to determine the melting point of HPTB-CBr₄ crystals (using a Perkin-Elmer DSC-1¹⁰³ set up at heating rates of 5 and 10 K/min.); it was found to be 165.5°C. The samples were composed of small crystals and their masses were 0.01-0.015 g. These crystals decompose on melting. A typical DSC plot is shown in Figure 3.5.

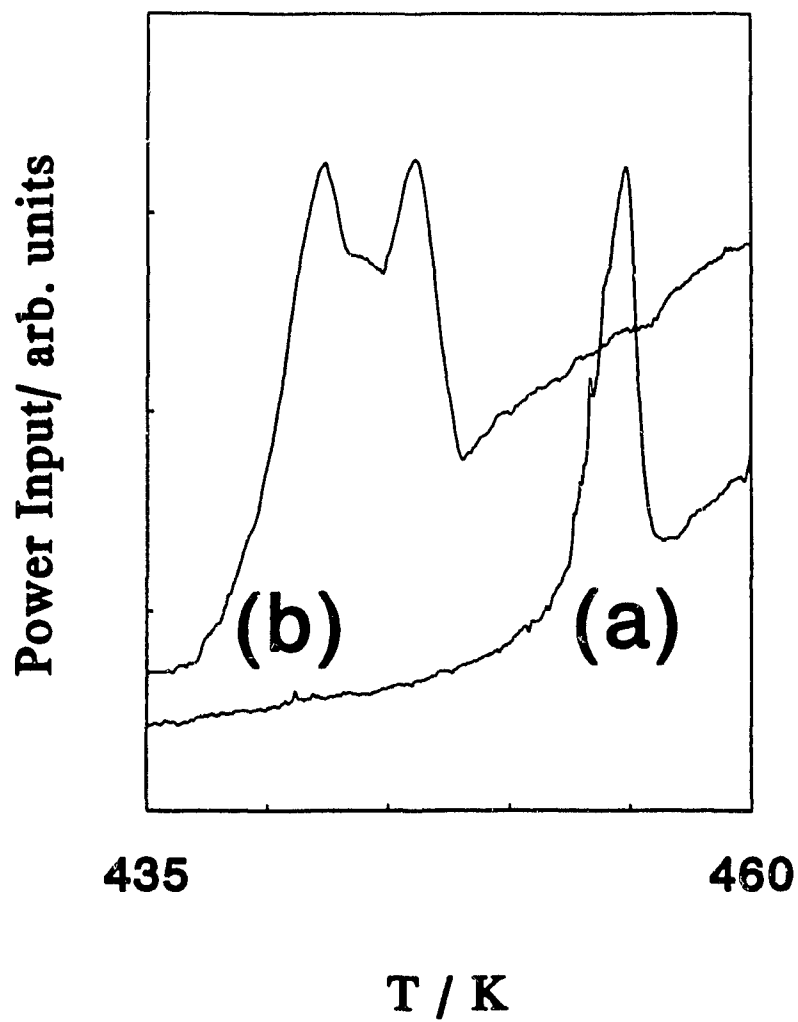


Figure 3.5 A DSC scan of (a) HPTB and (b) HPTB-CBr₄ measured on heating at 5 K min⁻¹.

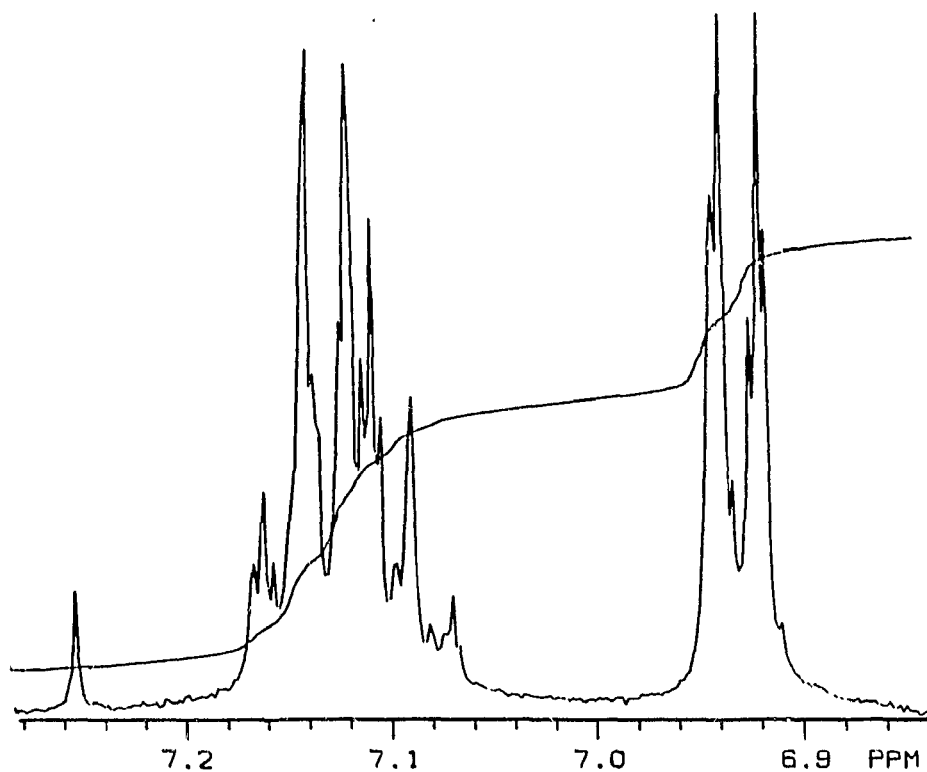


Figure 3.6 ¹H NMR spectrum of HPTB in chloroform. The doublet centred at 6.93 is due to the ortho-hydrogens; splitting is caused by the coupling between ortho- and meta-hydrogens of the phenyl group. The set of overlapping peaks about 7.10 ppm is due to the meta- and para-hydrogens and splitting stems from the coupling with their neighbouring hydrogens on the phenyl ring. The peak at 7.26 ppm is from the chloroform. The integrated peaks are in the ratio 3:2 which supports the given assignment.

3.3 CRYSTAL STRUCTURE OF HPTB AND ITS CBr₄ CLATHRATE¹⁰⁴

3.3.1 HPTB

The crystallographic parameters of HPTB are given in Table 3.1. Pure HPTB crystallizes in the space group $P\bar{1}$ (shown in Figure 3.7). The crystallographic axis passes through the C(20)-S(1) bond, so that half of the molecule is unique and the other half is related by the centre of symmetry (Figure 3.7; positional parameters and B(eq) are given in Appendix in Table A6). The C-S bond lengths are not unusual, the mean being 1.768(2) Å. The central and side chain phenyl rings are almost planar. The ability of HPTB to form clathrates stems from the very open molecular topology. The packing coefficient, *i.e.* the ratio of the van der Waals volume of the molecular content of the unit cell to the volume of the unit cell itself, determined by molecular mechanics¹⁰⁵ is 0.60. Organic molecular crystals typically have packing coefficients in the range 0.65 to 0.77.¹⁰

3.2.2 HPTB-CBr₄

The crystallographic parameters of HPTB-CBr₄ are given in Table 3.1. The CBr₄ clathrate of HPTB crystallizes in a trigonal crystal system, space group $R\bar{3}(h)$. Its structure, shown in Figure 3.8, is similar to its CCl₄ analogue.⁸⁹ A cavity, in the zone of the crystallographic *c*-axis, is formed by six host HPTB molecules. The guest molecules close the top and the bottom of the cage. The effective length of the cavity occupied by two guest species is *ca.* 17 Å. The elongated cavity is of the closed cage type. The gaps in the cage wall (determined from van der Waals radii)

Table 3.1 Crystallographic properties of HPTB and HPTB-CBr₄ at 22°C.

	HPTB	HPTB-CBr ₄
Formula	C ₄₂ H ₃₀ S ₆	C ₄₄ H ₃₀ S ₆ Br ₈
Formula weight	727.1	1390.3
Crystal system	triclinic	trigonal
Space group	P $\bar{1}$ (No. 2)	R $\bar{3}$ (No. 148)
<i>a</i> (Å)	9.589(2)	14.327(4)
<i>b</i> (Å)	10.256(1)	14.327(4)
<i>c</i> (Å)	10.645(2)	20.666(8)
α (°)	68.42(1)	90
β (°)	76.92(2)	90
γ (°)	65.52(1)	120
V (Å ³)	883(1)	3674(2)
Z	1	3
ρ_{calc} (g cm ⁻³)	1.368(2)	1.885(1)
ρ_{exp} (g cm ⁻³) ^a	1.365(5)	1.865(5)
melting point (°C) ^b	180.0±0.5	165.5±0.5 (decomp.)

^a The density was found at T=22°C by matching the crystal density with aqueous RbI solutions; the density of the CBr₄ clathrate of HPTB corresponds to 98% guest occupancy.

^b Determined by differential scanning calorimetry.

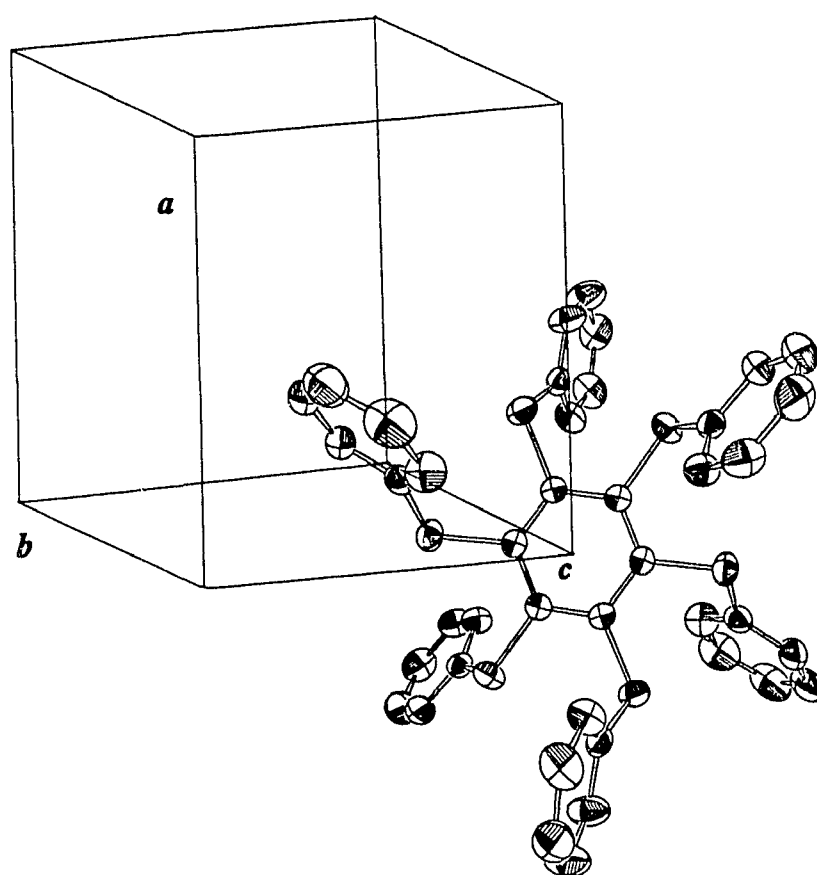
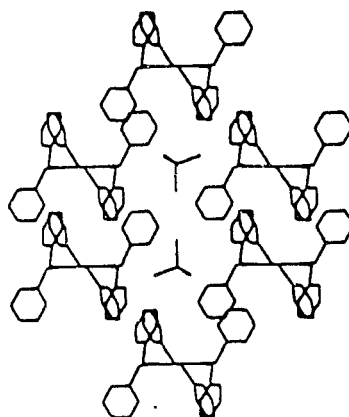
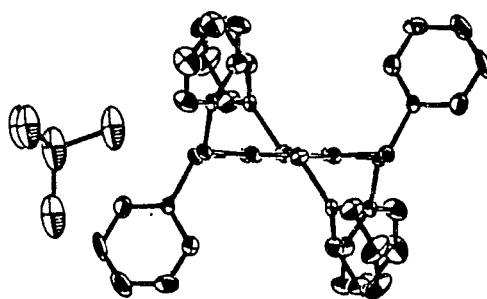


Figure 3.7 An ORTEP drawing of an HPTB molecule in pure HPTB.



(a)



(b)

Figure 3.8 (a) An illustration of the CBr_4 clathrate of HPTB showing the host-guest packing as projected onto the ac plane. For clarity, two HPTB molecules, one above and one below the cage as viewed in this direction, have been omitted.

(b) An ORTEP drawing of CBr_4 and HPTB molecules in the CBr_4 clathrate of HPTB.

are smaller than the effective sizes of the guest molecules.¹⁰⁵ The enclathrated guests are oriented such that the axial C-Br bond of the CBr₄ molecule is along the three-fold axis. The geometry of CBr₄ is tetrahedral, the mean Br-C-Br angle is 109.5(12)°. The axial C-Br distance (1.92(2) Å) is not significantly longer than the other C-Br distances (mean 1.904(1) Å). The corrected mean values for C-Br distances and Br-C-Br angles obtained after thermal motion analysis¹⁰⁶ are 1.945(14) Å and 109.5(11)° respectively.

The anisotropic thermal parameters of the nonhydrogen atoms are ordinary, with the exception of U₃₃[Br(1)] and U₁₁ and U₂₂[(Br(2))] (positional parameters and B(eq) are given in Appendix, Table A7). The large temperature factors of Br atoms are not unexpected since CBr₄ is a non-bonded guest molecule. The analysis of the thermal motion¹⁰⁶ of the CBr₄ molecule in terms of the translational, librational and screw matrices reveals a surprising degree of compliance with the rigid body model, R(U_{ij}) = 2.74%, Rw(U_{ij}) = 2.58%, rms(U_{ij}) = 0.0020 and rms[esd(U_{ij})] = 0.0014. The mean librational amplitudes about the three principle axes of libration are L₁, 3.94°; L₂, 9.40°; and L₃, 9.40°. The translation motion is essentially isotropic, with a mean principal displacement of ~ 0.24 Å. However, significant screw motion along the S₂ and S₃ directions is also apparent in the screw tensor:

$$\begin{array}{ccc} -0.50 & 0.00 & 0.00 \\ 0.00 & 0.25 & 0.00 \\ 0.00 & 0.00 & 0.25 \end{array} .$$

The intermolecular Br...Br distance of 3.310(7) Å is shorter than the shortest

intermolecular distance between Br atoms found in the structure of pure CBr_4 (3.78(2) Å in phase II)¹⁰⁷ but is comparable to that observed in the CBr_4 clathrate of the seleno analogue of HPTB, hexakisphenylselenobenzene.¹⁰⁸ The same type of shortening for the Cl...Cl contact with respect to the phase II of pure CCl_4 ¹⁰⁹ was also observed in the case of the previously reported structure of the CCl_4 clathrate of HPTB.⁸⁹ The origin of this effect is unclear although might be an artefact caused by thermal motion.

A crystallographic axis passes through the centre of the central phenyl ring. The sulphur atom is displaced by 0.064 and 0.137 Å from the centres of the phenyl substituent and central phenyl rings, respectively. Yet both the central and the side chain phenyl rings are considered to be satisfactorily planar. The bond lengths and angles are comparable with those of HPTB and its CCl_4 clathrate.

BRILLOUIN SCATTERING EXPERIMENT¹¹⁰

4.1 INTRODUCTION

The motion of particles in a crystal is described by the displacement, $u(\underline{r}, t)$, where \underline{r} denotes a position vector and t is time. Phenomenological treatment of lattice dynamics associates the restoring force, \underline{f} , of the vibrating particles with the displacement, $u(\underline{r}, t)$. These can be related to the thermodynamics of a solid and/or to the lattice elasticity, if $u(\underline{r}, t)$ and \underline{f} are replaced by the corresponding second-rank tensors of strain, $\underline{\epsilon}$ (ϵ_{ij}) and stress, $\underline{\sigma}$ (σ_{ij}). It is also convenient to change the volume dependence of relevant state functions to the configurational dependence. Thus the first and second laws of thermodynamics (equation (2.1)) for an anisotropic medium gives

$$dU = TdS + V \sum_{ij} \sigma_{ij} d\epsilon_{ij} \quad . \quad (4.1)$$

If stresses and strains are small and homogenous there is a linear dependence between them known as Hooke's law , *i.e.* (the Einstein summation scheme is used)¹¹¹

$$\epsilon_{ij} = s_{ijkl} \sigma_{kl} \quad (\sigma_{ij} = c_{ijkl} \epsilon_{kl}) \quad (4.2)$$

where s_{ijkl} and c_{ijkl} are the components of the fourth-rank tensors of the compliance and stiffness, respectively; s_{ijkl} and c_{ijkl} are usually written using Voigt notation in the simplified form as matrices s_{ij} and c_{ij} , respectively. Since the strain and stress tensors are symmetrical (*i.e.* $\epsilon_{ij} = \epsilon_{ji}$, $\sigma_{ij} = \sigma_{ji}$) the number of independent components of s_{ijkl} and c_{ijkl} is reduced from 81 to 36. On the other hand the adiabatic stiffness tensor can be expressed as strain derivatives of the internal energy ($c_{ijkl} = V^{-1} (\partial^2 U / \partial \epsilon_{ij} \partial \epsilon_{kl})$)⁵⁹ and the number of independent components is subsequently reduced to 21. Thus the tensors have the Voigt symmetry, *i.e.* $c_{ijkl} = c_{jikl} = c_{klij} = \dots$. The symmetry elements of the particular crystallographic system further decrease the number of independent components..

In the lattice dynamics description (Section 2.1) it was tacitly assumed that forces acting between particles are central and this is, in general, the case for organic molecular crystals. Such an assumption introduces additional symmetry to the tensor components known as the Cauchy relations.⁹¹ Then, if they hold, the number of independent elastic constants is reduced (in the general case) from 21 to 15. The deviation of elastic constants from the Cauchy relations indicates that angle-dependent forces act in the crystal.

The form of the elastic constant matrix depends also on the choice of the Cartesian reference coordinates with respect to the crystallographic axes. For all trigonal systems orthogonal coordinates can be chosen in such a way that the matrix has the same topology with six non-zero components. Yet, the usual choice for the RII system (R3 and $\bar{R}3$) follows "Standards on Piezoelectric Crystals" with $x \parallel a$ and

z || c.¹¹¹ This is shown in Figure 4.1. In this case the elastic stiffness constant matrix is

$$\begin{pmatrix} c_{11} & c_{12} & c_{13} & c_{14} & -c_{25} & 0 \\ & c_{11} & c_{13} & -c_{14} & c_{25} & 0 \\ & & c_{33} & 0 & 0 & 0 \\ & & & c_{44} & 0 & c_{25} \\ & & & & c_{44} & c_{14} \\ & & & & & (c_{11} - c_{11})/2 \end{pmatrix}$$

For the RII system, the inverse of c_{ij} , *i.e.* the elastic compliance constant matrix, s_{ij} , which is directly related to thermodynamical variables, has the form

$$\begin{pmatrix} s_{11} & s_{12} & s_{13} & s_{14} & -s_{25} & 0 \\ & s_{11} & s_{13} & -s_{14} & s_{25} & 0 \\ & & s_{33} & 0 & 0 & 0 \\ & & & s_{44} & 0 & 2s_{25} \\ & & & & s_{44} & 2s_{14} \\ & & & & & 2(s_{11} - s_{12}) \end{pmatrix}$$

The equation of motion of the anisotropic medium is given by¹¹²

$$\rho \frac{\partial^2 u_i}{\partial t^2} = \sum_{jkl} c_{ijkl} \frac{\partial^2 u_l}{\partial r_j \partial r_k} \quad (4.3)$$

which for the Debye crystal with $u(\underline{r}, t)$ as plane-waves can be rewritten as

$$(c_{ijkl} q_j q_k - \rho v_g^2 \delta_{il}) \Pi_l = 0 \quad (4.4)$$

where q_n are the direction cosines of wave propagation with respect to the coordinate system in which the elastic constant tensor is defined and Π_l is the polarization vector

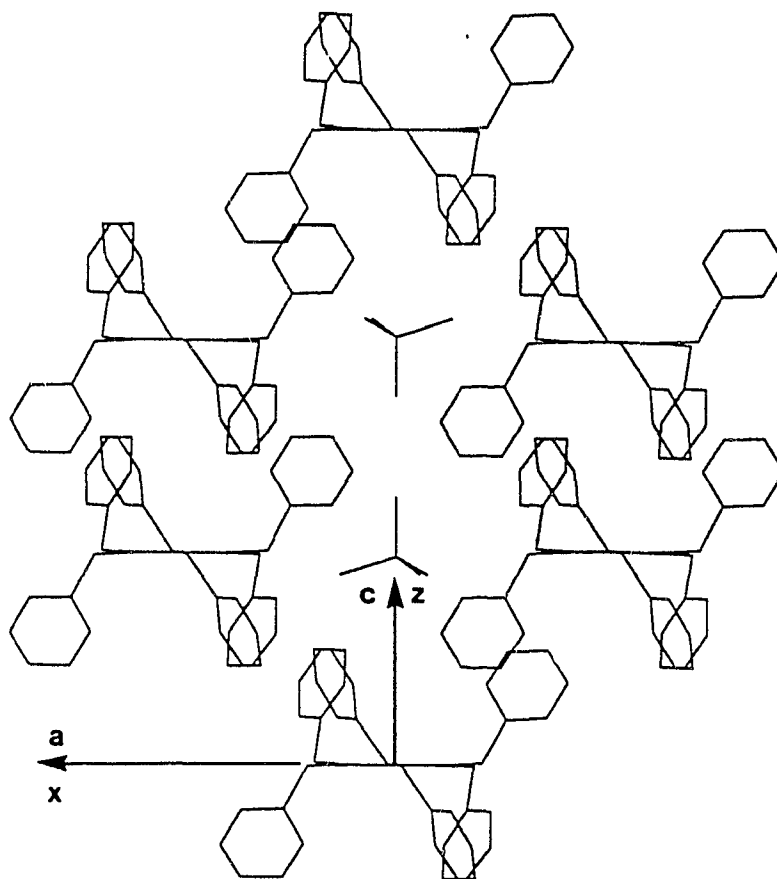


Figure 4.1 The Cartesian coordinate system in which the tensor is written with respect to the hexagonal axes of the crystallographic system (RII, *i.e.* $R3$ and $\bar{R}3$). This figure is equivalent to Figure 3.6; the projection is onto the xz -plane.

of the sound wave. The real symmetric matrix $D_{ij}(q) = c_{ijkl}q_jq_l$ is the dynamical matrix of the lattice motion and in the case of the RII system has the form (written in Voigt notation):

$$D_{11} = c_{11}(q_1^2 + \frac{1}{2}q_2^2) - \frac{1}{2}c_{12}q_2^2 + c_{44}q_3^2 + 2(c_{14}q_2q_3 - c_{25}q_1q_3) \quad , \quad (4.5)$$

$$D_{12} = \frac{1}{2}c_{11}q_1q_2 + \frac{1}{2}c_{12}q_1q_2 + 2c_{14}q_1q_3 + 2c_{25}q_1q_3 \quad , \quad (4.6)$$

$$D_{13} = c_{25}(q_2^2 - q_1^2) + c_{13}q_1q_3 + 2c_{14}q_1q_2 + c_{44}q_1q_3 \quad , \quad (4.7)$$

$$D_{22} = c_{11}(\frac{1}{2}q_1^2 + q_2^2) - \frac{1}{2}c_{12}q_1^2 - 2c_{14}q_2q_3 + 2c_{25}q_1q_3 + c_{44}q_3^2 \quad , \quad (4.8)$$

$$D_{23} = c_{13}q_2q_3 + c_{14}(q_1^2 - q_2^2) + 2c_{25}q_1q_2 + c_{44}q_2q_3 \quad , \quad (4.9)$$

$$D_{33} = c_{33}q_3^2 + c_{44}(q_1^2q_2^2) \quad . \quad (4.10)$$

For non-trivial solutions of equation (4.4) it is required that the Christoffel determinant vanishes, *i.e.*

$$\|D_{ij} - \rho v_g^2 \delta_{ij}\| = 0 \quad . \quad (4.11)$$

Thus for high symmetry systems knowledge of the stiffness, *i.e.* ρv_g^2 in special directions, allows for easy determination of the elastic constants.

4.2 RÉSUMÉ OF THE EXPERIMENTAL METHOD

Brillouin scattering provides a noncontactual probe for viscoelastic properties and it has proven to be a serviceable tool in the examination of many types of materials.^{112,113,114} In this technique the scattering of light is explained by fluctuations in the optical dielectric constant of the medium; in crystals this is caused by the thermally excited sound waves or equivalently this process can be explained as Bragg diffraction from the moving grating formed by the acoustically vibrating periodic lattice. Thus for a crystal the spectrum consists of three sets of doublets, Doppler shifted symmetrically with respect to the incident frequency. In the language of corpuscular theory Brillouin scattering is the inelastic scattering of photons from acoustic phonons. This is shown schematically in Figure 4.2. The conservation of energy and quasimomentum is equivalent to the selection rule for one phonon scattering:

$$\omega_i = \omega_s \pm \omega_p \quad (4.12)$$

$$\underline{k}_i = \underline{k}_s \pm \underline{k}_p \quad (4.13)$$

where ω and \underline{k} with subscripts i , s and p refer to the incident light, scattered light and to the phonon respectively. The phonon emission (Stokes process) and absorption (anti-Stokes process) are denoted by $+$ and $-$, respectively. The frequency shifts measured in the experiment are directly related to the phonon velocities by the

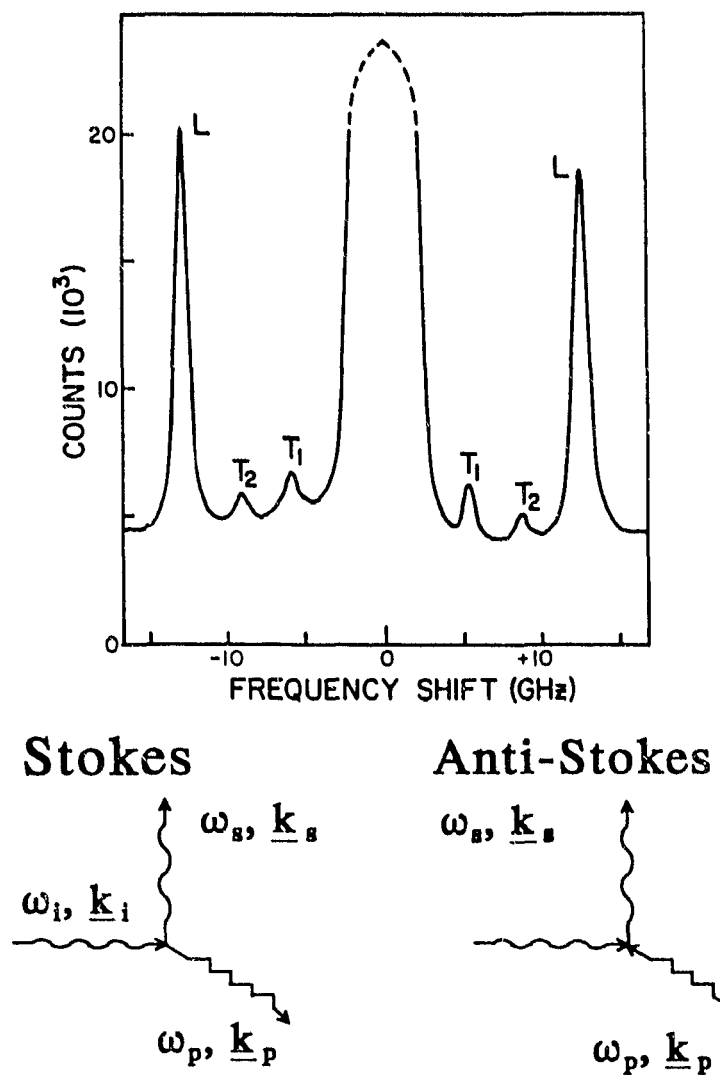


Figure 4.2 Representative 2-h Brillouin spectrum of $[0.470, 0.882, -039]$ phonons in the CBr_4 clathrate of HPTB. Number of counts for the central peak is of the order 10^7 . There are three doublets denoted by L, T_1 and T_2 corresponding to quasi-longitudinal, slow and fast quasi-transverse phonons. The peaks on the left correspond to Stokes processes and the peaks on the right correspond to anti-Stokes processes.

Brillouin equation

$$v_{\mu} = (\Delta v / v_0) c (n_i^2 + n_s^2 - 2n_i n_s \cos\theta)^{-1/2} \quad (4.14)$$

where v_{μ} is the phonon velocity of the μ th mode, c is the velocity of light in a vacuum, ν_0 is the frequency of light, $\Delta\nu$ is the Brillouin shift, n_i and n_s are the refractive indices of the incident and scattered light respectively and θ is the scattering angle.

Elastic constants can be determined from solution of the secular equation (equation. (4.11)), although this is not trivial for low-symmetry systems. In general these equations are highly nonlinear due to coupling through products of elastic constants. One can use particular directions in the crystal for which these equations can be factored to give components of the c_{ij} matrix or for which they can be simplified to the degree that particular c_{ij} values can be found. Yet, subsequent determination of the elastic constants gives rise to the propagation and accumulation of the errors associated with the sound velocities. Another disadvantage is that the phonon velocities can lead to ambiguous results due to the existence of quadratic and/or cubic equations, and then the elastic constant determination relies on an educated guess rather than on the experimental findings. This method is also limited because there are only a few experimentally accessible directions with purely longitudinal and transverse phonons. Their number decreases dramatically as the space group symmetry is lowered. The low-symmetry RII trigonal system has only a

single direction, along the c -axis, which allows direct calculation of the components, c_{33} and c_{44} , of the elastic stiffness constant matrix.¹¹²

These difficulties can be circumvented through a least-squares minimization of the compliance tensor (equation (4.11)) using its reasonable initial approximation (although it is not necessary since the program used allows for the thorough examination of the behaviour of an investigated function; *vide infra*). The only inconvenience of this approach is that it requires the measurement of a rather large number of phonon velocities. In principle the special directions should be measured first and then quasimodes should be investigated (*vide infra*). Ideally this can be achieved either by having a spherical sample or a sample immersed in liquid with identical refractive index but this is very difficult to realize in practice. In this case the only viable method to access different directions was to cut the crystal.

This procedure does not depend on the special directions and thus eliminates the need to use purely longitudinal or purely transverse phonons. In general, modes of any arbitrary directions may be utilized. They are referred to as quasi-longitudinal and quasi-transverse. This is the only tractable method for this crystallographic system.

The computer program used in this optimization,¹¹⁵ based on the MINUIT package (a system for function minimization and analysis of the parameter errors and correlations),^{116,117} started from an arbitrary set of elastic constants and fit all elements of the elastic constant tensor to experimental mode stiffnesses, ρv_{exp}^2 , where v_{exp} is the experimental acoustic velocity. With every iteration an error vector is computed and

its square

$$\sum_i \sigma_i^{-2} |\rho v_{\text{exp},i}^2 - \rho v_{\text{cal},i}^2|^2, \quad (4.16)$$

where σ_i is the standard deviation error of the experimental value, was minimized by systematically varying the elastic constants until the fit was optimized.

4.3 EXPERIMENTAL PROCEDURE

Brillouin scattering measurements were carried out at room temperature on the CBr_4 clathrate of HPTB, in the laboratory of Prof. Harry Kiefte in the Physics Department of Memorial University, Newfoundland. Identification of the crystal faces was achieved by goniometry and morphological examination and was confirmed by X-ray diffraction. The c -axis (of the hexagonal system) was identified with the slightly longer body diagonal of the crystal samples. The facets of the samples were $\{10\bar{1}1\}$. Measurements were made on four different samples, of average dimension $(4\text{mm})^3$. They were cut using a wire saw manufactured by South Bay Technology Inc. with a wire blade (diameter 0.025 mm), and the crystal polished using silicon carbide grains of grade 600, 1000 and 1400. This was done to comply with the condition of 90° scattering.

Refractive indices of the CBr_4 clathrate of HPTB at room temperature were determined by comparison with standard liquids (Cargille Laboratories) of known refractive indices. They were found to be $n_x=n_y=1.803 \pm 0.003$ and $n_z=1.803 \pm 0.003$.

A schematic diagram of the experimental Brillouin scattering setup is shown in Figure 4.3. Incident radiation of wavelength $\lambda=514.5$ nm was provided by a single-mode argon laser (Spectra Physics 2020-03) and filtered by neutral density filters to a power of about 40 mW. The free spectral range utilized in the experiments was 35.57 GHz, determined by employing a standard block of fused quartz with known Brillouin shifts. The scattered light was collected at 90° . It was analysed by a

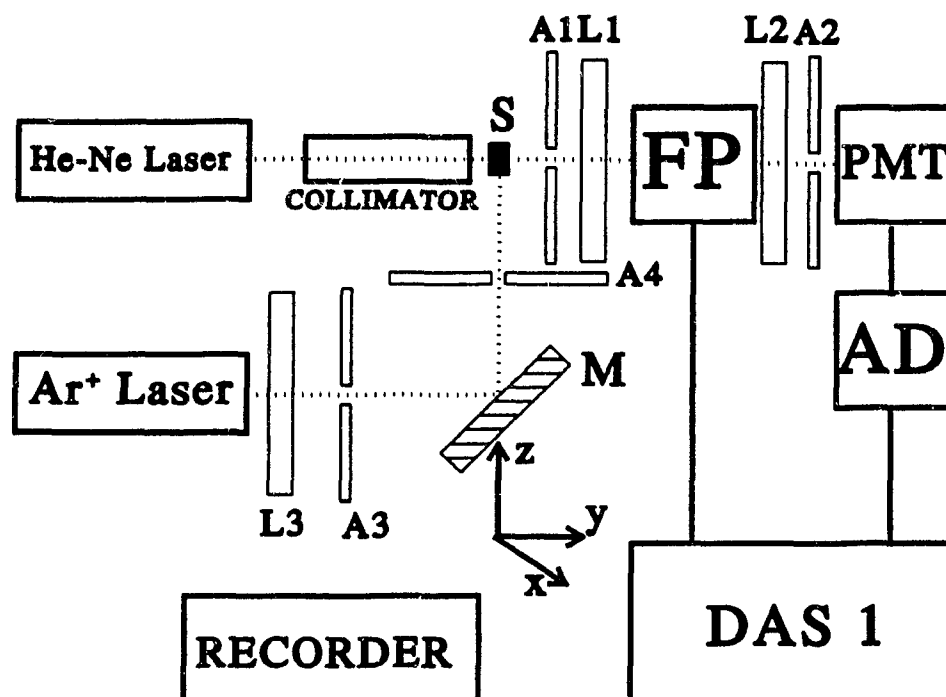


Figure 4.3 A schematic diagram of the experimental setup for the Brillouin scattering experiment. The following abbreviations denote: S is the sample, A1-A4 are the apertures, L1-L3 are the lenses, FP is the triple-pass Fabry-Perrot interferometer, PMT is the cooled photomultiplier tube, AD is the amplifier-discriminator and DAS 1 is the data acquisition and stabilization system. The He-Ne laser was used to set a proper geometry for the experiment.

commercial triple-pass piezoelectrically scanned Fabry-Perot interferometer Burleigh RC 110 followed by a cooled photomultiplier connected to the multichannel analyzer of the data acquisition and stabilization system Burleigh DAS 1 that automatically corrected for frequency and any other drifts in the system. For these experiments the error in the determination of the frequency shifts was about 1%. Alphanumeric readout on the DAS 1 allowed for convenient and accurate determination of the spectra and shifts. The setup is described in detail elsewhere.¹¹⁸

4.4 RESULTS AND DISCUSSION

4.4.1 EXPERIMENTAL FINDINGS

The shifts were measured in seven directions giving 16 velocities. A representative Brillouin scattering spectrum is shown in Figure 4.2. The results of the fitting procedure for the components of the elastic and stiffness matrices are presented in Table 4.1. Velocities calculated from these values of the c_{ij} matrix were compared with the experimental ones, giving an average error of 4.1% for the slow quasi-transverse modes, 3.0% for the fast quasi-transverse modes and 3.3% for the quasi-longitudinal modes.

In order for an elastic stiffness matrix to be physically meaningful in terms of crystal stability, certain conditions for the components must be fulfilled. For this crystallographic system these conditions, *i.e.*

$$(c_{11}+c_{12})c_{33}>2c_{13}^2 \quad , \quad (4.17)$$

$$(c_{11}-c_{12})c_{44}>2(c_{14}^2+c_{15}^2) \quad , \quad (4.18)$$

$$c_{33} \quad , \quad c_{44}>0 \quad , \quad (4.19)$$

were met.

During the optimization procedure the error in the function value was calculated. This indicated how much an elastic constant value could vary before it caused a 1% change in the function. It was expressed to resemble the standard deviation. From this the relative uncertainties in the elastic constants were estimated

Table 4.1 The seven independent components of the stiffness (c_{ij}) and compliance (s_{ij}) matrices for the CBr_4 clathrate of HPTB; c_{ij} and s_{ij} in units of 10^{10} N m^{-2} and 10^{-10} $\text{m}^2 \text{N}^{-1}$, respectively.

ij	11	12	13	14	25	33	44
c_{ij}	$1.20 \pm$	$0.11 \pm$	$0.39 \pm$	$0.14 \pm$	$0.21 \pm$	$1.69 \pm$	$0.29 \pm$
	0.03	0.04	0.02	0.02	0.02	0.03	0.02
s_{ij}	1.24	-0.36	-0.20	-0.79	-1.16	0.69	5.88

to be less than $0.04 \times 10^{10} \text{ N m}^{-2}$ (details in Table 4.1). The major source of error is the quality of samples, rather typical for these types of crystals. The optical clarity was relatively poor and there were cracks which might have been introduced by cutting and polishing during the preparation of these small crystals. The surface and any bulk defects can affect the Brillouin lines and increase the intensity of the central component. (On the other hand, in some cases small crystals have an advantage over big crystals in that they have lower concentrations of innate imperfections.) In addition to errors due to defects, there is uncertainty (few degrees) in the crystal orientation associated with cutting and polishing, and from alignment in the experimental setup. In view of all sources of error the fit is quite good.

The elastic anisotropy of the CBr_4 clathrate of HPTB can be assessed from ratios that stem from conditions for the appropriate components of the c_{ij} matrix for an isotropic material. For an elastically isotropic RII system $c_{11} = c_{33}$, $c_{12} = c_{13}$, $2c_{44} = (c_{11} - c_{12})$ and $c_{14} = c_{15} = 0$. For HPTB- CBr_4 , $c_{14} = 0.14 \times 10^{10} \text{ N m}^{-2}$ and $c_{15} = -0.21 \times 10^{10} \text{ N m}^{-2}$ and the anisotropic factors, c_{11}/c_{33} , c_{12}/c_{13} , $2c_{44}/(c_{11} - c_{12})$, were found to be 0.71, 0.28, 0.53, respectively. HPTB- CBr_4 is elastically more anisotropic than the ethanol clathrate of Dianin's compound¹¹⁹ (also RII system, $\bar{R}\bar{3}$ structure) for which $c_{15} = 0$, $c_{14} = 0.03 \times 10^{10} \text{ N m}^{-2}$ and the respective anisotropic factors were 1.02, 0.49, 0.86. This is seen further in Figure 4.4.

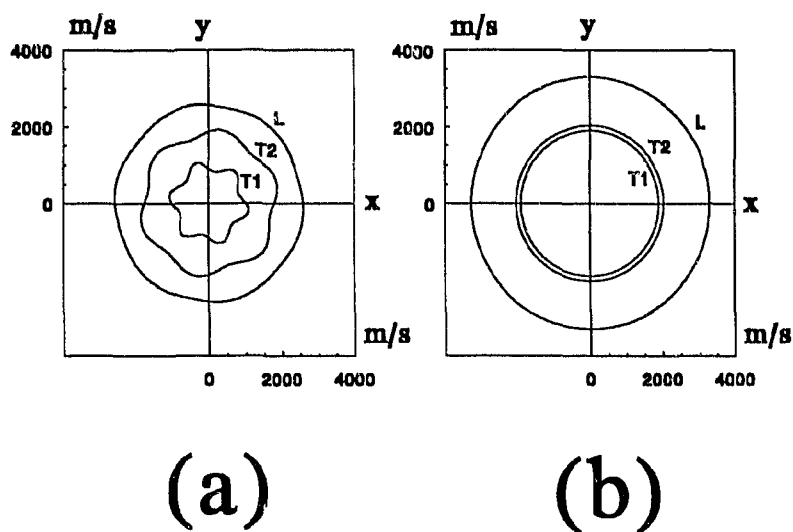


Figure 4.4 Sound velocities in the xy -plane for (a) the CBr_4 clathrate of HPTB and (b) the ethanol clathrate of Dianin's compound. T1, T2 and L represent the slow quasi-transverse, the fast quasi-transverse and quasi-longitudinal modes. The anisotropy of the sound velocities in HPTB- CBr_4 , although not large, gives a view of the rotation of the six-fold symmetry of the velocity contour away from the Cartesian x, y axes.

4.4.2 DERIVED PARAMETERS AND OTHER SYSTEMS

The $\bar{R}3$ system can be described as a link between the hexagonal classes and those of trigonal symmetry. It may be characterized by hexagonal axes of alternating symmetry, or by a three-fold axis with inversion. It appears that the only $\bar{R}3$ trigonal systems for which the full elastic constant tensors have been determined are the ethanol clathrate of Dianin's compound¹¹⁹ and now HPTB-CBr₄. The elasticity of the former was successfully approximated by hexagonal symmetry. In contrast, the anisotropy of the elasticity of the CBr₄ clathrate of HPTB differs considerably from that represented by systems with purely hexagonal symmetry. Given that the ethanol adduct of Dianin's compound is elastically hexagonal, HPTB-CBr₄ appears to be one of the lowest symmetry solids for which elastic information has been obtained.

It is instructive to compare some parameters derived from the elastic constants as they very often have more direct physical significance than the tensor itself.

The adiabatic bulk modulus, B_s , *i.e.* the ratio of applied hydrostatic pressure to resultant fractional change in volume, which can be expressed as

$$B_s = \left[\sum_{ij} s_{ijj} \right]^{-1} \quad , \quad (4.20)$$

is $6.1 \times 10^9 \text{ N m}^{-2}$ for the CBr₄ clathrate of HPTB. This is not greatly different from that of other clathrates, *e.g.* the ethanol clathrate of Dianin's compound¹¹⁹ ($B_s = 7.8 \times 10^9 \text{ N m}^{-2}$), tetrahydrofuran clathrate hydrate¹²⁰ ($B_s = 8.5 \times 10^9 \text{ N m}^{-2}$) although smaller than the dioctanoyl peroxide clathrate of urea¹²¹ ($B_s = 12.2 \times 10^9 \text{ N m}^{-2}$).

HPTB-CBr₄ is similar to molecular crystals such as stilbene¹⁰ ($B_s=6.4\times 10^9$ N m⁻²) and naphthalene¹⁰ ($B_s=5.3\times 10^9$ N m⁻²). The values of B_s for these inclusion compounds show them to be less compressible than some orientationally disordered molecular solids. For example, their values of B_s are about twice that of solid CCl₄ in its orientationally disordered rhombohedral Ib phase¹²² ($B_s=3.35\times 10^9$ N m⁻²) and in its metastable disordered cubic Ia phase¹²³ ($B_s=3.30\times 10^9$ N m⁻²), and also about twice that of the disordered fcc structure of CBr₄¹²⁴ ($B_s=3.65\times 10^9$ N m⁻²). However, high compressibility is not exclusively associated with disorder; it can also be due to other packing and interaction considerations as in crystals of rather flat molecules, *e.g.* anthracene¹²⁵ ($B_s=3.84\times 10^9$ N m⁻²), toluene¹⁰ ($B_s=3.89\times 10^9$ N m⁻²) and biphenyl¹⁰ ($B_s=4.46\times 10^9$ N m⁻²).

Experimental studies of clathrate hydrates with different guest species show that the guest-host force constant stiffens as the mass or size of the guest increases.¹²⁰ In consideration of results from molecular dynamics simulations, this can be ascribed to a coupling of the motion of the guest molecules with that of the host lattice.¹²⁶ The coupling of the dynamical disorder of the guest molecules with low-frequency vibrations of the host lattice is thought to be responsible for the unusually low thermal conductivity of some inclusion compounds.^{82,86} As a result, the temperature profile of their thermal conductivity is more glass-like than that usually associated with crystalline matter. On the basis that the ethanol clathrate of Dianin's compound and tetrahydrofuran clathrate hydrate have both similar thermal conductivities and similar compressibilities, it would not be unexpected to observe in HPTB-CBr₄, with its

similar B_3 and similar topology, a qualitatively similar thermal conductivity profile.

This is discussed in detail in Chapter 7.

Another physical property, the linear compressibility, β , is the fractional change in length per unit of applied hydrostatic pressure. It varies with direction and in the hexagonal and trigonal systems depends on an angle, α , between the direction and the c -axis. Thus for axial systems it is expressed as¹¹¹

$$\beta = \beta_I + \beta_{II} \cos^2 \alpha \quad (4.20)$$

where $\beta_I = s_{11} + s_{12} + s_{13}$ and $\beta_{II} = s_{13} + s_{33} - s_{11} - s_{12}$. For the CBr_4 clathrate of HPTB, $\beta_I = 0.68 \times 10^{-10} \text{ m}^2 \text{ N}^{-1}$ and $\beta_{II} = -0.39 \times 10^{-10} \text{ m}^2 \text{ N}^{-1}$. For the ethanol clathrate of Dianin's compound these compressibilities are $0.49 \times 10^{-10} \text{ m}^2 \text{ N}^{-1}$ and $-0.22 \times 10^{-10} \text{ m}^2 \text{ N}^{-1}$, respectively.¹¹⁹ The deviation of the $(|\beta_I| + |\beta_{II}|) / |\beta_I|$ ratio from unity is a measure of anisotropy, and these values show again HPTB- CBr_4 (ratio = 1.57) to be more anisotropic than the ethanol clathrate of Dianin's compound (ratio = 1.45).¹¹⁹ Nevertheless, both crystals present highly anisotropic linear compressibilities and in both cases the c/a ratio strongly depends on hydrostatic pressure.

The elastic constants of HPTB- CBr_4 (as the ethanol-Dianin clathrate,¹¹⁹ the dioctanoyl peroxide clathrate of urea¹²¹ and urea¹²⁷) are almost an order of magnitude larger than these of the very soft hexagonal crystals of $\beta\text{-N}_2$ and $\beta\text{-CO}$,¹¹⁸ much smaller (by a factor of 10 to 50) than harder crystals such as Al_2O_3 ,¹²⁸ but, in fact, very similar to those of ice Ih.¹²⁹ The exception in the latter case is c_{12} which is larger by a factor of 7 in ice Ih (and by 3 in the ethanol clathrate of Dianin's

compound¹¹⁹). The elastic constant c_{12} appears to be low in the present system, HPTB-CBr₄ (*vide infra*).

Although the Cauchy conditions are not fulfilled even for ideal systems because of the contribution of the temperature-dependence of the phonons, deviations of Cauchy ratios from unity clearly indicate the character of the potential in a crystal, *i.e.* the presence of angular forces between atoms and/or torsional interactions between molecules that contribute to the crystal potential. The geometry of CBr₄-HPTB reduces the six general Cauchy ratios to only two, *i.e.*, c_{13}/c_{44} and c_{12}/c_{66} ($c_{66}=(c_{11}-c_{12})/2$). These ratios are 1.34 and 0.20 respectively for HPTB-CBr₄ and 1.48 and 0.63 respectively for the ethanol clathrate of Dianin's compound.¹¹⁹ The Cauchy ratios for the dioctanoyl peroxide clathrate of urea are 2.26 and 6.32 respectively.¹²¹ The low values of c_{12} for the ethanol clathrate of Dianin's compound and especially for HPTB-CBr₄ are responsible for the significant deviation of the second Cauchy ratio from unity. The c_{12} value is also very low in the case of urea¹²⁷ ($c_{12}=-0.05 \times 10^{10}$ N m⁻²). This molecular compound crystallizes in a tetragonal system with an elastic constant matrix topology similar to the hexagonal system. Such a low value of c_{12} was obtained for the adiabatic constant. The isothermal elastic constant is 0.89×10^{10} N m⁻².¹²⁷ Cauchy c_{13}/c_{44} ratios exceeding unity have been associated with rotational-translational coupling in N₂, CO and Ar-O₂ mixtures,^{118,130} low values of c_{44} are characteristic of soft transverse modes that are susceptible to rotational-translational coupling. Such a coupling between the guest and the host lattice of this system is a manifestation of anharmonic behaviour that could significantly affect

properties which are sensitive to the higher (than quadratic) order terms in the expansion of the crystal's potential energy in the Taylor series.

THERMAL EXPANSION AND RELATED PROPERTIES

5.1 INTRODUCTION

Harmonic theory of crystal lattice dynamics determines vibrational frequencies and thus it can be used to explain the properties which depend mainly on these frequencies. Yet there are some properties which exist exclusively due to anharmonicity of the lattice, *e.g.* the difference between isochoric and isobaric heat capacity or elastic constants; the temperature dependence of the latter; the behaviour of heat capacity at high temperatures; melting; thermal conductivity; thermal expansion.⁹³

For crystals with a monatomic motif, the simplified view of thermal expansion is that with rising temperature the average displacement of a vibrating atom increases and depends monotonically on the temperature; an even simpler explanation is that the amplitudes of the vibration increase causing the crystal to expand.⁹³ Although this can hold for simple solids like close-packed crystals of rare gases⁵⁸ thermal expansivity is a much more complicated phenomenon for other materials,^{131,132} *e.g.* it does not explain the negative thermal expansion in certain directions for some crystals (*e.g.* Cd or Zn). The situation in molecular solids is more complicated still because of two domains of forces acting in the crystal, *e.g.* the molecules might change their relative orientations or the temperature increase could activate the motion of certain

molecular moieties which might have a noticeable effect on thermal expansivity.

Thermodynamically thermal expansion can be viewed as a volumetric response of the solid to minimize Gibbs energy, which is a function of the temperature. The equation of state (given in the universal form by equation (2.2)) in the quasi-harmonic approximation (*vide supra*) is⁹⁴

$$P(V_0) = -\frac{\Delta V}{\beta} + \sum_{ki} \gamma_{ki} \hat{e}_{ki} \quad (5.1)$$

where \hat{e}_{ki} is the mean energy of phonons in the state ki and γ_{ki} defined as $\gamma_{ki} = -\partial \ln \omega_{ki} / \partial \ln V$ is the Grüneisen function of the ki mode (the so-called mode Grüneisen parameter). Since thermal expansion is the fractional volume change at zero pressure the thermal expansion coefficient can be written as

$$\alpha_V = \frac{\beta}{V} \sum_{ki} \gamma_{ki} C_{V(ki)} \quad (5.2)$$

where $C_{V(ki)}$ is the isochoric heat capacity of the ki mode. Introducing a mode-independent (or bulk) Grüneisen parameter ($\gamma = \sum_{ki} \gamma_{ki} C_{V(ki)} / \sum_{ki} C_{V(ki)}$) one can rewrite this expression in terms of experimentally determined thermal properties of the solid as

$$\alpha_V = \frac{\beta_{isothermal}}{V} \gamma C_V = \frac{\beta_{adiabatic}}{V} \gamma C_P \quad (5.3)$$

provided that the material is isotropic. Thus any unusual behaviour of thermal

expansion is due to peculiarities of the behaviour of the Grüneisen parameter, which reflects anharmonicity in the crystal lattice. On the other hand, the negative of the $\gamma\alpha_V$ factor, itself, has clear physical meaning as the mean temperature coefficient of the lattice vibration frequencies.¹³³

The anisotropic version of equation (5.3) is (the Voigt notation is used)¹³¹

$$\alpha_\lambda = \frac{C_\sigma}{V} \sum_{\mu=1}^6 s_{\lambda\mu} \gamma_\mu \quad (5.4)$$

where α_λ is the component of the thermal expansion tensor, $s_{\lambda\mu}$ is the component of the adiabatic compliance matrix and γ_μ is the Grüneisen parameter in a particular direction.

5.2 EXPERIMENTAL PROCEDURE

Thermal expansion measurements were performed by determination of the lattice parameters of powder samples of HPTB and HPTB-CBr₄ by neutron diffraction within the temperature range $25 < T < 295$ K. The samples were prepared by rapid crystallization as described in Chapter 3.

The C2 neutron powder diffractometer in the NRU reactor of AECL Research, Chalk River, Ontario was used. The instrument consists of an 800-wire detector spanning 80° in 2θ , giving a 0.1° channel interval. During the measurements the detector was stepped once so that the measured step size for the profile refinements was 0.05° . The samples were loaded into cylindrical vanadium cans (internal diameter 4 mm) and placed in an open cycle He-cryostat. The sample was photographically centred in the beam before the experiment began. The temperature stability was ± 1 K during each measurement. The experiment used the reflection from a Si531 monochromator at a take-off angle of approximately 110° . The calibration was performed using a standard Si powder. The wavelength was determined by Rietveld fitting the Si profile and found to be $1.50506(3)$ Å. The incident collimation used during the experiment was 0.4° and a cooled sapphire filter was used to reduce second-order contamination of the beam. The spectrum was fitted using the GSAS program¹³⁴ from 6° to 36° .

5.3 RESULTS AND DISCUSSION

5.3.1 EXPERIMENTAL FINDINGS

The results of the room-temperature single crystal X-ray measurement of the CBr_4 clathrate of HPTB at $T=291$ K (see Table 3.1) agree very well with the values extracted from the neutron diffraction experiment at $T=295$ K : $a=14.328\pm 0.003$ Å, $c=20.663\pm 0.006$ Å and $V=3674\pm 1$ Å³.

There is satisfactory correspondence for the values obtained for HPTB at $T=295$ K with $a=9.565\pm 0.09$ Å, $b=10.279\pm 0.007$ Å, $c=10.629\pm 0.010$ Å, $\alpha=68.46\pm 0.06^\circ$, $\beta=77.09\pm 0.09^\circ$, $\gamma=65.81\pm 0.07^\circ$ and $V=883\pm 0.6$ Å³ as determined by neutron powder diffraction, compared with values (see Table 3.1) from single crystal X-ray measurements.

Two factors might contribute to slight differences between the X-ray and neutron diffraction results. First, HPTB contains a significant number of hydrogen atoms which results in a high background in the neutron diffraction pattern. Secondly, an intrinsic feature of organic molecular crystals is weak intermolecular interactions which, with the low symmetry of the HPTB crystal and its open structure, make the structure susceptible to easy distortion by thermal and mechanical effects. For example, it is known that the structure of powdered samples of the CCl_4 clathrate of Dianin's compound is easily disturbed on grinding.⁹⁹

5.3.2 TEMPERATURE EVOLUTION OF UNIT CELL PARAMETERS

The changes in the unit cell dimensions of the CBr_4 clathrate of HPTB with

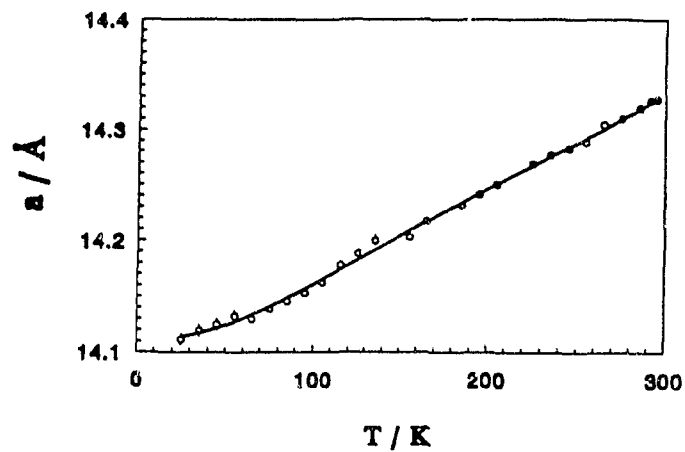
temperature are shown in Figure 5.1. The value of the a -axis decreases monotonically with decreasing temperature. For the c -axis, two regions can be distinguished; above and below *ca.* 200 K (Figure 5.2). Similar behaviour was observed in Dianin's clathrates which have the same space group.^{99,135} The stronger effect of temperature on the a -axis than the c -axis can be attributed to more accessible space in the cavity in the a -direction than in the c -direction.

Knowledge of the temperature dependence of the unit cell dimensions of HPTB-CBr₄ allows for the determination, through smooth fitting, of the values of the thermal expansion tensor as a function of temperature. Due to the symmetry of the system the tensor for HPTB-CBr₄ has only two non-zero independent components defined as $\alpha_a = (\partial \ln a / \partial T)_p$ and $\alpha_c = (\partial \ln c / \partial T)_p$, *i.e.* $\alpha_{11} = \alpha_{22} = \alpha_a$ and $\alpha_{33} = \alpha_c$ respectively (Figures 5.1 and 5.2).

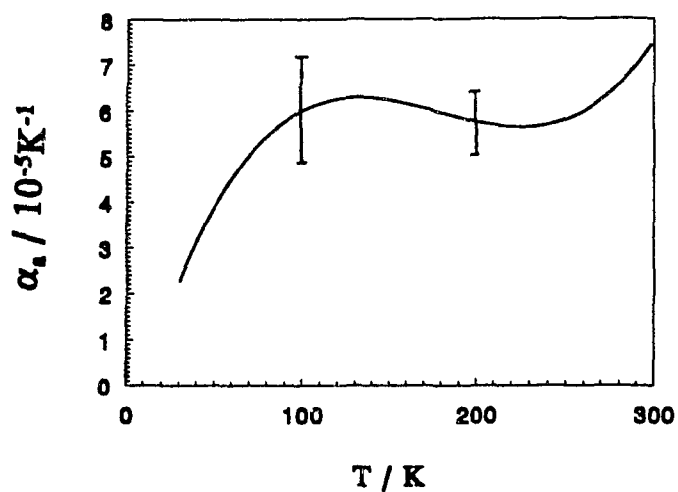
The dependence of the unit cell volume on temperature for HPTB and HPTB-CBr₄ is shown in Figures 5.3 and 5.5. The volume thermal expansivities, *i.e.* $\alpha_v = (\partial \ln V / \partial T)_p$, of both systems are similar in character with slightly higher values for pure HPTB.

In the case of pure HPTB the largest temperature-dependence in the unit cell dimension is for the b -axis. (See Figure 5.4 for unit cell dimensions and volume as functions of temperature.) The values of a and c change only very slowly with temperature. It is difficult to interpret this on the basis of the topological features of the crystal because of the very low symmetry of the structure.

Although both HPTB and HPTB-CBr₄ have anisotropic thermal expansivity



(a)

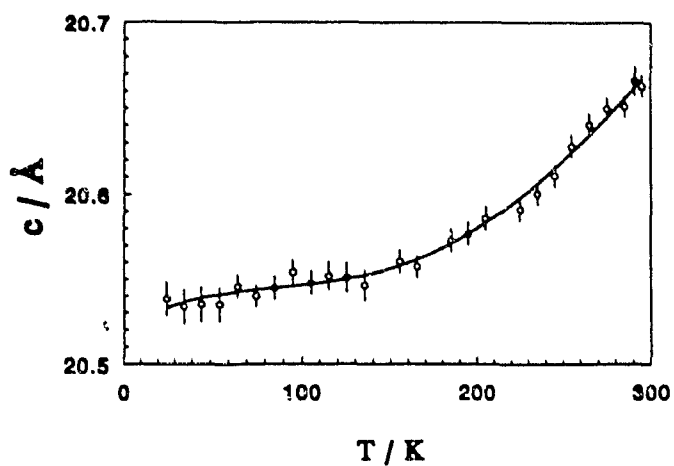


(b)

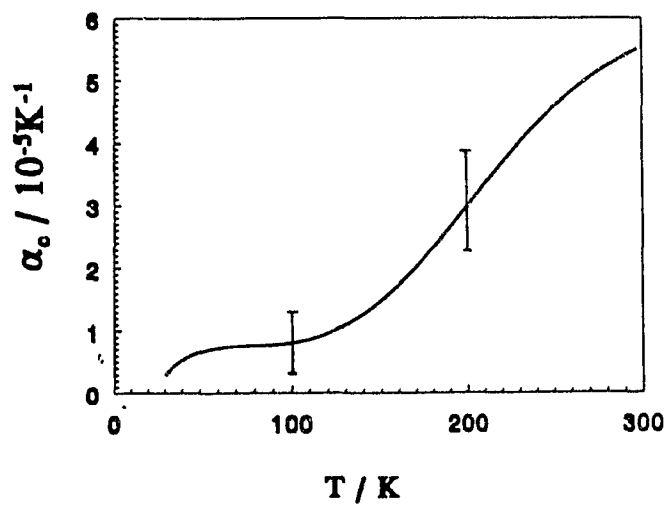
Figure 5.1 (a) HPTB-CBr₄ *a*-axis lattice parameter as a function of temperature.

○, neutron powder diffraction results (most error bars are smaller than the data circles); ●, X-ray single crystal diffraction result. The solid line is the least-square fit.

(b) The thermal expansion coefficient along this axis as a function of temperature.



(a)

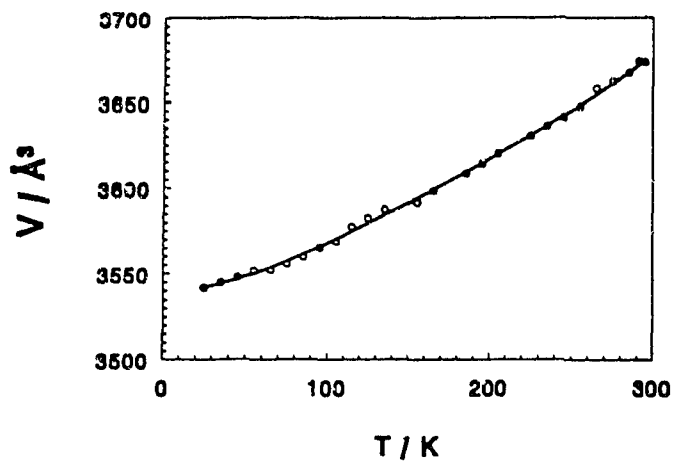


(b)

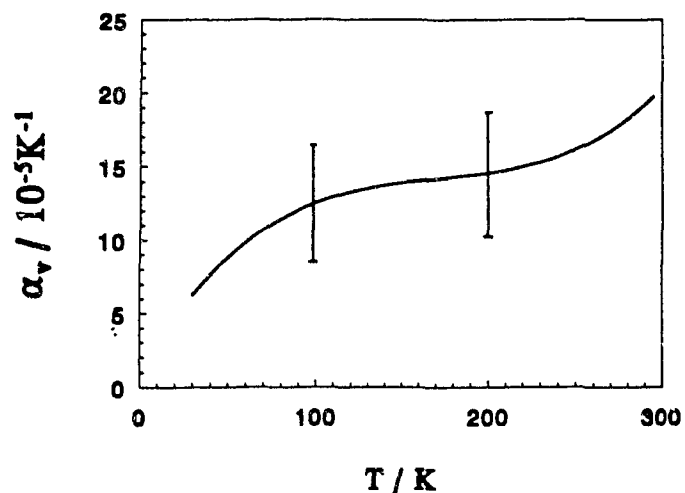
Figure 5.2 (a) HPTB-CBr₄ *c*-axis lattice parameter as a function of temperature.

○, neutron powder diffraction results; ●, X-ray single crystal diffraction result. The solid line is the least-square fit.

(b) The thermal expansion coefficient along this axis as a function of temperature.



(a)



(b)

Figure 5.3 (a) HPTB-CBr₄ unit cell volume as a function of temperature. ○, neutron powder diffraction results (error bars are smaller than the data circles); ●, X-ray single crystal diffraction result. The solid line is the least-square fit.

(b) The volume thermal expansion coefficient as a function of temperature.

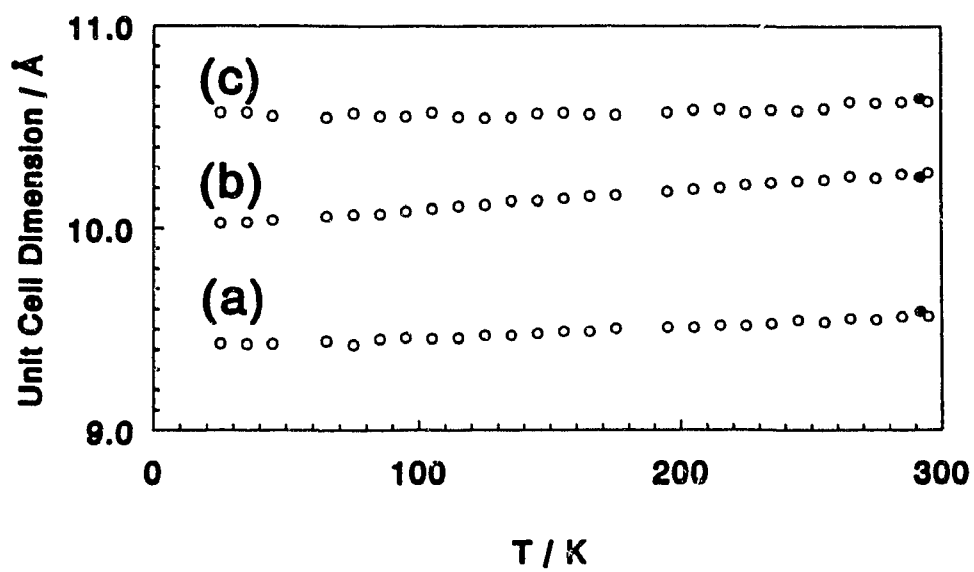
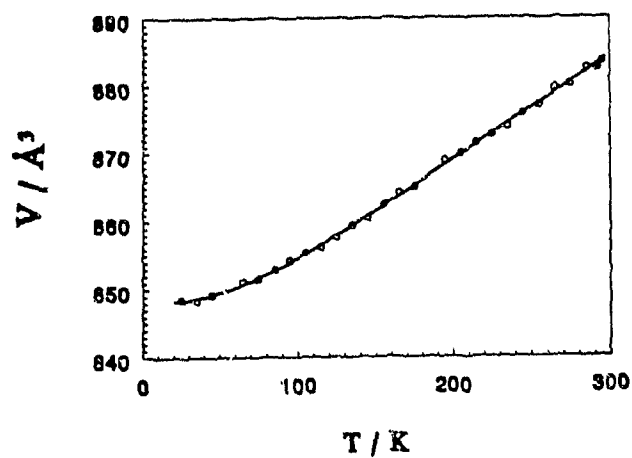
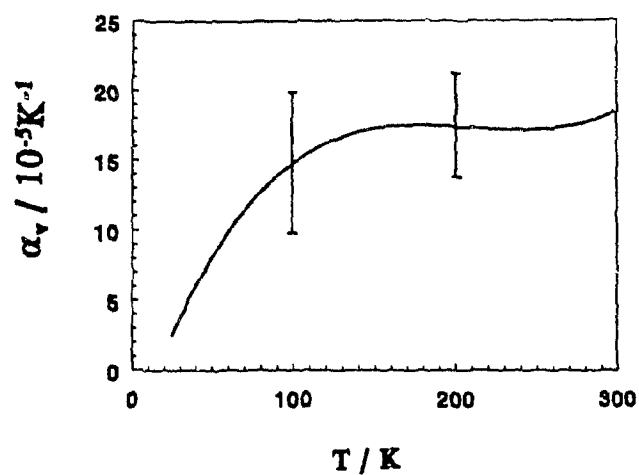


Figure 5.4 HPTB: (a) *a*-axis, (b) *b*-axis and (c) *c*-axis as a function of temperature: ○, neutron powder diffraction results, ●, X-ray single crystal result (error bars are smaller than the data circles)



(a)



(b)

Figure 5.5 (a) HPTB unit cell volume as a function of temperature. \circ , neutron powder diffraction results (error bars are smaller than the data circles); \bullet , X-ray single crystal result. The solid line is the least-square fit. (b) The volume thermal expansion coefficient as a function of temperature.

neither displays any unusual behaviour (*e.g.* negative thermal expansion).

5.3.3 OTHER INCLUSION LATTICE SYSTEMS

These findings can be compared to thermal expansivity results for clathrate hydrates^{78,79} and Dianin's system.^{99,164} Both these systems exhibit enhanced thermal expansion of the clathrate lattice with respect to the framework composed of host compound (*i.e.* ice or the clathrand of Dianin's compound). For the former a phenomenological explanation was proposed:⁷⁸ the increased thermal expansivity was attributed to the weakened interactions between the water molecules of the host lattice due to pressure exerted on the walls of cavities by the guest molecules. This internal pressure was ascribed to the kinetic motion of the guest molecules. It would seem even more reasonable (*vide infra*) to assume the same mechanism for the Dianin's systems.

The guest molecules in hydrates were treated classically and the equation of the ideal gas was applied in order to assess the internal pressure.⁷⁸ Molecular dynamics simulations seemed to corroborate this view,^{78,79} although the premises of this explanation may oversimplify the physical picture of the guest presence in the cavities as described further below.

5.3.4 THE ROLE OF THE GUEST IN THERMAL EXPANSION

In light of recent studies^{16,17} of the stability of the hydrate structures, the picture of the guest molecule trapped in cages within an *inert* framework composed of

water molecules appears to be too simple. The guest molecules seem to play an essential role in creating the clathrate hydrates through mechanical stabilization of the host lattice by attenuation of the water lattice vibrations that result in rearrangement of the *unstable* host matrix.^{16,17} It is also known that the interaction of motion of the guests with lattice modes lead to coupling of the localized vibrations of guest molecules to the acoustic modes of the host lattice.^{82,126} It was also shown that enhancement of phonon density for selective vibrational states occurs in the hydrates.¹²⁶

Guests experience motion within the molecular field of the crystal. For obvious reasons the character of this motion is less restrained than that of bonded chemical species or even molecular clusters. It can be assumed that for clathrates of a particular host compound, thermodynamical variables such as V , C_v and β are very similar at a given temperature (this is certainly true in Dianin's system⁵⁶). Since equation (5.3) relates the thermal expansion and the Grüneisen constant, if all other variables are constant then the Grüneisen parameter is directly responsible for any differences between thermal expansivities of different clathrates. On the other hand, it has been shown that the thermal expansion can be viewed as a response to the change in the dynamical internal pressure which is equivalent to the radiation pressure of the elastic waves on crystal walls.¹³⁶ Since in the clathrate hydrates and in Dianin's system the guests introduce additional motion (in comparison to the lattice of the pure host compound) the dynamical internal pressure is higher and therefore the thermal expansivity is higher.

5.3.5 VOLUME THERMAL EXPANSION OF HPTB SYSTEMS

It could be concluded that absence of an effect of guest molecules on the thermal expansivity for HPTB and HPTB-CBr₄ might stem from differences between their structures and those of the clathrate hydrates and Dianin's clathrates. All three systems conform to the aforementioned topological definition of a clathrate compound, *i.e.* a structure based on lattice lacunae. Yet a subtle, but most significant, distinction lies in the constitution of these assemblies. Dianin's clathrate and clathrate hydrates form better-defined cavities. The clathrate edifice is composed of the host molecules associated through hydrogen bonds, and the steric barriers which limit the volume of the voids are tight; this lets the guest have noticeable impact on the thermal expansion. In contrast, the HPTB clathrates are more open. Two supramolecular hexamers close the cage tightly in the Dianin's assemblies; the cavity in HPTB clathrate is created by six host molecules which correspond to a Dianin's hexamer. The guests in HPTB can be considered as space fillers that are loosely retained in the lattice. This also explains why some guests such as CCl₄ or CH₃CCl₃ are easily lost from HPTB.

5.3.6 GRÜNEISEN FUNCTION OF HPTB SYSTEMS

Attention is turned now to anharmonic properties of HPTB and the CBr₄ clathrate of HPTB since relevant values of the thermal properties are available to quantify this.

For axial systems there are only two non-zero independent anisotropic

Grüneisen parameters¹³¹

$$\gamma_1(=\gamma_2)=(V/C_\sigma)(c_{11}+c_{12})\alpha_1+c_{13}\alpha_3 \quad (5.5)$$

$$\gamma_3=(V/C_\sigma)(2c_{13}\alpha_1+c_{33}\alpha_3) \quad (5.6)$$

where c_{ij} are the adiabatic elastic constants and C_σ is the heat capacity at constant stress (*vide infra*). Since the volume thermal expansion is a combination of α_1 and α_3 (*vide supra*), employing equation (5.3), one can express the bulk Grüneisen parameter as¹³¹

$$\gamma = \frac{2\beta_1\gamma_1 + \beta_3\gamma_3}{\beta} \quad (5.7)$$

where β_1 and β_3 are the linear adiabatic compressibilities along the a - and c -axes, respectively (equation (4.20)). This allows for determination of the γ functions.

It is reasonable to assume that the value of the adiabatic compressibility of the HPTB (no experimental values are available) will be similar to that of the clathrate since the features of the composition of the molecular crystals indicate similarity of mechanical properties. By virtue of this premise the overall Grüneisen parameter was determined for pure HPTB. Plots of the bulk Grüneisen parameters for HPTB and HPTB-CBr₄ are shown in Figures 5.6 and 5.7. The anisotropic Grüneisen parameters for the CBr₄ clathrate are shown in Figure 5.8.

The arbitrariness of the choice of the HPTB compressibility does not affect the

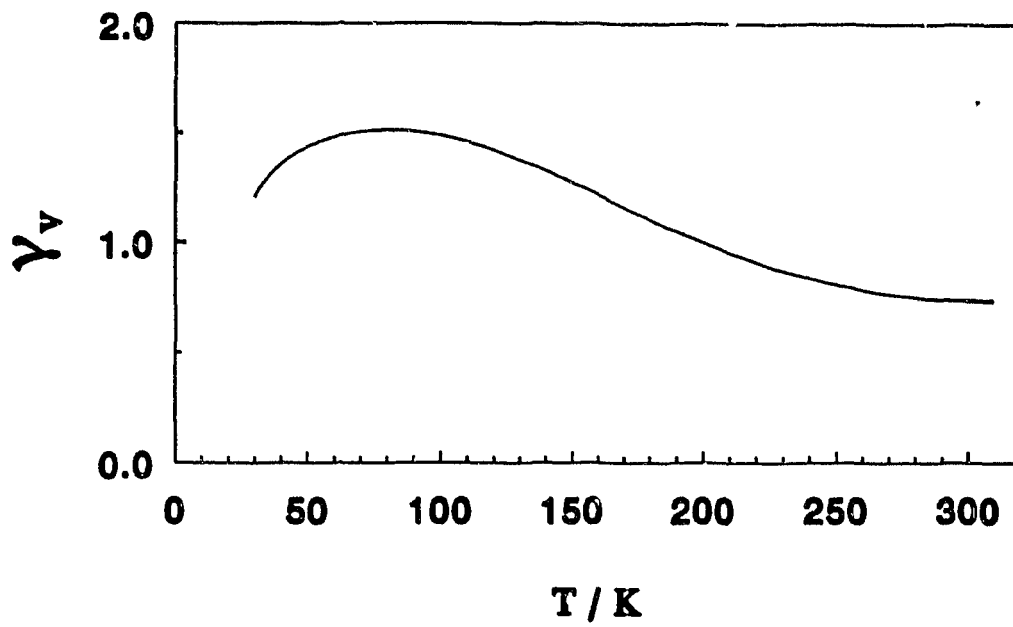


Figure 5.6 Temperature dependence of the overall Grüneisen parameter, γ_v , for pure HPTB.

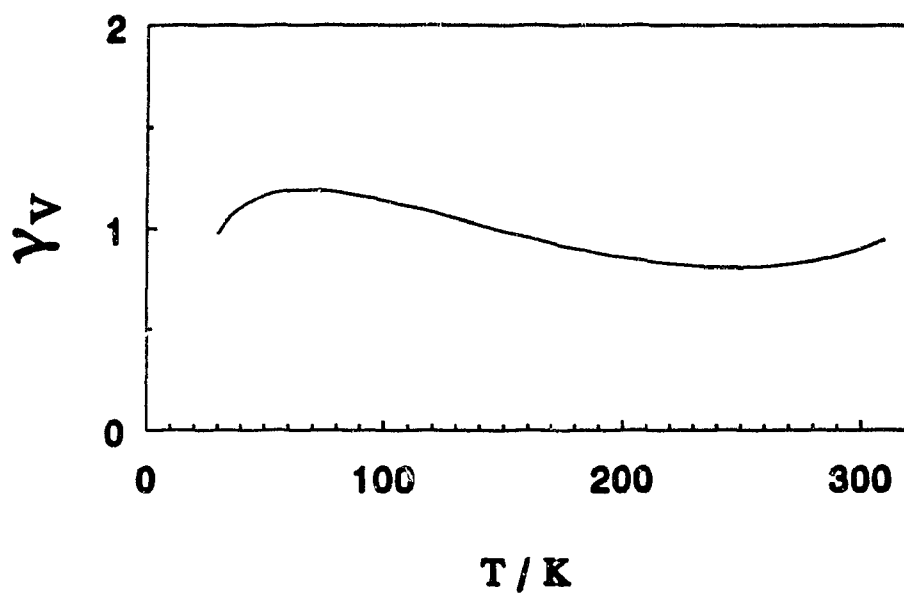


Figure 5.7 Temperature dependence of the overall Grüneisen parameter, γ_V , for HPTB-CBr₄.

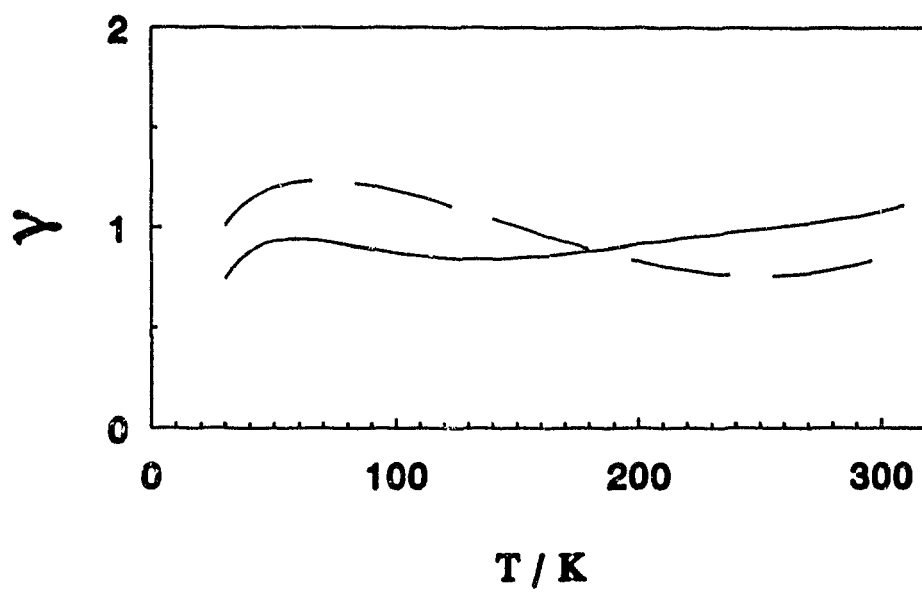


Figure 5.8 Temperature dependence of the Grüneisen parameters, γ_a (- -) and γ_c (-), for HPTB-CBr₄.

character of the temperature dependence of the Grüneisen parameter especially elevation of the Grüneisen constant at lower temperatures, particularly since the compressibility is nearly independent of temperature. This was confirmed by calculations with compressibilities ranging from $1.0 \times 10^{-9} \text{ m}^2 \text{ N}^{-1}$ to $1.0 \times 10^{-8} \text{ m}^2 \text{ N}^{-1}$, which is the range of values for different molecular crystals found in the literature.¹⁰

The values of γ are comparable to those characteristic for non-metallic solids with γ of the order of unity.¹³¹ The low-temperature increase of the Grüneisen parameter reflects the thermal expansion. Although it is not typical because for most materials γ decreases with decreasing temperature, the same trend was observed for other substances like Dianin's systems,⁵⁶ tetrahydrofuran hydrate,¹³⁷ disordered materials and crystals doped with impurities.¹³¹ In solid CO this elevation was attributed to the presence of low-frequency librational modes,¹³¹ which also will exist in the materials investigated here. In amorphous materials it was partially attributed to the linear temperature dependence of the heat capacity¹³¹ which is also observed here (see Chapter 6).

5.3.7 GRÜNEISEN FUNCTION OF CBr_4

Since the thermal expansion and the compressibility of pure solid CBr_4 is available from the literature,^{138,139} combined with the heat capacity results of Chapter 6, this allows the calculation of the overall Grüneisen function of pure CBr_4 from equation (5.3). The temperature dependence of the Grüneisen parameter of CBr_4 is shown in Figure 5.9. Its temperature evolution is similar to that found here for the

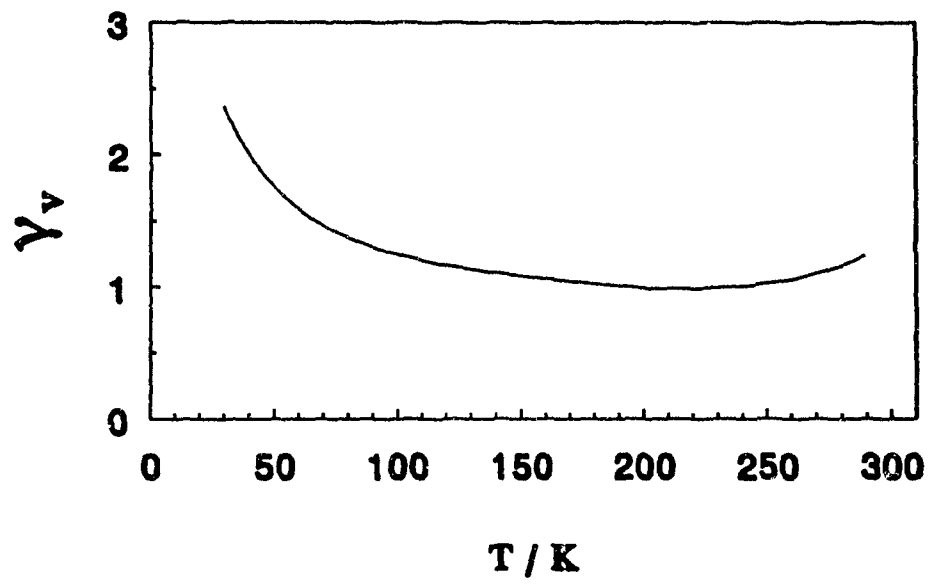


Figure 5.9 Temperature dependence of the overall Grüneisen parameter, γ_v , for pure CBr_4 .

HPTB systems.

Pure CBr_4 is a molecular solid. It has an orientationally ordered monoclinic structure¹⁰⁷ (phase II) below 320 K and an orientationally disordered face-centred-cubic structure¹⁴⁰ (phase I) between 320 K and its melting point, 365 K. The dynamics of phase I CBr_4 have been extensively studied due to its representative character for orientationally disordered solids. The simplified picture is that of six different orientations of the molecules which undergo discrete jumps between these positions.¹⁴¹ However, molecular dynamics simulations revealed much more complex behaviour with a wider range of orientations and additional sporadic free spinning.^{142,143} It was also suggested that some molecules (with sufficiently high kinetic energy) might experience jumps just below 320 in phase II. This represents highly anharmonic behaviour. The Grüneisen function increase in the high-temperature region could be a reflection of this. The origin of the low-temperature behaviour of the Grüneisen parameter in CBr_4 seems to be analogous to that discussed for the HPTB systems (*vide supra*).

5.3.8 CONCLUDING REMARKS ON THE GRÜNEISEN PARAMETER

Intermolecular forces determine many properties of organic molecular crystals, particularly thermal and mechanical properties, since they define the character of the potential between the chemical species building a crystal. The knowledge of the spatial as well as the harmonic/anharmonic character of the intermolecular interaction is crucial in understanding the lattice dynamics. The Grüneisen parameter has been

the useful quantity for discussion of the anharmonic properties of solids especially those displaying significant long-range interactions as ionic crystals. To date, organic molecular crystals and especially multicomponent systems such as clathrates have not been investigated so extensively. It is worthwhile to make a caveat concerning the physical meaning of Grüneisen parameter in the case of molecular crystals.

The strain (and stress) for these materials can be split into external and internal components.⁹¹ The former is due to the displacement of points of the ideal Bravais lattice. The homogeneous deformation formalism identifies the external stress with the elastic strains. The latter is due to a change in relative placement of atoms or molecules in the unit cell.⁹¹ The question is: how much do the overall Grüneisen parameter or the directional Grüneisen parameters as calculated here, reflect the anharmonicity of the crystal lattice potential?

Ideally the Grüneisen parameter calculation would be based on the mode γ determination. Their contributions define the relevant parameters. In the case of this investigation where organic molecular crystals with a wide range of internal vibrations were studied, the thermodynamics of internal strains¹⁴⁴ are complicated. This can significantly affect the values of γ 's obfuscating the physical meaning of this parameter, *e.g.* the mode γ 's due to internal modes are anomalously small despite absolutely no repressed anharmonicity of these modes.^{144,145} The same was postulated for the modes due to rigid-molecule librations.¹⁴⁶ Since both types of modes are present in the investigated materials, the temperature evolution of the calculated γ 's is definitely influenced by the internal coupling between internal and external modes.

HEAT CAPACITY DETERMINATIONS

6.1 INTRODUCTION

Many types of experimental investigations of thermal phenomena can be carried out using calorimeters.^{47,49} The character of physical or chemical processes of interest (*e.g.* the temperature region or time scale of the process) dictates the type of calorimeter and method of measurement employed in the study. In principle calorimeters are simple devices. Each consists of a thermometer, a vessel with a sample, a heat supply and possibly a thermal shield that determines the measurement constraints. The temperature of the sample can be either maintained constant or changed during the measurement (*i.e.* the initial temperature can differ from the final one). Adiabatic calorimetry belongs to the latter category.

Adiabatic calorimetry relies on the absence of heat flux between the measured system (*i.e.* the sample and addenda) and the surroundings. Practical difficulties in realization of this constraint are caused by heat transfer phenomena such as conduction, convection and radiation. To minimize these problems and to create as near to ideal adiabatic conditions as possible, the sample is either isolated from the surroundings by an infinite thermal resistance or the temperature of the measured system is matched with that of the surroundings. In addition, if the sample undergoes the reaction it must be sufficiently rapid to prevent any appreciable heat exchange

during the data collection.

The approach of temperature match to the surrounding was applied in the calorimeter used here. High vacuum, an adiabatic shield and a heat sink for the electrical leads allow for adequate approximation to adiabatic conditions. The temperature of the adiabatic shield is controlled so as to correspond to that of the sample and addenda. Then the unwanted undetermined energy loss/gain by the sample is reduced below an acceptable threshold. A schematic diagram of the heat pulse adiabatic calorimeter is shown in Figure 6.1. It operates with energy pulses, Q , to elevate the sample temperature. Thus the experimental measurement of the heat capacity, C_{exp} , at a given temperature yields always the average over a certain temperature increment, ΔT , *i.e.*

$$C_{exp} = Q/\Delta T . \quad (6.1)$$

The value of C_{exp} can be regarded as exact if the increment ΔT is chosen reasonably. For a solid, C_{exp} , is the heat capacity of the solid in equilibrium with its saturated vapour which is related to the isobaric heat capacity, C_p , by

$$C_{exp} = C_p - T \left(\frac{\partial P}{\partial T} \right)_{sat} \left(\frac{\partial V}{\partial T} \right)_P \quad (6.2)$$

where the subscript *sat* denotes the saturated vapour. For involatile solids $C_{exp} \approx C_p$. Thus the experimentally determined heat capacity, using equation (2.4), can yield the isochoric heat capacity, C_v . In principle for crystals C_p is not really the value of

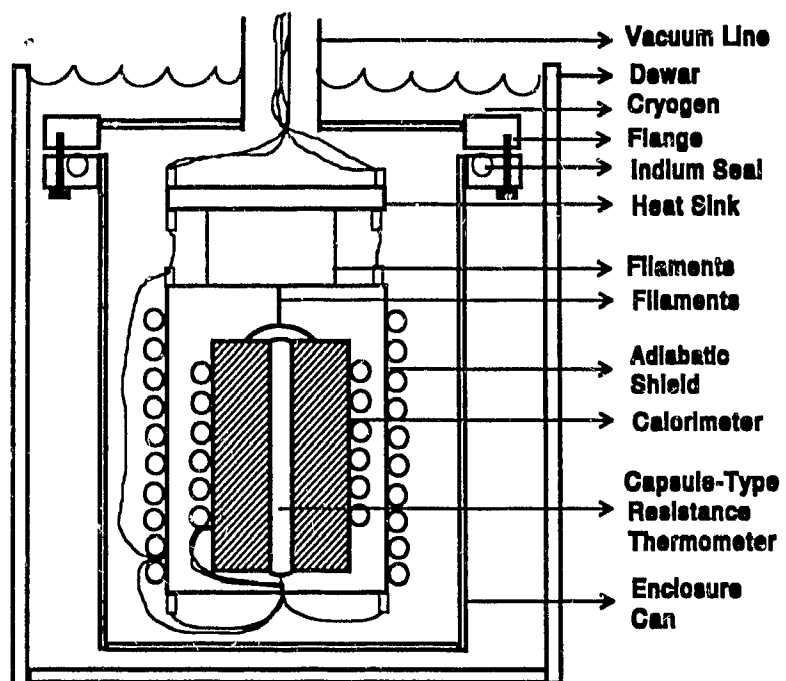


Figure 6.1 Schematic diagram of the adiabatic calorimeter.

interest and moreover equation (2.4) is valid only for isotropic materials. The constraints relevant to anisotropic materials are constant stress and constant strain, *i.e.* C_σ and C_ϵ , respectively. The equation equivalent to equation (2.4) takes the form

$$C_P - C_V \cong C_\sigma - C_\epsilon = VT \sum_{ijkl} c_{ijkl} \alpha_{ij} \alpha_{kl} \quad (6.3)$$

where c_{ijkl} is the isothermal elastic constant tensor and the α_{ij} is the thermal expansion tensor. Since it can be assumed that the vapour pressure of the solid is approximately zero, $C_P \cong C_\sigma$.

6.2 EXPERIMENTAL SETUP

The adiabatic calorimeter used for this research project consists of a calorimeter vessel which holds a known amount of the investigated sample and its electrical heater; a platinum resistance thermometer and a constant current power supply; an adiabatic shield and its controller; a vacuum system; an immersion cryostat; a digital multimeter and computer.¹⁴⁷ All electronic elements of the experimental station were interfaced with a Hewlett-Packard 87A personal computer (Figure 6.2) which allowed for full control of all crucial experimental variables including a fully automated mode of operation. The readings were taken by a Hewlett-Packard 3456D Digital Voltmeter. The time frame of the data collection was monitored and controlled with 0.02% accuracy by the HP 87A internal clock. Software enables one: a) to heat the sample for a specified time or to a specified temperature, b) to adjust the control of the adiabatic shield, and c) to gather temperature data at specified rate for a given period of time. The data processing was built into the program.

The calorimeter had been tested with Calorimetry Conference (NBS-49) benzoic acid from 35 K to 310 K. The results agreed with the literature to within 0.5%.¹⁴⁷

A cylindrical vacuum enclosure can was made out of copper. It surrounded the copper heat anchor that kept the adiabatic shield with the calorimetric vessel inside. The can was fastened to a flange of the vacuum line. An indium vacuum seal was made between the can and the rim. After the sample had been loaded (*vide infra*)

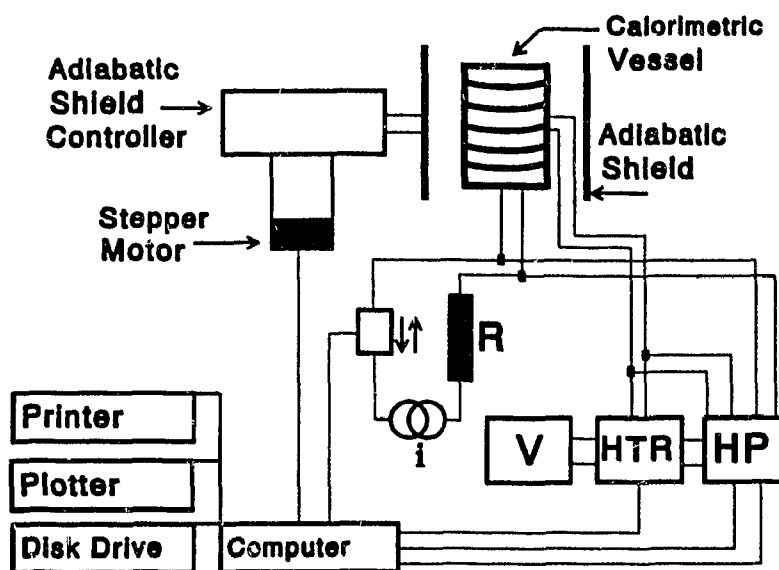


Figure 6.2 A schematic diagram of the computer system controlling the automated adiabatic calorimeter.¹⁵¹ The abbreviations in the diagram denote the following: i is the constant current supply; $\downarrow \uparrow$ is the computer-controlled current direction relay; R is the standard 100 Ohm resistor; V is the constant voltage supply; HTR are the heater/thermometer relays; HP is the Hewlett-Packard 3456A digital multimeter.

the contents of the enclosure can were evacuated in order to provide satisfactory insulation and prepare the assembly for the quasi-adiabatic conditions. The vacuum system which enabled a pressure lower than 10^{-5} Torr consists of a roughing pump and a oil diffusion pump. Sub-ambient temperatures were obtained immersing the enclosure can in an appropriate refrigerant stored in a glass Dewar. For the particular temperature range either only liquid nitrogen (for the temperatures 77 K and up) or liquid helium (for the temperatures 20 K and up) were used. In the latter case the enclosure can was submerged in a Dewar with liquid helium and this Dewar sat inside another containing liquid nitrogen. To facilitate cooling helium exchange gas was introduced to the enclosure can; afterwards it was pumped away.

The sample container and heater/thermometer assembly constitute the heart of the apparatus. This is shown in Figure 6.3. Apiezon T grease was used to improve thermal contact between the sample vessel and the heater/thermometer assembly. The sample container has a volume of approximately 5 cm^3 and mass *ca.* 11 g. It is closed hermetically from the top by a lid and an indium O-ring. The heater/thermometer assembly is made of thin-walled copper with a centrally located thermometer well where a calibrated miniaturized Pt resistance thermometer (Lake Shore Cryotronics Pt-103, 100 Ohms at 273 K) sat. In order to have good sensitivity, the Pt resistance thermometer was connected in a circuit in series with a standard resistor (100 Ohms). A small constant current (1 mA) was passed through the circuit and the ratio of the voltage drop across the thermometer relative to the drop across the standard resistor was measured with a HP 3456A digital multimeter (thermometer

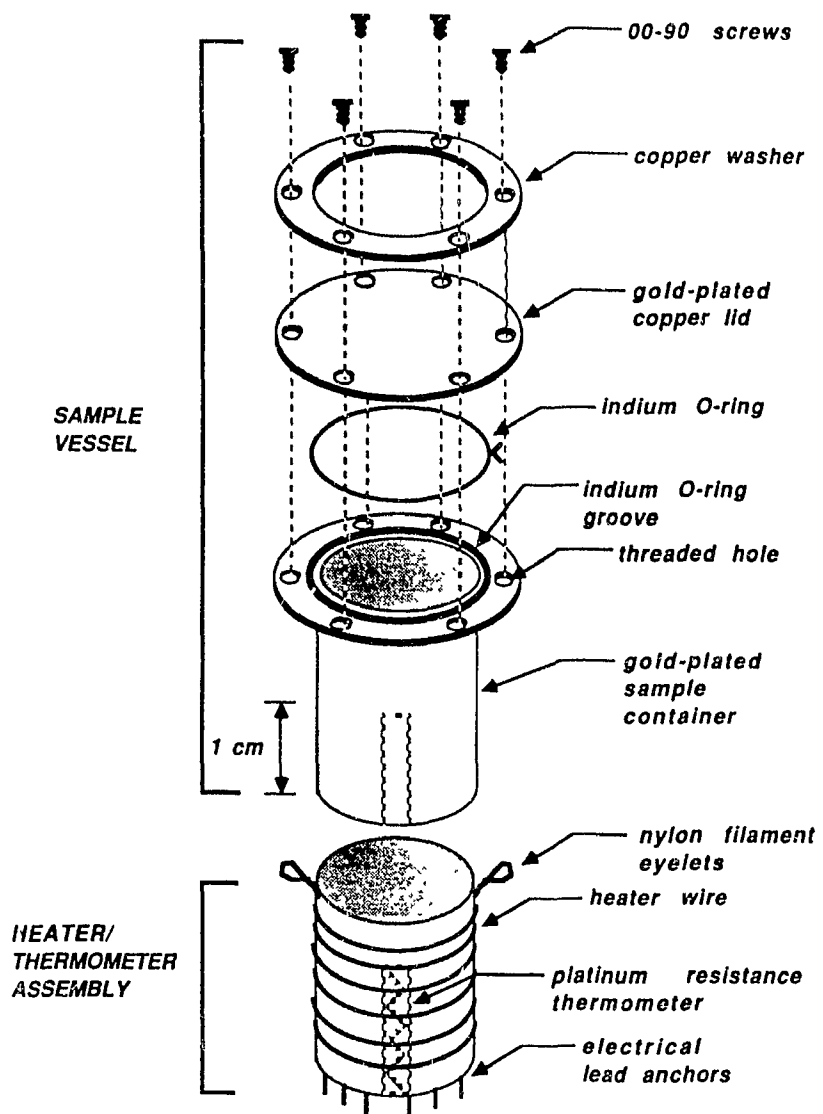


Figure 6.3 The sample container and heater/thermometer assembly of the calorimetric vessel.¹⁵¹

resistance ratio readings were taken in either direction to correct for thermal electromotive force). A schematic diagram of the circuit is shown in Figure 6.2. The thermometer was calibrated by the supplier from 4 K to 380 K against a platinum resistance thermometer that had been calibrated based on the 1976 Provisional 0.5 to 30 K temperature scale (EPT-76)¹⁴⁸ below 30 K and International Practical Temperature Scale of 1968 (IPTS-68)¹⁴⁹ above 30 K. The accuracy of this calibration also satisfies the 1990 International Temperature Scale.¹⁵⁰ The claimed accuracy of the calibration is ± 10 mK above 27 K and ± 15 mK below 27 K.¹⁵¹ The heater was made of approximately 2.6 m of double-silk wound Karma wire (590 Ohms) which was wound bifilarly around and varnished to the heater/thermometer assembly.

The sample vessel and heater/thermometer assembly (Figure 6.3) was suspended inside the adiabatic shield. This prevented unknown energy exchange between the surroundings and the system. Copper-constant thermocouple junctions placed on the shield and on the bottom of the sample container (as a reference) permitted control of the temperature gradient. The shield had an outer heater which was 15 m manganin wire wound bifilarly on the surface of the shield. This thermocouple was connected to an Artronix 5301-E shield controller which contained the power supply for the shield heater. An admissible thermal drift in the calorimetric vessel was within 0.003 K/min and it was achieved and sustained through an appropriate set point of the shield controller.

A more detailed description of the calorimeter can be found elsewhere.¹⁵¹

6.3 EXPERIMENTAL PROCEDURE

A sample container loaded to maximum capacity with a compound of interest was placed in a desiccator for evacuation. The evacuated desiccator was moved to a dry box with helium gas where the sample vessel was closed. Helium gas provided better thermal diffusivity among sample, the container and the thermometer. The mass of the sample was determined by weighing the empty and loaded calorimetric vessel. Then it was installed below the heat sink and all previously described steps were carried out in order to commence measurements.

The data collection consisted of a preheating and a postheating period. First the conditions were set to maintain equilibrium conditions in the calorimeter, *i.e.* with the temperature drift within ± 0.003 K/min. The resistance ratio readings (thus the temperature readings) were taken for an arbitrary period of time which was usually 30 to 60 minutes. Then the sample was heated for a period, t , by applying voltage across the vessel heater. The voltage, U , had been measured three times and averaged. The heater resistance, R , had been measured twice, *i.e.* before and after heating, and averaged. Thus the energy provided to the system is given by $Q=tU^2/R$. Depending on the temperature region, the set point on the shield controller was accordingly changed during the heating to adjust to the new temperature and new prospective temperature gradient between the vessel and the shield.

After heating the resistance ratio readings were taken once again. The preheating and postheating resistance ratios were projected to the midpoint of the heating where their values were calculated (giving the corresponding temperature of

the sample before heating, T_1 , and the temperature of the sample after heating, T_2) in order to determine the temperature increment ($\Delta T = T_2 - T_1$) and the averaged value of the temperature, T , for which the heat capacity is calculated ($T = (T_2 + T_1)/2$). The total heat capacity (sample and addenda) was calculated from equation (6.1). The actual value of the heat capacity of the sample was obtained subtracting the heat capacity of addenda, *i.e.* the empty calorimeter, indium metal and Apiezon T grease; these temperature-dependent values were obtained from the fitting to the experimental findings using a spline method. Inaccuracy in the determination of the mass of Apiezon T grease and indium seal can be neglected since it contributes less than 0.04% to the total heat capacity of the empty vessel.¹⁵¹

The heat capacities of three compounds, *i.e.* pure CBr_4 , pure HPTB, and the CBr_4 clathrate of HPTB, were determined using the foredescribed heat pulse adiabatic calorimeter. The masses of these samples were 9.2904 g, 2.8241 g and 3.6546 g, respectively. Preparation of HPTB systems was as described in Chapter 3. The CBr_4 sample was obtained from Aldrich Chemical Company at a stated purity of 99%. It was then sublimed to further remove impurities. This method was reported to be more effective for CBr_4 than recrystallization from solution.¹³⁹

6.4 RESULTS AND DISCUSSION

6.4.1 EXPERIMENTAL FINDINGS

The raw experimental findings of the measured compounds, given per mole of the substance, are presented in the Appendix (Tables A1, A2, A3); the relevant plots are shown in Figures 6.4 and 6.5. The corresponding smoothed values of the isobaric heat capacity for these compounds are presented in Tables 6.1, 6.2, and 6.3.

All compounds behaved well thermally. No thermal history effects, which can indicate properties such as frozen disorder, were observed. The relaxation times after heating did not exceed 15 minutes for CBr_4 and 10 minutes for HPTB and HPTB- CBr_4 . For all compounds the times were slightly decreased at lower temperatures.

The heat capacity of the sample with respect to the heat capacity of the calorimeter varied with (increasing) temperature from > 90% to 50% for pure CBr_4 , from 40% to 30% for pure HPTB and from 60% to 35% for the CBr_4 clathrate of HPTB.

The heat capacity functions are smooth for all three compounds with no singularities due to phase transitions. The heat capacity of CBr_4 reported previously¹³⁹ above 295 K is also plotted in Figure 6.4. Agreement with these results is within experimental error.

6.4.2 HEAT CAPACITY OF CBr_4 GUEST IN HPTB- CBr_4

It is reasonable to assume, as a first approximation, additivity of the host and guest contributions to the total heat capacity of HPTB- CBr_4 , as had been done in the

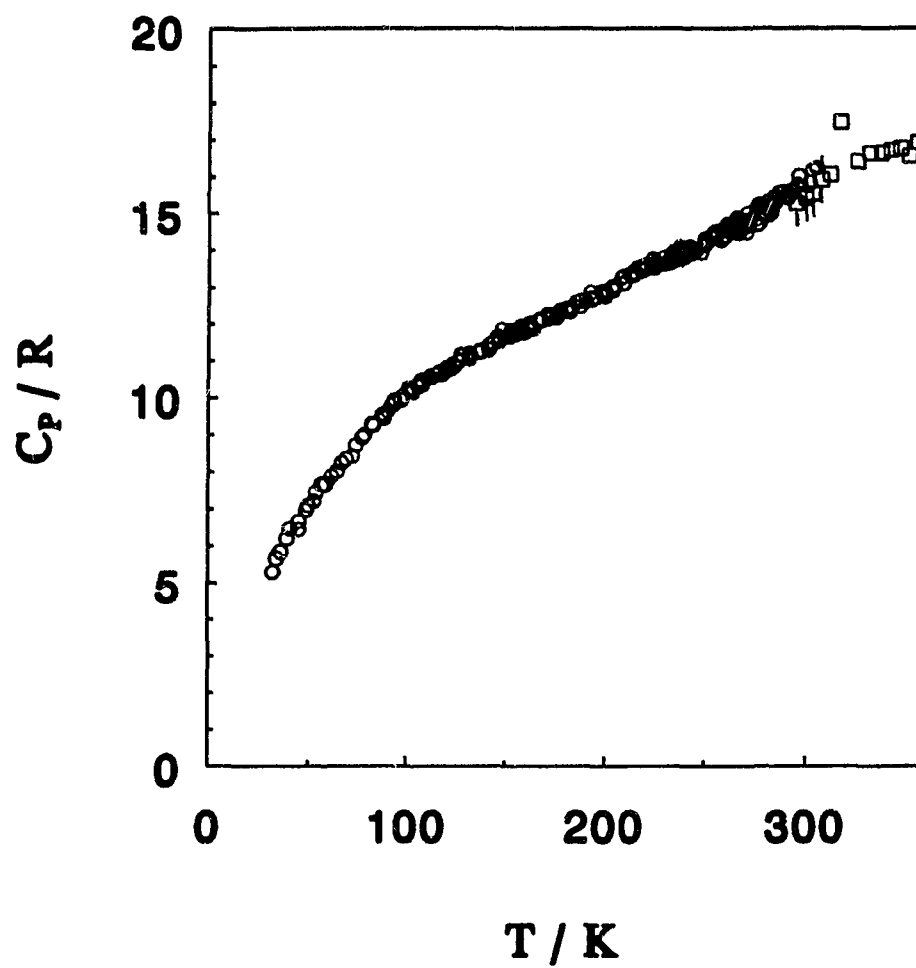


Figure 6.4 Experimental molar heat capacity of CBr_4 as determined in this experiment (O) and from literature¹³⁹ (□).

Table 6.1 Smoothed values of C_p for CBr_4 .

T / K	$C_p / \text{J K}^{-1} \text{mol}^{-1}$	T / K	$C_p / \text{J K}^{-1} \text{mol}^{-1}$
30.0	43.09	175.0	102.18
35.0	47.29	180.0	103.18
40.0	51.24	185.0	104.17
45.0	54.94	190.0	105.17
50.0	58.42	195.0	106.17
55.0	61.69	200.0	107.17
60.0	64.75	205.0	108.19
65.0	67.62	210.0	109.23
70.0	70.31	215.0	110.28
75.0	72.83	220.0	111.34
80.0	75.19	225.0	112.43
85.0	77.41	230.0	113.54
90.0	79.48	235.0	114.68
95.0	81.43	240.0	115.83
100.0	83.27	245.0	117.02
105.0	84.99	250.0	118.22
110.0	86.62	255.0	119.46
115.0	88.15	260.0	120.71
120.0	89.60	265.0	121.99
125.0	90.98	270.0	123.29
130.0	92.29	275.0	124.62
135.0	93.54	280.0	125.96
140.0	94.74	285.0	127.32
145.0	95.89	290.0	128.70
150.0	97.00	295.0	130.09
155.0	98.08	300.0	131.49
160.0	99.13	305.0	132.90
165.0	100.16	310.0	134.31
170.0	101.18		

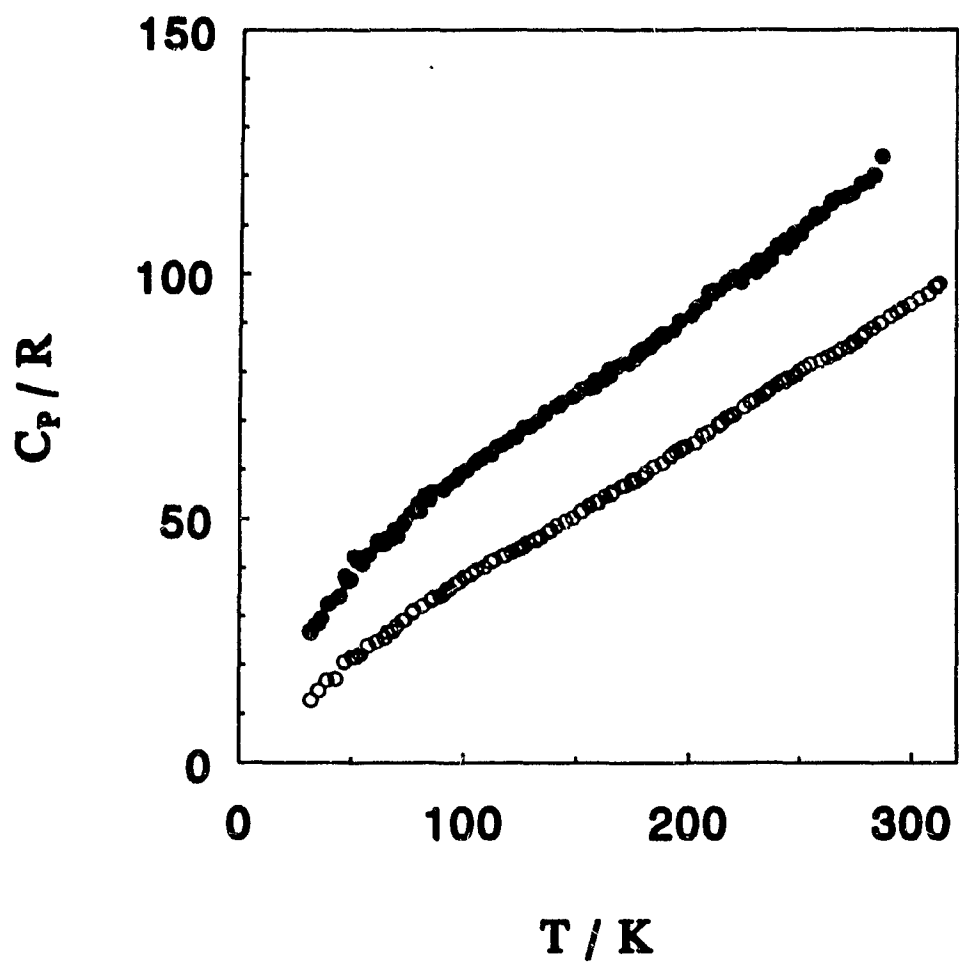


Figure 6.5 Experimental heat capacities of HPTB (○) and HPTB-CBr₄ (●), with the latter expressed per mole of HPTB.

Table 6.2 Smoothed values of C_p for HPTB.

T / K	$C_p / \text{J K}^{-1} \text{mol}^{-1}$	T / K	$C_p / \text{J K}^{-1} \text{mol}^{-1}$
30.0	96.65	175.0	481.23
35.0	118.52	180.0	493.19
40.0	138.83	185.0	505.23
45.0	157.74	190.0	517.32
50.0	175.40	195.0	529.46
55.0	191.97	200.0	541.63
60.0	207.56	205.0	553.82
65.0	222.30	210.0	566.03
70.0	236.32	215.0	578.23
75.0	249.70	220.0	590.41
80.0	262.56	225.0	602.57
85.0	274.97	230.0	614.69
90.0	287.01	235.0	626.78
95.0	298.77	240.0	638.81
100.0	310.30	245.0	650.79
105.0	321.65	250.0	662.72
110.0	332.89	255.0	674.60
115.0	344.06	260.0	686.44
120.0	355.19	265.0	698.24
125.0	366.31	270.0	710.03
130.0	377.46	275.0	721.81
135.0	388.66	280.0	733.61
140.0	399.92	285.0	745.46
145.0	411.26	290.0	757.40
150.0	422.69	295.0	769.45
155.0	434.21	300.0	781.67
160.0	445.82	305.0	794.67
165.0	457.54	310.0	806.82
170.0	469.34		

Table 6.3 Smoothed values of C_p for HPTB-CBr₄, per mole HPTB.

T / K	C_p / J K ⁻¹ mol ⁻¹	T / K	C_p / J K ⁻¹ mol ⁻¹
30.0	217.27	175.0	691.05
35.0	244.94	180.0	704.41
40.0	270.99	185.0	717.94
45.0	295.55	190.0	731.64
50.0	318.72	195.0	745.52
55.0	340.61	200.0	759.57
60.0	361.31	205.0	773.79
65.0	380.93	210.0	788.16
70.0	399.57	215.0	802.68
75.0	417.30	220.0	817.33
80.0	434.23	225.0	832.09
85.0	450.43	230.0	846.94
90.0	465.99	235.0	861.84
95.0	480.97	240.0	876.76
100.0	495.46	245.0	891.68
105.0	509.52	250.0	906.54
110.0	523.22	255.0	921.32
115.0	536.61	260.0	935.96
120.0	549.76	265.0	950.41
125.0	562.72	270.0	964.62
130.0	575.54	275.0	978.53
135.0	588.26	280.0	992.08
140.0	600.94	285.0	1005.20
145.0	613.60	290.0	1017.83
150.0	626.29	295.0	1029.90
155.0	639.03	300.0	1041.32
160.0	651.85	305.0	1052.02
165.0	664.78	310.0	1061.92
170.0	677.84		

case of quinol systems,¹⁵² the THF hydrate⁵⁴ and Dianin's systems.⁵⁵ For the latter the heat capacity of the host lattice was measured directly since the clathrand of this compound exists. The heat capacity of the empty host lattice of the quinol was extrapolated from the heat capacity of clathrates with different guest concentrations. For HPTB-CBr₄ the situation is analogous to that of THF clathrate hydrate. Neither the clathrand exists nor is there data available (since the clathrates of HPTB seem to have fixed compositions) to have or extract the heat capacity of the empty host lattice. Thus the heat capacity of pure HPTB was used as the only feasible approximation for the empty host framework of HPTB-CBr₄. The molar "bulk" and "molecular", *i.e.* guest, heat capacity of CBr₄ are shown in Figure 6.6.

From the figure the heat capacities of the CBr₄ molecules in bulk or cages of the HPTB clathrate above 130 K are the same, within the experimental error. This is also the temperature region where the heat capacity is a very linear function of the temperature. Below 130 K the enclathrated CBr₄ molecules exhibit higher heat capacity than that of pure CBr₄. The difference increases with decreasing temperature to *ca.* R (R is the gas constant) at 30 K. This shows that, within the assumption of guest-host heat capacity additivity, CBr₄ has more freedom in the voids of the clathrate than in the bulk. The "single molecule" molar heat capacity at the temperature 30 K exceeds $6R$ which is the harmonic equipartition limit to the heat capacity from vibrational rattling and rigid-body rotation of the CBr₄ molecule (even after subtraction of the intramolecular contribution to the total heat capacity; *vide infra*). The total molar heat capacity approaches *ca.* $16R$ at 300 K. Thus the guest

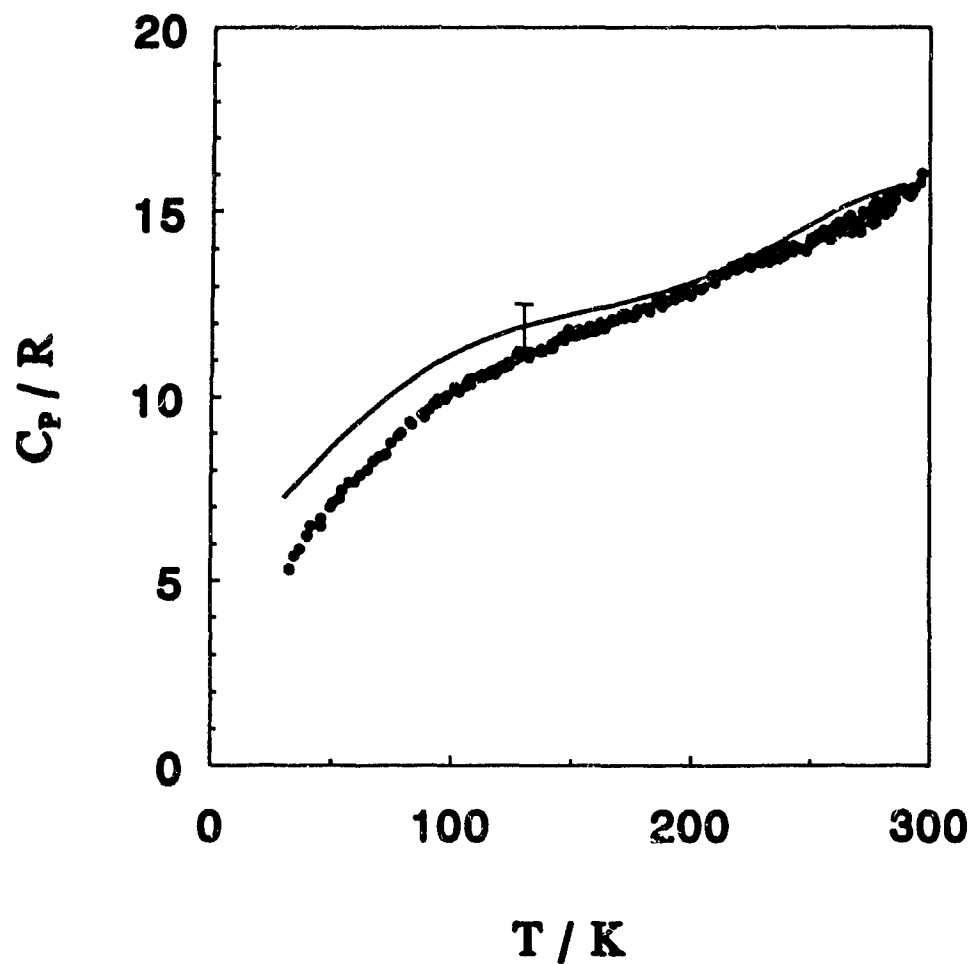


Figure 6.6 The molar heat capacities of the CBr_4 molecule as a function of temperature for bulk CBr_4 (\bullet) and as determined by difference between the heat capacity of HPTB- CBr_4 and the heat capacity of HPTB ($-$). The error bar represents the error in the molar heat capacity of the CBr_4 molecule in the clathrate.

rigid-body motion appears to be fully excited between 30 K and 300 K, with additional contributions to the heat capacity from internal vibrations.

6.4.3 ISOCHORIC HEAT CAPACITY

Since the necessary thermodynamic variables are available for CBr_4 ^{138,139} and for HPTB- CBr_4 the calculation of their isochoric heat capacities is possible. For CBr_4 the isochoric heat capacity is computed by means of equation (2.4) with values of the isothermal compressibility and the volume thermal expansion taken from literature.^{138,139} For HPTB- CBr_4 the thermal expansion tensor and elastic constants determined here were used. This allows for the calculation of the heat capacity at constant stress by means of equation (6.3), which for this crystal symmetry, takes the form (in Voigt notation)¹⁰

$$C_\epsilon = VT(2(c_{11} + c_{12})\alpha_a^2 + 4c_{13}\alpha_a\alpha_c + c_{33}\alpha_c^2) . \quad (6.4)$$

The relevant plots are shown in Figures 6.7 and 6.8, *i.e.* for pure CBr_4 and HPTB- CBr_4 , respectively. The smoothed values are given in Appendix (Table A4 and A5).

C_V of CBr_4 is quite linear above 100 K. C_V of HPTB- CBr_4 is linear in the whole measured temperature range. The relative difference between the isobaric and isochoric heat capacities for these materials is negligibly small at low temperatures, increasing with the increasing temperature to 12% for CBr_4 , and 8% (C_V), or 1% (C_V) for HPTB- CBr_4 at the highest measured temperature.

The linear character of the heat capacity functions is most likely caused by

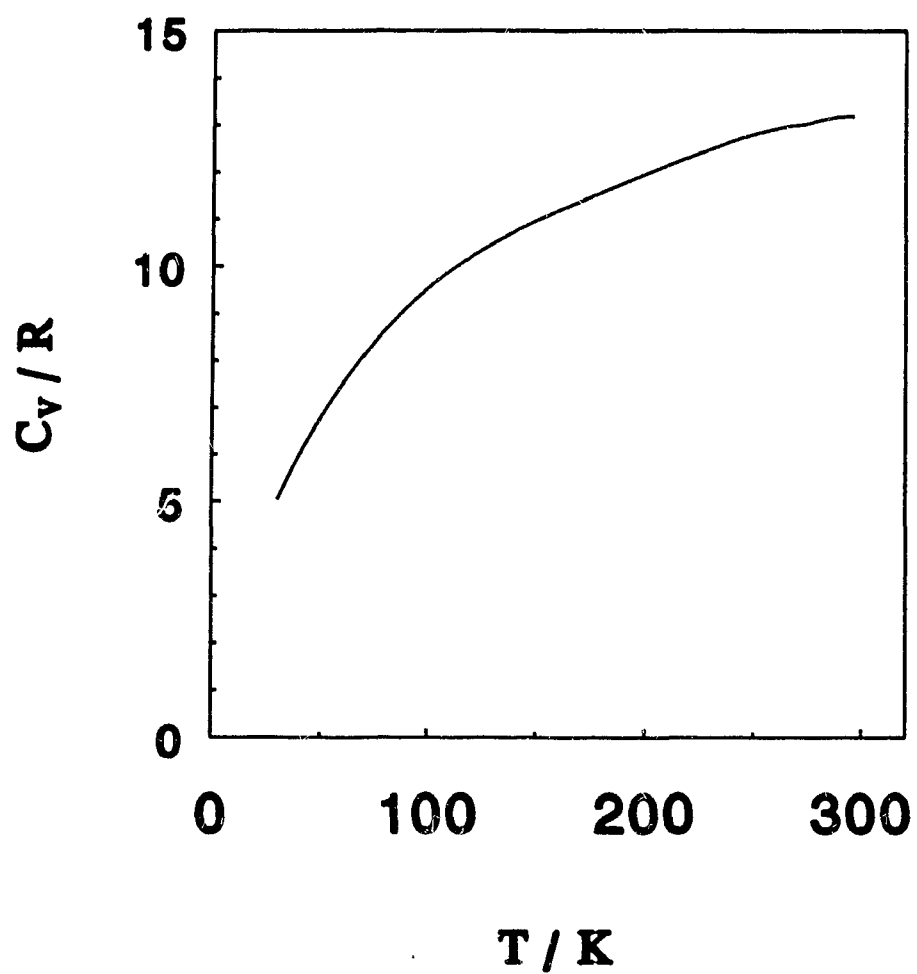


Figure 6.7 Molar isochoric heat capacity of pure CBr_4 as a function of temperature.

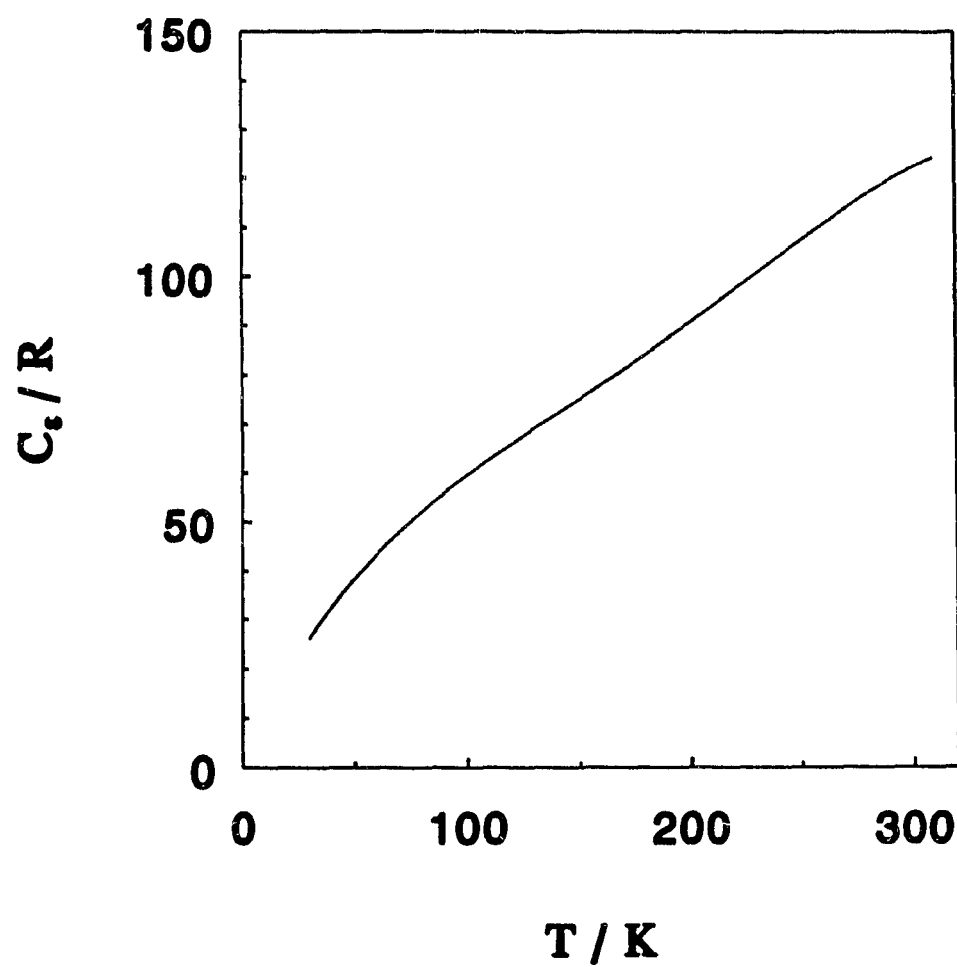


Figure 6.8 Molar isochoric heat capacity of HPTB-CBr₄ as a function of temperature.

internal modes which exist in these molecular solids. The reported¹⁵³ Raman spectrum of CBr_4 reveals vibrations with frequencies between 15 cm^{-1} and 677.7 cm^{-1} . The Raman spectrum of HPTB reveals vibrations between 15 cm^{-1} and 3000 cm^{-1} .¹⁵⁴ It is expected that internal vibrations within HPTB molecules will remain the same in its CBr_4 clathrate. Similar linear behaviour of C_V was observed in the Dianin's system⁵⁶ with internal modes ranging between 40 cm^{-1} to 3000 cm^{-1} , and in the monomer and polymer of p-toluene sulphonate with the stretching vibrational modes contributing to C_V proportionally to the temperature¹⁵⁵, as well as in other molecular organic crystals.⁴⁶

6.4.5 CHARACTERISTIC TEMPERATURES

The isochoric heat capacity allows for the calculation of Debye temperature by means of equation (2.14). All three systems are molecular crystals and application of this equation requires appropriate modification of the understanding of n which in the case of a simple atomic crystal is the number of atoms in the unit cell, each of which contribute $3k_B$ to the heat capacity in the high-temperature limit. In light of the previously described structural features as well as the energetic makeup of the molecular solids, n should be regarded as the number of potential contributors to the high-temperature heat capacity or equivalently as the number of sites in the unit cell. Organic molecular crystals exhibit a wide variety of molecular motions;⁴⁶ either the entire molecule or a particular group of atoms undergoes diverse rotational and/or translational motions, *e.g.* various types of dynamics of methyl groups.¹⁵⁶ The

question is: how many degrees of freedom one can ascribe to the molecule? In the case of the CBr_4 molecule the most likely answer seems to be six, *i.e.* translational vibration (three degrees of freedom; one site) and libration of the molecule (another three degrees of freedom; another site).

For the CBr_4 clathrate of HPTB this assignment is more arbitrary. The host molecule can be treated as a rigid unit and then there are six degrees of freedom. If the phenyl moieties are able to move then the number of degrees of freedom increases. The phenyl rings might display translational vibrations¹⁵⁷ as well as librations¹⁵⁸ and then the HPTB molecule can be treated either as 8 or 14 sites. Since the assignment is, of necessity, arbitrary in nature it should be treated as a reasonable simplification of the real thermal behaviour of HPTB systems. The value of n , *i.e.* the number of generalized sites, or the corresponding number of degrees of freedom should not be taken too literally since molecular crystals and especially complex structures like those of HPTB and its clathrate do not lend themselves to the straightforward application of Debye or Einstein theory. There are approaches based on hybrids of these two models but they cannot be applied here owing to the absence of auxiliary data (*e.g.* lack of a complete assignment for internal modes).

Since the Debye model describes acoustic modes, the contribution of intramolecular vibrations to the total heat capacity should be subtracted before determination of the Debye temperature. Although complete assignment of intramolecular vibrations for these compounds is not known, the Raman spectrum of CBr_4 has been reported.¹⁵³ These values of intramolecular vibrations were used for

CBr_4 and the CBr_4 guest of HPTB- CBr_4 since the internal frequencies are practically insensitive to the molecular environment. The simplified assessment of the molar intramolecular vibrational contribution of CBr_4 to the total molar heat capacity, based on the values from literature,¹⁵³ is

$$C_{\text{intra}} = R \sum_{i=1} w_i \frac{x_i^2 e^{x_i}}{(e^{x_i} - 1)^2} \quad (6.5)$$

where w_i is the appropriate weighing factor for frequency ω_i and $x_i = \hbar\omega_i/k_B T$. The temperature-dependent value of C_{intra} was appropriately subtracted from the isochoric heat capacities of CBr_4 and HPTB- CBr_4 before the evaluation of the temperature-dependent Debye temperature. Since the compressibility of HPTB is not known, θ_D of this compound was evaluated from the experimental heat capacities, rather than C_p .

The plots with the Debye temperatures as functions of temperature are shown in Figures 6.9, 6.10, and 6.11 for CBr_4 , HPTB, and HPTB- CBr_4 , respectively. Details are given in the captions. θ_D of CBr_4 is comparable to that of other halomethanes (CCl_4 with θ_D about 90 K,¹⁵⁹ CBrCl_3 with $\theta_D = 63.48$ K and CBr_2Cl_2 with $\theta_D = 58.4$ K;¹⁶⁰ these values were extracted from low-temperature heat capacity data). For HPTB- CBr_4 , in the low-temperature region, both curves seem to approach values between 90 K and 110 K. Increasing in temperature from $T=0$ K one would expect these curves, relatively close in values, decrease and subsequently increase as was observed for other solids.⁶¹ In all cases the θ_D decrease with the increasing temperature is likely caused by increasing anharmonicity in these systems and by not

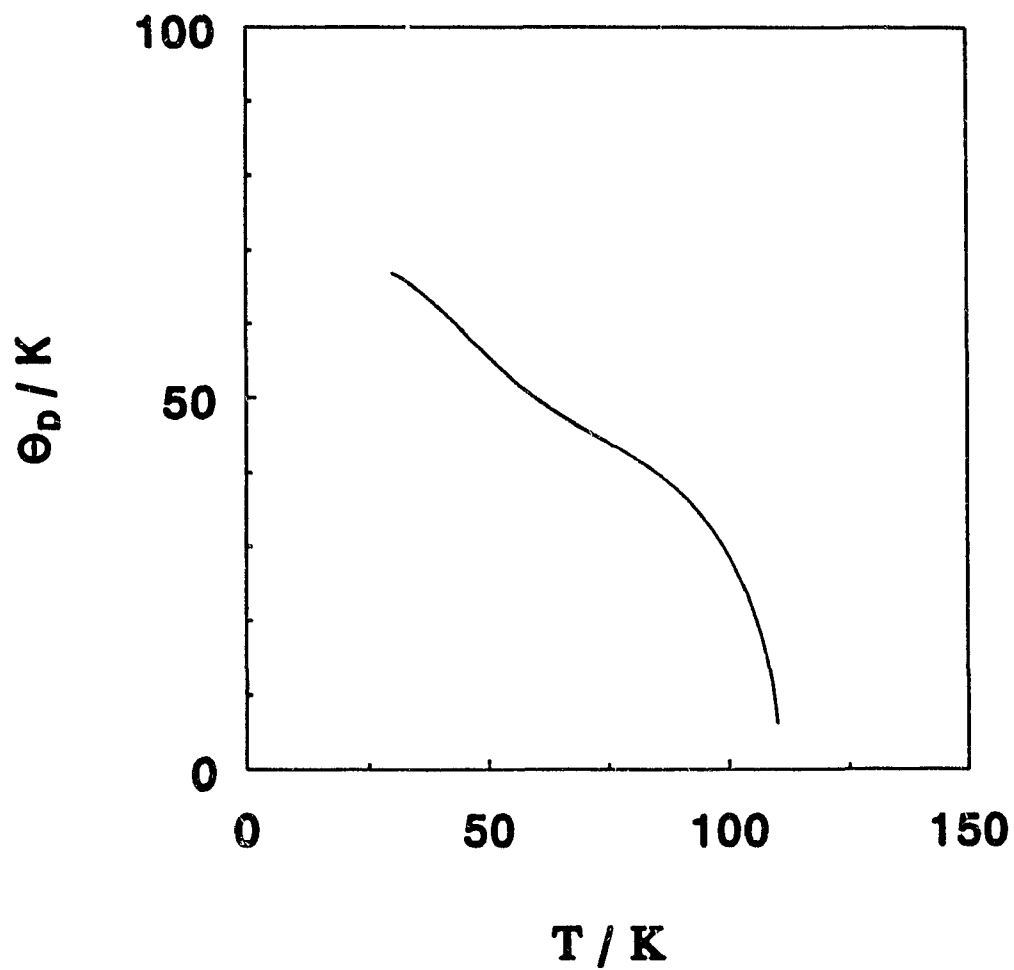


Figure 6.9 The Debye temperature for pure CBr_4 as a function of temperature, calculated for six degrees of freedom per molecule. This was calculated from the isochoric heat capacity with intramolecular contribution removed.

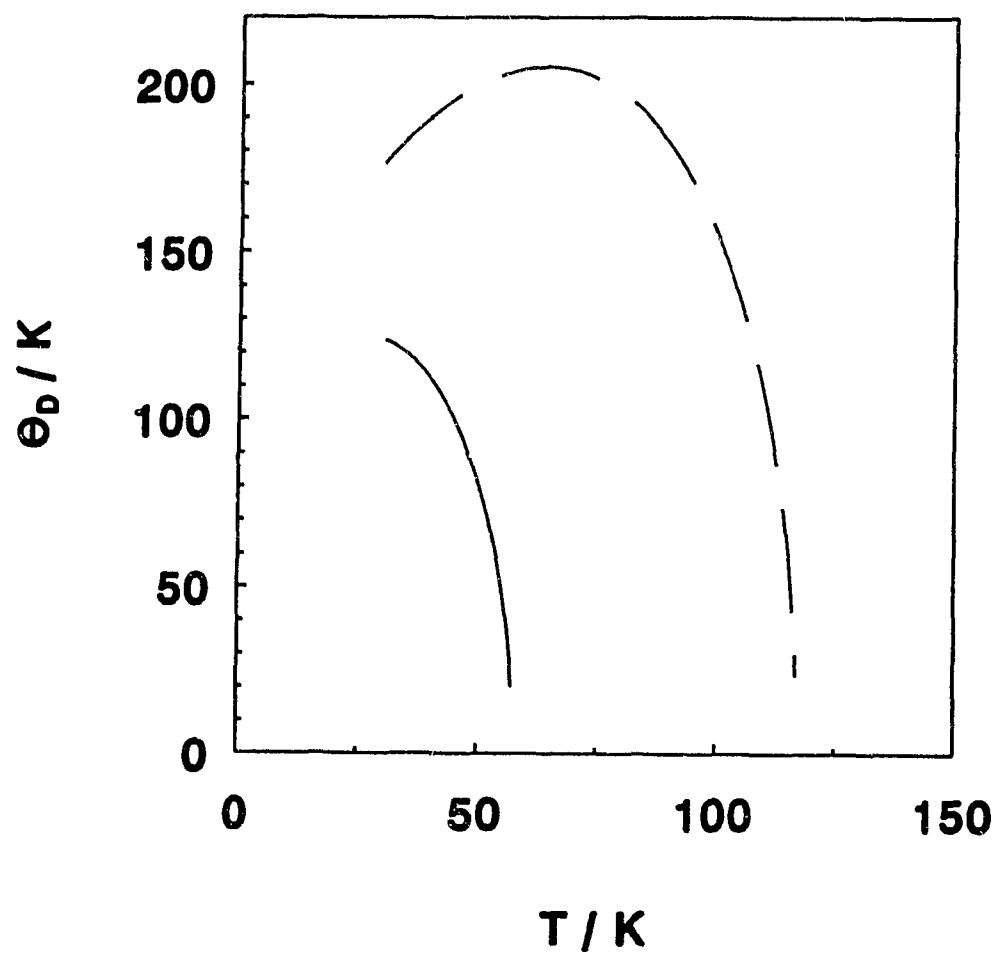


Figure 6.10 The Debye temperature for pure HPTB as a function of temperature calculated from experimental heat capacity; (—) calculated for 24 degrees of freedom per molecule, (- -) calculated for 42 degrees of freedom per molecule.

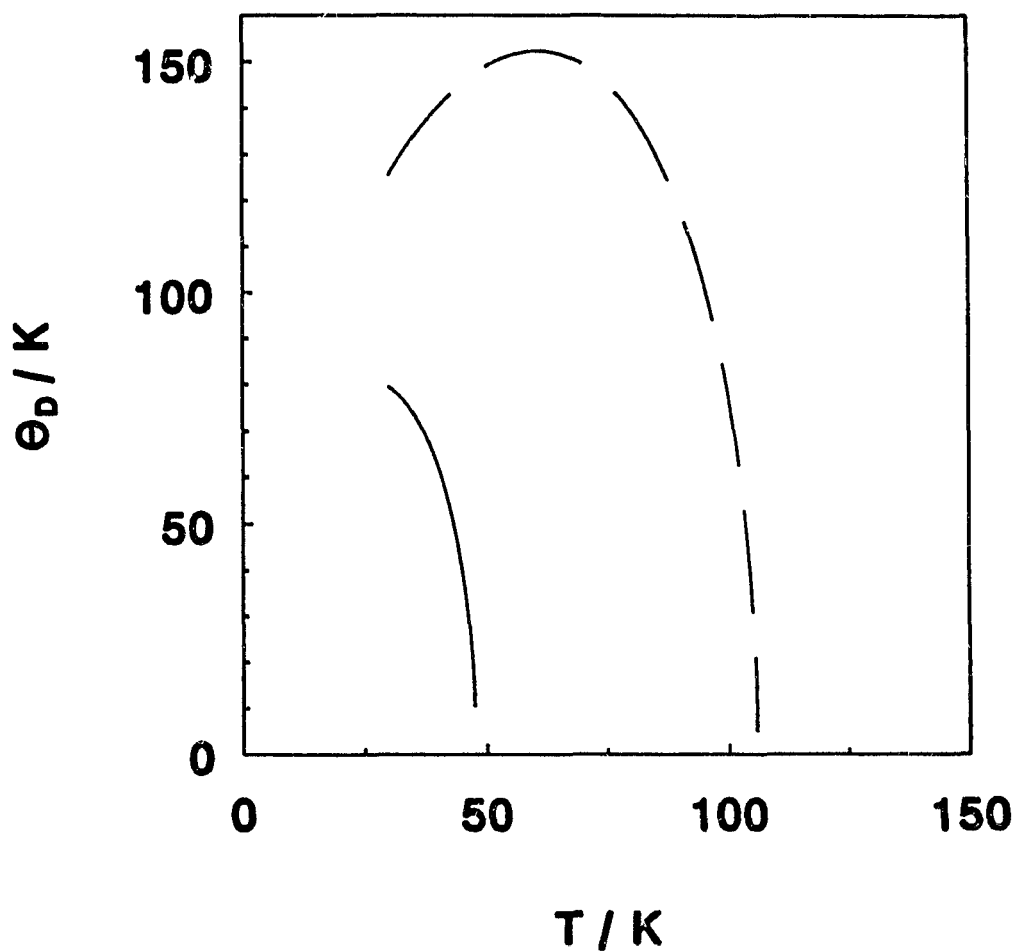


Figure 6.11 The Debye temperatures for HPTB-CBr₄ as functions of temperature calculated from isochoric heat capacity with intramolecular contribution from the CBr₄ molecules removed; (—) calculated for 24 degrees of freedom per the HPTB molecule, (---) calculated for 42 degrees of freedom per HPTB molecule, and 6 degrees of freedom per CBr₄ molecule in both cases.

taking into account all contributions to the total heat capacity arising, most likely, from rotational modes.

Knowledge of elastic constants of the CBr_4 clathrate of HPTB permits the calculation of sound velocities along the c -axis. These values can be used to compute θ_D from equation (2.14). Once again assignment of n in this equation is somewhat arbitrary. For $n=36$, $\theta_D=90$ K; for $n=54$, $\theta_D=103$ K. These values correspond quite well with the calorimetric Debye temperature despite the fact that sound velocities used in the calculation were, out of necessity, from an arbitrary direction. In other solids the calorimetric Debye temperature at $T=0$ K is in reasonable agreement with the θ_D derived from the sound velocities.⁵⁹ The above results indicate that this is also the case here.

7.1 FORMAL THEORY OF THERMAL CONDUCTIVITY

The microscopic expression for heat flow in a solid was given by equation (2.17). One of the main conclusions drawn from this equation is that a net flow of heat is possible only if the phonon distribution function departs from the thermal equilibrium value. Thus the Bose-Einstein function (Section 2.1) which is a function of position, time and temperature, lays the theoretical ground for formulation of a mathematical description of heat transport in insulators.

Spatial dependence of temperature in a crystal causes phonon diffusion at a particular rate. On the other hand phonons are scattered by various mechanisms. At steady state the phonon drift must be balanced by the phonon scattering and this is expressed in the form of the Boltzmann equation⁶²

$$-c_{kj} \nabla T \frac{\partial n_{kj}}{\partial T} + \frac{\partial n_{kj}}{\partial t} = 0 . \quad (7.1)$$

The first term is due to the drift of phonons; c_{kj} is the group velocity of phonon kj , n_{kj} is the relevant phonon distribution. The second term is due to scattering. Solution of this equation relies on simplifications taking into account valid physical approximations. It is linearized to yield an analytic solution.

It can be assumed that the departure of the Bose-Einstein distribution from equilibrium due to the temperature gradient is small and the phonon distribution n_{kj} can be replaced by its equilibrium value, N_{kj} , in the derivative with respect to temperature. A similar assumption for the temporal dependence of the phonon distribution function (that this function can be expanded in a Taylor's series around its equilibrium value and higher than the first term neglected) allows for replacement of its time derivative with $(n_{kj} - N_{kj})/\Delta t$. Thus the linearized Boltzmann equation for phonons has the form⁶²

$$-c_{kj} \nabla T \frac{\partial N_{kj}}{\partial T} = \frac{n_{kj} - N_{kj}}{\tau_{kj}} \quad (7.2)$$

where τ_{kj} is a relaxation time. The right-hand side reflects the fact that in this approximation the scattering process restores the phonon distribution to the thermal equilibrium distribution at a rate proportional to its departure from the equilibrium value.

Thus the departure of the phonon distribution from its equilibrium value in equation (7.2) can be put into equation (2.17) for heat flow, rewritten for simplicity for the z -axis

$$\mathcal{H} = - \sum_{kj} \hbar \omega_j(k) c_{kj} \tau_{kj} \frac{\partial N_{kj}}{\partial T} \frac{\partial T}{\partial z} \quad (7.3)$$

From equation (2.18) ($\kappa = -\mathcal{H}/\Delta T$) this permits one to calculate the thermal conductivity coefficient, κ , which is

$$\kappa = \sum_{kj} \hbar \omega_j(k) c_{kj}^2 \tau_{kj} \frac{\partial N}{\partial T} . \quad (7.4)$$

For the Debye crystal and heat capacity model, equation (7.4) can be written as

$$\kappa = \frac{k_B}{2\pi^2 v_g} \left(\frac{k_B}{\hbar} \right)^3 T^3 \int_0^{\theta_D/T} \tau(x) \frac{x^4 e^x}{(e^x - 1)^2} dx . \quad (7.5)$$

If the relaxation time is expressed as the ratio of a mean free path of a phonon to its velocity then equation (7.5) corresponds exactly ($\kappa = 1/3 v \int C(x) l(x) dx$, where $C(x)$ is the heat capacity) to κ derived from kinetic theory (equation (1.1)). Thus the temperature dependence of κ described in the General Preamble is a result of the behaviour of heat capacity (Section 2.2) and the mean free path l (limited due to scattering at high temperatures and due to sample dimension and/or defect concentration at low temperatures). The ideal case of the temperature evolution of κ , with main heat resistant mechanisms depicted in the relevant temperature regions, is shown in Figure 7.1.

In the relaxation time approach due to Callaway¹⁶¹ it is assumed that all scattering processes act independently and the total rate of scattering, τ_R^{-1} , can be expressed as

$$\tau_R^{-1} = \tau_S^{-1} + \tau_P^{-1} \quad (7.6)$$

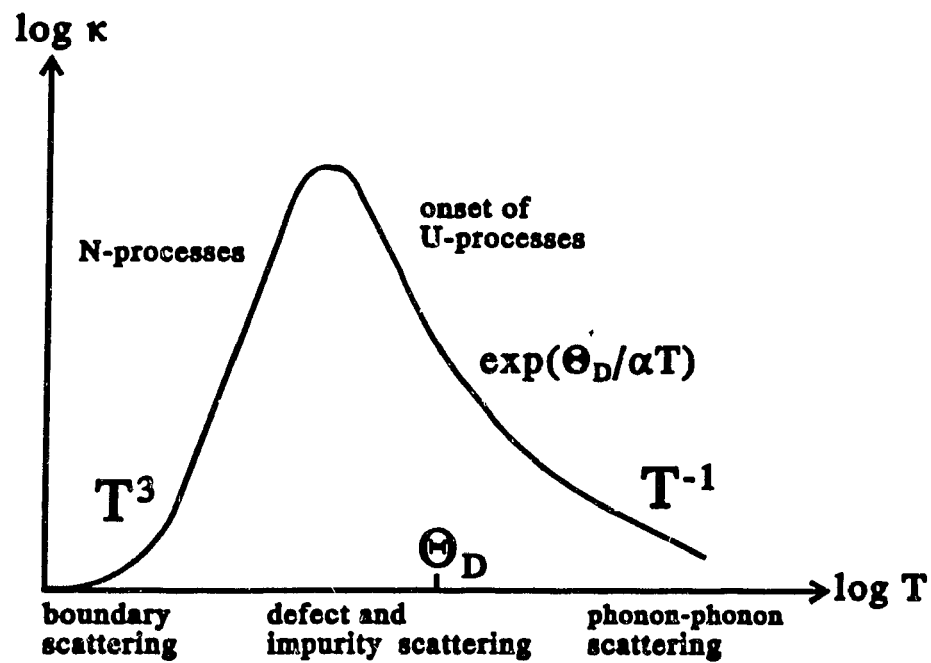


Figure 7.1 Schematic illustration of a typical temperature profile of the thermal conductivity for an insulating crystal depicting the major processes and mechanisms responsible for the thermal resistance in particular temperature regions.

where τ_S is the phonon relaxation time ascribed to different mechanisms of elastic scattering (the equivalent total scattering rate is a sum of the particular scattering rates) and τ_P is due to phonon-phonon scattering. Callaway assumed that the Normal processes also contribute to the thermal conductivity and the rate of change of the phonon distribution is^{62,161}

$$\frac{\partial n}{\partial t} = -\frac{n-N}{\tau_R} - \frac{n-N'}{\tau_N} \quad (7.7)$$

where τ_N is due to N-processes. This yields the thermal conductivity as a sum of two components κ_1 and κ_2 , *i.e.*¹⁶¹

$$\kappa_1 = C \int_0^{\theta/T} \frac{\tau_{tot} x^4 e^x}{(e^x - 1)^2} dx \quad (7.9)$$

and

$$\kappa_2 = C \frac{\left(\int_0^{\theta/T} (\tau_{tot}/\tau_N) x^4 e^x (e^x - 1)^{-2} dx \right)^2}{\int_0^{\theta/T} (\tau_{tot}/\tau_N \tau_R) x^4 e^x (e^x - 1)^{-2} dx} \quad (7.10)$$

where $C = k_B^4 T^3 / (2\pi^2 v \hbar^3)$. Thus if N-processes are dominant, $\tau_P \approx \tau_N$ and $\tau_U \gg \tau_N$, and κ_2 is the main term. If resistive processes are dominant, $\tau_P \approx \tau_U$ and $\tau_N \gg \tau_U$, and κ_1 is a major component. For the case when all resistive processes are excluded $\tau_U \rightarrow \infty$ and $\tau_P = \tau_N$. The denominator of equation (7.10) approaches 0 and the thermal conductivity tends to infinity as required for a perfect crystal.

7.2 RÉSUMÉ OF THE EXPERIMENTAL METHOD

Thermal conductivity of solids can be determined by a number of experimental techniques, the application of which depends on the type of sample, the temperature range as well as the range of thermal conductivity values.¹⁶² Although in principle the measurements are not overly complicated the thermal conductivity determination is laborious and tedious. The various techniques fall into two classes: the non-steady state methods and steady-state methods. In the former, the temperature distribution in the sample varies with time and it is thermal diffusivity, λ_d , (where $\lambda_d = \kappa \rho^{-1} C_p^{-1}$) which is determined through measurements of the rate of the temperature change.

In steady-state methods the sample is subjected to a time-invariant temperature profile. The thermal conductivity is determined directly by simultaneous measurement of the rate of heat flow per unit area and the temperature gradient after steady-state conditions have been reached. This experimental approach was utilized here.

The determination of thermal conductivity was carried out using the standard steady-state potentiometric method¹⁶³ in which heat is supplied at a known rate dQ/dt at one end of a single crystal sample of cross-sectional area \tilde{A} and this heat is removed at the other end. Thermometers are attached at two places along the sample at a separation d . The thermal conductivity, κ , is given by

$$\kappa = \frac{(dQ/dt)d}{\tilde{A}\Delta T} \quad (7.11)$$

where ΔT is the temperature difference between the thermometers. In the present measurement the value of κ at a given temperature was obtained from a linear fit of (dQ/dt) as a function of ΔT with several different power values and the consequent variation in temperature gradients. In this way the random errors due to temperature differential determinations were minimized. A typical plot is shown in Figure 7.2.

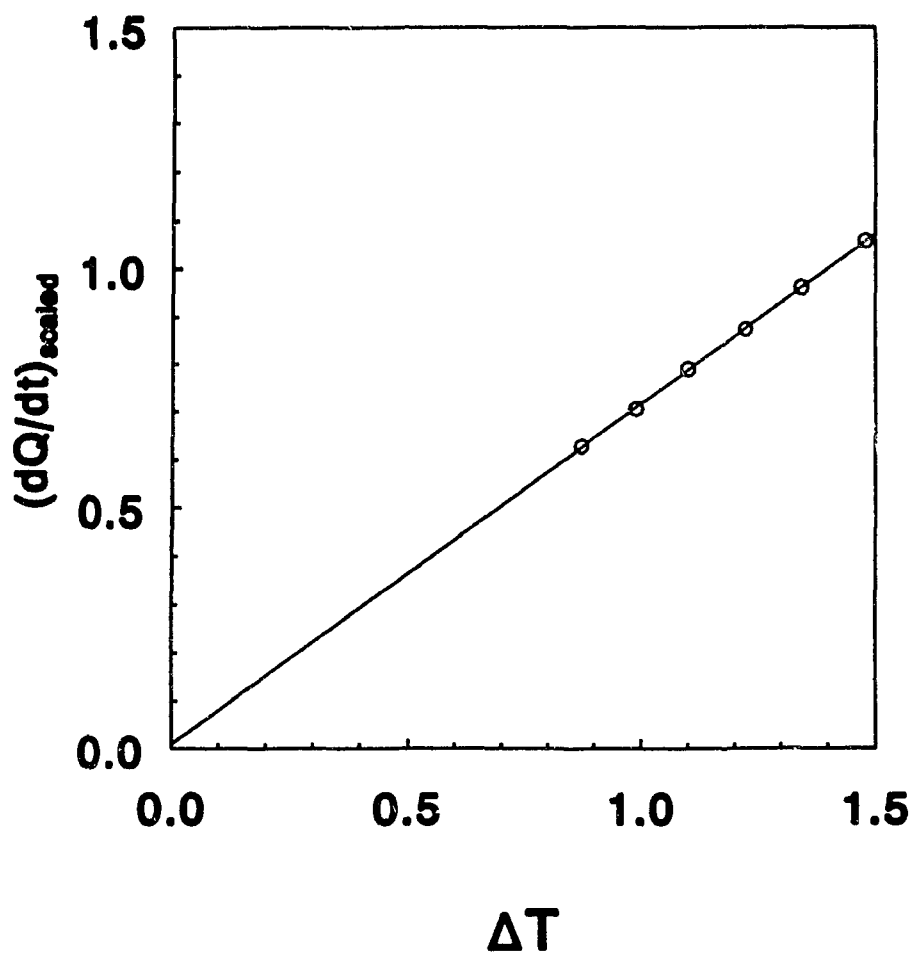


Figure 7.2 A typical plot for Dianin- CCl_4 of the scaled rate of heating, $(dQ/dt)_{scaled}$ (where $(dQ/dt)_{scaled} = \tilde{A}^{-1} d(dQ/dt)$), as a function of the temperature difference, ΔT , between the thermocouple junctions. The measurement was taken at the temperature 146.6 K yielding $\kappa = 0.71 \text{ W m}^{-1} \text{ K}^{-1}$. The thermal conductivity is a slope of the linear fit as shown.

7.3 EXPERIMENTAL PROCEDURE

7.3.1 EXPERIMENTAL SETUP

A schematic diagram of the apparatus for thermal conductivity measurements is shown in Figure 7.3. It utilizes the previously described potentiometric steady-state method. It had been tested by measurements of a high-purity single crystal of NaCl (Harshaw) and results were found to be within the range of the literature values.^{81,82}

This fully automated experimental setup consisted of a platinum resistance thermometer and a constant current power supply, an adiabatic shield and its heater, a digital multimeter Hewlett-Packard 34401A, an Artronix 5301-E shield controller, a vacuum system, the heaters for the crystal and for the heat sink, and a personal computer (PC IBM clone) for data collection.

The sample was mounted on the copper heat sink (Figure 7.3). The platinum resistance thermometer (Pr-100B, Cryoc Inc., St. Paul, Minnesota, R (25° C) ~ 100 Ohms) was placed inside the central cavity of the heat sink. It was secured underneath by a protective lid. The heat sink had 43 SWG Karma wire (230 Ohm/m; 600 Ohms resistance) bifilarly wound around it to provide required heating in order to raise and/or maintain the required temperature. The heat sink was mounted below the thermal anchor by means of copper rods that went through the perimeter of the heat sink.

The role of thermal anchor is to provide a thermal buffer for electrical leads that go outside this system.

The adiabatic shield, which performed the same function as in the adiabatic

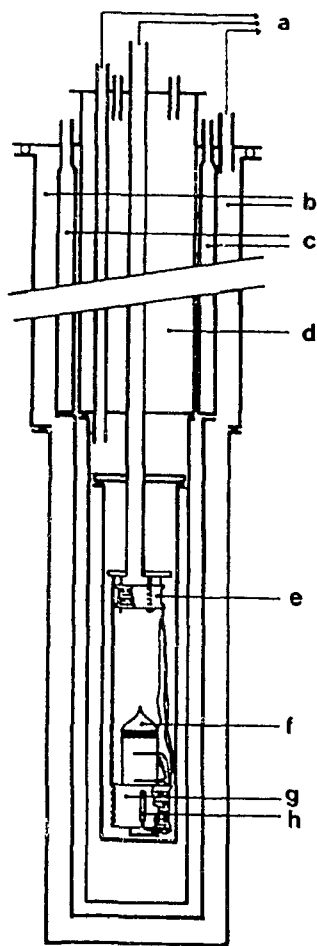


Figure 7.3 Plan of the thermal conductivity apparatus.⁸² The following letters denote: a) connection to the vacuum system, b) vacuum, c) liquid nitrogen, d) either liquid nitrogen or liquid helium, e) thermal anchor, f) single crystal with heater and thermocouples, g) copper heat sink and h) Pt resistance thermometer.

calorimeter, was placed around the sample. One copper-constantan thermocouple junction was varnished (GE 7031, Tri Research, Inc) to the inside wall of the shield, another was placed below a small detachable monel plate affixed to the top of the heat sink. This plate was used as a base for the crystal sample. An Artronix-E shield was used as a constant current power supply for the shield. The shield was suspended just above the heat base by nylon filaments attached to the thermal anchor.

A computer program, developed for this experimental setup, allowed for taking all electrical readings, *i.e.* heater resistance, heater voltage, thermocouple emf and resistance ratio of the platinum resistance device relative to a standard resistor; it also controlled all conditions by changing relevant variables. This totally automated the operation of the apparatus.

The vacuum system that provided thermal insulation consisted of a roughing pump and an oil diffusion pump. The pressure during experiments was lower than 10^{-5} Torr. Each of three separate regions of the cryostat (Figure 7.3) had its own valve allowing appropriate handling of the thermal conditions. The temperature range of experiments (30 K to 210 K) was limited by heat leaks in the low-temperature region and heat losses at high temperatures.

The cryostat in this apparatus was of the aneroid type. The cylindrical reservoirs for refrigerants had been placed centrally on the top of the setup in such a way that one was surrounded by another. Liquid nitrogen and liquid helium were used to carry out measurements in relevant temperatures. The outer chamber was filled with liquid nitrogen during the whole experiment. Depending on the

temperature range, either liquid nitrogen or liquid helium was in the inner chamber (above or below 77 K, respectively).

At the beginning the whole system was evacuated and an exchange gas (helium) was allowed into the middle region of the cryostat in order to facilitate cooling. In order to decrease the temperature below 77 K exchange gas was also pumped into the innermost chamber. In either case the gas was removed before commencement of the data collection.

The overall uncertainty in the determination of the thermal conductivity was assessed to *ca.* $\pm 20\%$. It stems from systematic errors in the determination of the cross-sectional area ($\pm 10\%$) and the thermocouple separation distance ($\pm 5\%$), and from random errors from the temperature differential ($\pm 3\%$) and the power input ($\pm 3\%$).

The power applied to the crystal heater was chosen to optimize conditions of the data collection. An increase of signal-to-noise ratio was achieved by a reasonably high temperature gradient, *i.e.* such that it did not jeopardize crystal mechanical stability. Thus a temperature difference between the thermocouple junctions ranged between 0.7 K to 1.8 K during measurements.

7.3.2 SAMPLE PREPARATION

The thermal conductivities of the CCl_4 clathrate of Dianin's compound and the CBr_4 clathrate of HPTB were measured. The crystal structure and method of growth of have already been described in Chapter 3.

The crystals produced were colourless and transparent with no cloudiness or internal cracks. The uniformity of extinction of polarised light inspected on an optical microscope for all orientations confirmed that crystals were single with respect to twinning and grain boundaries.

The Dianin- CCl_4 crystal used in the experiment was 3.5 mm in maximum lateral dimension and 17.0 mm long, with a cross-sectional area of 7.5 mm^2 . The lateral dimension measurement was done using a polarizing microscope equipped with an engraved scale. The crystallographic c -axis was identified by morphological inspection and goniometry as the longitudinal direction, along which κ was measured.

One end of the crystal was polished to allow a good contact of the crystal sample with the monel plate on the heat sink. This was done using a filter paper soaked in CCl_4 .

A crystal heater was wrapped on the other end of the sample. Karma wire (approximately 32 cm long; resistance of 66 Ohms) was folded in half to allow bifilar winding. Varnish (GE 7031, Tri Research, Inc) was used to attach the heater to the crystal.

The temperature gradient (ΔT ; *vide infra*) was determined using the AuFe (one piece; 0.08 mm in diameter and 125 mm long, 0.03%Fe)/Chromel (two pieces;

0.08 mm in diameter and 150 mm long each) differential thermocouples (Johnson Matthey; provided and calibrated by Cryogenic Calibrations Ltd., England with accuracy ± 0.05 K in the investigated temperature region). The AuFe thermocouple wire of this length minimized the flow of heat along the thermocouple wires. The thermocouple wires were coiled prior to welding to expedite their final placement inside the shield. The junctions were made with spark welding in a helium atmosphere.¹⁶⁴ They were attached symmetrically to the crystal with varnish (GE 7031, Tri Research, Inc). The separation between them for Dianin- CCl_4 was 8.630 mm, determined by means of a travelling microscope originally used for measuring Debye-Scherrer films with accuracy ± 0.001 mm.

The crystal was kept in thermal contact with the monel plate by general purpose silicone sealant (no. 67-0859-0, Canadian Tire).

The above procedure was repeated to prepare the HPTB- CBr_4 crystal. These crystals grew as rhomboids so definite determination of the direction of heat flow after appropriate polishing with the filter paper soaked with chloroform was not possible. The crystal used in the experiment was 4.0 mm in maximum lateral dimension and 6.4 mm long with a cross-sectional area of 14 mm^2 . The junctions of the thermocouple were placed symmetrically with the separation of 2.375 mm. Since chloroform is not trapped into the clathrate cavities and it is volatile, it was used in this case to solvate GE varnish to facilitate the sample preparation.

In order to prevent any damage to the HPTB- CBr_4 crystal due to possible guest escape, after the crystal placement in the thermal conductivity apparatus but prior to

evacuation of the cryostat, the crystal was cooled to about 250 K. A similar procedure was used in the case of THF clathrate hydrate.⁸²

7.4 RESULTS AND DISCUSSION

7.4.1 THE CCl_4 CLATHRATE OF DIANIN'S COMPOUND

7.4.1.1 EXPERIMENTAL FINDINGS

The temperature profile of the thermal conductivity of the CCl_4 clathrate of Dianin's compound is shown in Figure 7.4, and the data are presented in Table 7.1. In contrast with most simple crystalline materials in which $(\partial\kappa/\partial T)$ is negative in this temperature range ($T \approx$ Debye temperature), $(\partial\kappa/\partial T)$ is positive for Dianin- CCl_4 throughout the temperature range of this experiment (60 to 210 K); a similar result was found for Dianin- $\text{C}_2\text{H}_5\text{OH}$ and for the clathrand.⁸⁶

The results show that κ for Dianin- CCl_4 is virtually identical with values found for the corresponding clathrand, whereas κ of the ethanol clathrate is significantly lower than that of the clathrand.⁸⁶ This is somewhat surprising in light of the thermal expansion (which, like thermal conductivity, reflects anharmonic intermolecular interactions) of Dianin- CCl_4 ,⁹⁹ which is slightly greater than the clathrand but slightly less than Dianin- $\text{C}_2\text{H}_5\text{OH}$; similar ordering of thermal conductivities might have been expected. It appears that the thermal expansivity and the thermal conductivity reflect different subtleties of the anharmonicity of the intermolecular interaction.

Similarly, if guest concentration were the dominant factor in controlling κ , as would be the case, for example, if the guests were scattering phonons as hypothetical point defects,⁸⁴ the CCl_4 clathrate of Dianin's compound (with one guest molecule per cage) would be expected to fall intermediate between the clathrand (no guests) and the ethanol clathrate (two guest molecules per cage). That Dianin- CCl_4 is more like the

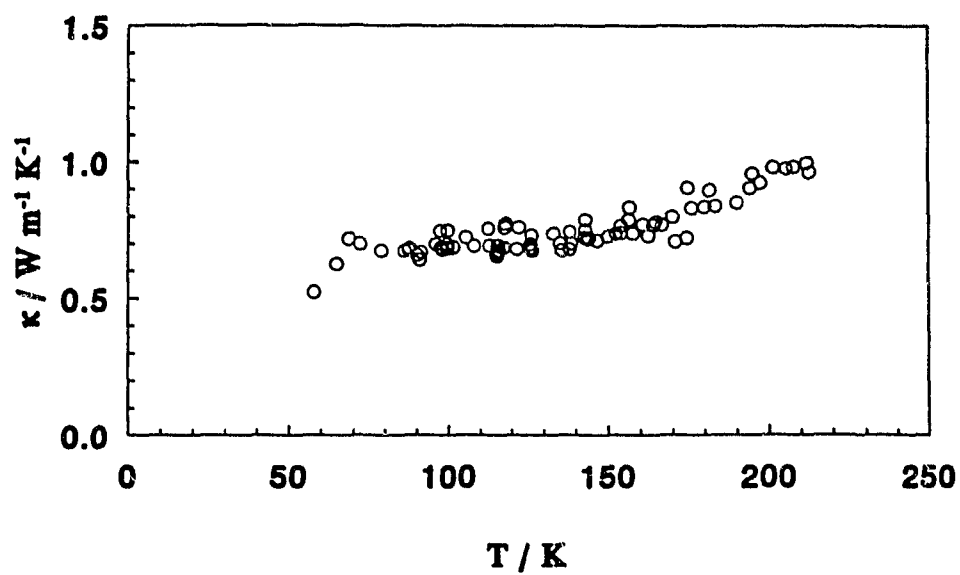


Figure 7.4 The thermal conductivity of Dianin- CCl_4 as determined in this experiment.

Table 7.1 The thermal conductivity of the CCl_4 clathrate of Dianin's compound.

T	κ	T	κ	T	κ
[K]	[W K ⁻¹ m ⁻¹]	[K]	[W K ⁻¹ m ⁻¹]	[K]	[W K ⁻¹ m ⁻¹]
57.78	0.523	126.00	0.685	183.43	0.839
64.90	0.626	126.11	0.731	190.12	0.852
68.58	0.719	126.17	0.730	194.27	0.905
72.20	0.700	126.30	0.675	195.16	0.959
78.88	0.675	132.81	0.737	197.52	0.924
86.28	0.674	134.94	0.702	201.54	0.981
87.68	0.678	135.52	0.676	205.57	0.978
87.73	0.683	138.00	0.681	207.99	0.983
90.28	0.659	138.04	0.744	211.98	0.996
90.95	0.642	138.50	0.702	212.73	0.962
91.34	0.670	142.71	0.723		
96.00	0.699	142.90	0.751		
97.31	0.747	142.92	0.789		
97.50	0.686	143.67	0.718		
98.07	0.678	144.00	0.721		
99.50	0.685	146.61	0.712		
99.60	0.698	149.98	0.728		
99.68	0.748	152.45	0.738		
99.70	0.685	154.00	0.766		
101.50	0.686	154.07	0.740		
105.38	0.723	156.46	0.788		
107.98	0.693	156.78	0.834		
112.59	0.755	157.71	0.738		
113.00	0.693	160.74	0.771		
115.42	0.665	162.33	0.730		
115.44	0.656	164.00	0.768		
115.73	0.692	164.59	0.781		
116.00	0.674	166.55	0.769		
117.50	0.684	169.87	0.800		
117.84	0.760	170.77	0.709		
118.00	0.773	174.31	0.723		
121.60	0.681	174.59	0.906		
122.11	0.760	175.88	0.832		
125.82	0.699	180.05	0.837		
125.99	0.686	181.58	0.896		

clathrand indicates that the type (not concentration) of guest plays an important role in determining thermal conductivity in this system (*vide infra*).

In light of the finding that the clathrand, the ethanol clathrate and the CCl_4 clathrate of Dianin's compound all show similar temperature profiles, with characteristics more usually associated with glassy materials than with crystalline solids, it is appropriate to begin the discussion of origins of thermal resistance in systems with similar features.

7.4.1.2 GLASSY-LIKE BEHAVIOUR

In most other crystalline materials exhibiting the same type of thermal behaviour, highly effective thermal resistance mechanisms were found on the basis of individual (system-specific) analysis. For example, in alkali cyanide mixed crystals the ability of the cyanide ions to perform rotational motions at high temperature resulting in low-energy states seems to be the origin of the thermal conductivity behaviour.¹⁶⁵ In Zr:Nb alloys small atomic motions cause fluctuations between two coexisting phases and thus give rise to low-energy states.¹⁶⁶

Universal behaviour of glass-like thermal conductivity can be deduced if a scaling procedure rewriting the thermal conductivity in a universal dimensionless form is employed. This is given by⁶⁷

$$\kappa(T)/\text{K} = \left(\frac{T}{\theta_D} \right)^3 \int_0^{\theta_D/T} \frac{k_B \theta_D \tau}{h} \frac{x^4 e^x}{(e^x - 1)^2} dx \quad (7.12)$$

where $\mathbf{K} = 4\pi k_B^3 \theta_D^2 / (\hbar^2 \nu)$, the Debye temperature θ_D is 170 K here,⁵⁶ and τ is the total relaxation time. It is believed that external modes are principally responsible for mechanical properties of organic molecular crystals. Here, as well as in all other relevant expressions, by virtue of the experimental findings that the structure of the clathrates of Dianin's compound is insensitive to the presence of the guest, the value of $\nu = 2250 \text{ m s}^{-1}$ reported for the ethanol clathrate of Dianin's compound⁸⁶ was used for the CCl_4 clathrate. The scaling of equation (7.12), applied to the Dianin clathrates (ethanol clathrate and now CCl_4 clathrate) puts them into the same pattern of the temperature evolution as for many glassy materials.

The scaled κ for the crystals investigated here (Dianin- CCl_4 and HPTB- CBr_4), as well as for other materials exhibiting typical glass-like temperature evolution of the thermal conductivity are shown on Figure 7.5.

7.4.1.3 MEAN FREE PATH

Preliminary examination of κ of Dianin's clathrates using the temperature-dependence of the phonon mean free path derived from the Debye formula once again indicates similarity with glassy materials. The phonon mean free path, derived from the Debye formula (equation (1.1)), in the CCl_4 clathrate (and other Dianin's systems) is shown in Figure 7.6. The mean free path drops from 30 Å to about 10 Å (very similar to the decrease for the clathrand) and from above 10 Å to about 5 Å in the ethanol clathrate. The short mean free path suggests that rather localized oscillations are partly responsible for the behaviour of the thermal conductivity, and these are

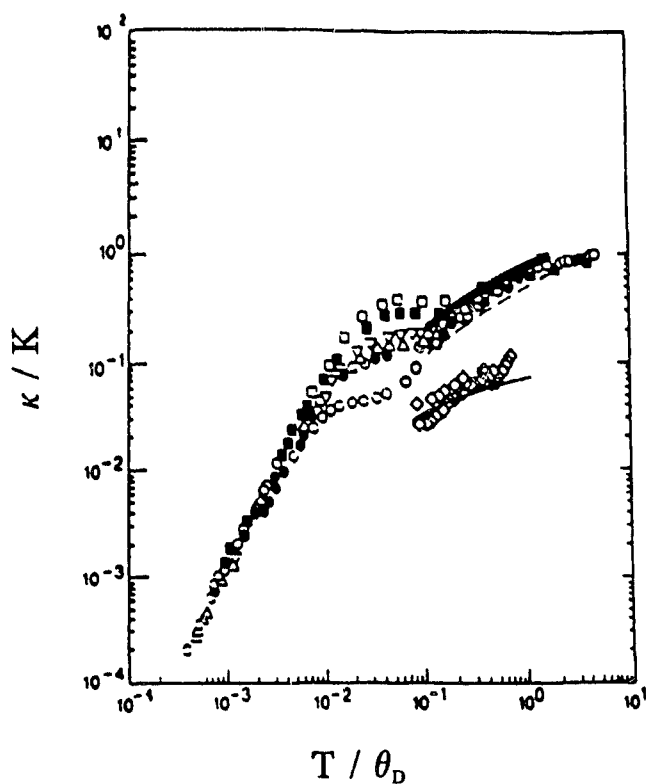


Figure 7.5 The scaled thermal conductivities for Dianin- CCl_4 and HPTB- CBr_4 , and other materials exhibiting similar types of glass-like thermal behaviour. Abbreviations: \circ is SiO_2 , \blacktriangle is B_2O_3 , \square is polybutadiene, ∇ is poly(ethylene terephthalate), \bullet is polystyrene, \blacksquare is poly(methyl methacrylate),⁶⁷ \diamond is the tetrahydrofuran clathrate hydrate.⁸² Heavy solid line is Dianin- CCl_4 , light solid line is HPTB- CBr_4 , and the dashed line is Dianin- $\text{C}_2\text{H}_5\text{OH}$.⁸⁶

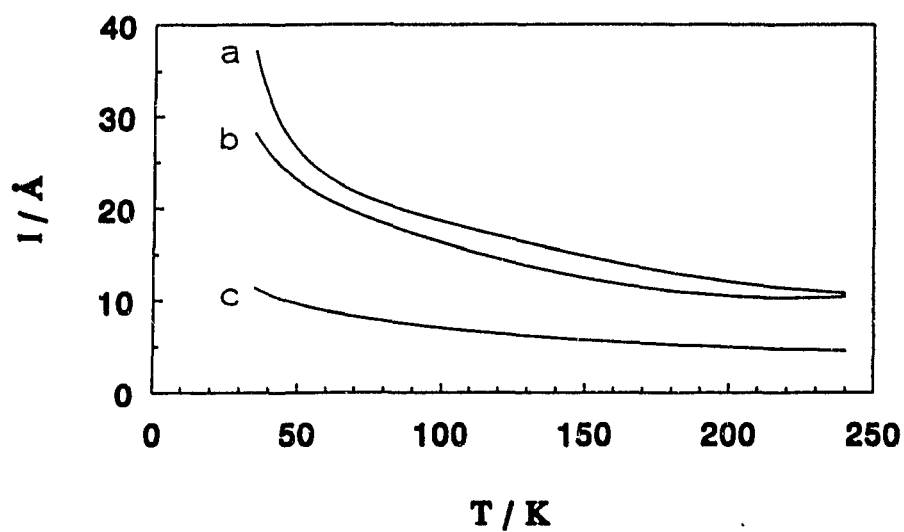


Figure 7.6 Phonon mean free paths as functions of temperature as calculated from equation (1.1); (a) the clathrand of Dianin's compound; (b) Dianin- CCl_4 ; (c) Dianin- $\text{C}_2\text{H}_5\text{OH}$. Data for (a) and (c) are taken from refs. 55 and 86.

more localized for Dianin-C₂H₅OH than for Dianin-CCl₄ or the clathrand.

7.4.1.4 MINIMUM THERMAL CONDUCTIVITY

In studies of glasses, the concept of "minimum thermal conductivity" has attracted considerable attention. In Slack's model¹⁶⁷ of the minimum thermal conductivity the minimum phonon mean free path is arbitrarily assumed to be of the order of one phonon wavelength. κ of the clathrand of Dianin's compound is greater than the predicted minimum thermal conductivity, $\kappa_{Smin\infty}$, by a factor of 30.⁸² Slack's model extrapolates phenomenological theory of heat resistivity of perfectly ordered structures to topologically disordered systems. A similar concept, but of different origin, was proposed by Cahill and Pohl⁶⁸ who modified Einstein's classical analysis of coupled oscillators by inclusion of Debye's model of lattice vibrations and larger oscillating entities. The physical picture of energy transport is that of a random walk of energy between near-neighbour localized quantum-mechanical oscillators of varying sizes and frequency. Although both models seem to be similar they differ significantly in the physics of the phenomena. Slack postulates that heat is always carried by waves and for this to be true the mean free path cannot be shorter than one wavelength. This assumption seems to be controversial since it is difficult to accept that waves that short are present in a crystal. On the other hand the Cahill-Pohl approach is based on independent oscillators with a lifetime of one half of the period of vibration ($\omega=2\pi/\lambda$ where $\lambda=2d$ and d is the size of the site in the crystal) and this appears to depict heat transport more realistically.

In Cahill-Pohl model the minimum thermal conductivity, κ_{CP} , for a single polarization i is given by⁶⁸

$$\kappa_{CP} = \left[\frac{\pi}{6} \right]^{1/3} k_B n_d^{2/3} v_i \left[\frac{T}{\theta_i} \right]^2 \int_0^{\theta_i/T} \frac{x^3 e^x}{(e^x - 1)^2} dx \quad (7.13)$$

where v_i is the speed of sound for this polarization, $\theta_i = v_i \hbar (6\pi^2 n)^{1/3} / k_B$ is the cutoff frequency for this polarization and n_d ($= 6$ per Dianin's molecule⁵⁶) is the number density of rigid groups. Although the phonon mean free path above 70 K (Figure 7.6) becomes so short that lattice vibrations seem to be more appropriately described as those of damped oscillators with random phases, the Cahill and Pohl approach yielded minimum values of κ for the Dianin system only slightly larger than those obtained from Slack's model. This indicates that phonon-phonon scattering causing thermal resistance is at less than maximum effectiveness in the Dianin system, in contrast with mixed crystals such as $\text{KBr}_{1-x}(\text{CN})_x$ which approach the minimum calculated thermal conductivity.¹⁶⁸

7.4.1.5 RESONANCE SCATTERING MODEL

The Callaway relaxation-time approach for a Debye crystal was used to analyze the experimental data. Theoretical prediction of κ relies on the postulate concerning the phonon scattering rate, τ^{-1} ,

$$\tau^{-1} = \sum_i \tau_i^{-1}, \quad (7.14)$$

i.e. it is the sum of all independent scattering rates. Since even a rudimentary look at the character and values of the thermal conductivity of Dianin-CCl₄ shows that thermal resistant mechanisms are much in effect, κ is approximated by the first component of Callaway's model, *i.e.*

$$\kappa(T) = \frac{1}{2\pi^2 v} \int_0^{\omega_p} \tau \frac{\hbar^2 \omega^4}{k_B T^2} \frac{e^{\hbar\omega/k_B T}}{(e^{\hbar\omega/k_B T} - 1)^2} d\omega . \quad (7.15)$$

In this case the overall phonon scattering rate, τ^{-1} , consists of three different terms, *viz.*: τ_U^{-1} , phonon-phonon Umklapp scattering rate; τ_B^{-1} , boundary scattering rate; τ_R^{-1} , resonant scattering rate.

The postulate of resonant scattering follows from studies of clathrate hydrates, Dianin's compounds, and other systems, in which one can distinguish groups that give rise to low-frequency optic modes that can act as scatterers for acoustic phonons.^{82,86,169} For example, molecular dynamics studies of clathrate hydrates revealed coupling between the low-frequency translational and vibrational motion of the guest molecules with the host lattice motion,¹²⁶ confirmed for CH₄ clathrate hydrate by incoherent inelastic neutron scattering,¹⁷⁰ and these localized modes might scatter thermal phonons quite effectively, resulting in low thermal conductivity. Motion of the guest molecule in the cages, as deduced from analysis of the heat capacity of THF clathrate hydrate⁵⁴ and Dianin-C₂H₅OH,⁵⁵ has been proposed as a source of resonance scattering in these systems. The low value of the elastic constant, c_{44} ($= 0.44 \times 10^{10}$ N m⁻²), for the ethanol clathrate of Dianin's compound¹¹⁹ is

characteristic of soft transverse modes that are prone to rotational-translational coupling that might have an effect on the thermal behaviour. Furthermore, the Cauchy (elastic constant) ratio, c_{11}/c_{44} , for the ethanol clathrate of Dianin's compound¹¹⁹ is 1.48; as was mentioned in Section 4.4.2, values of this ratio exceeding unity have been associated with rotational-translational coupling in N₂, CO and Ar-O₂ mixtures,^{118,130} and this could also be the case with the Dianin's system. This is in accord with conclusions concerning mixed crystals where glass-like behaviour was associated with motion¹⁶⁵ and with conclusions from a study of thermal properties of a crystalline polymeric molecular solid where acoustic phonons appear to be scattered by low-energy modes arising from the motions of hydrocarbon side chains.¹⁶⁹ The interaction between low-frequency librational motions of anions and acoustic modes has been shown to take place in crystalline KCl doped with NO₂⁻ and CN⁻.¹⁷¹

Because the thermal conductivities of the clathrates and the clathrand of Dianin's compound are qualitatively unchanged by the presence of the guests, the dominant role in the thermal resistivity mechanism in this system can be identified with scattering from modes which arise from internal degrees of freedom of the host molecule. Methyl groups with frequencies of the order of 10¹¹ s⁻¹ estimated from ¹³C NMR¹⁷² seem to be the most likely candidates for scattering.

The theoretical Umklapp scattering rate in the analysis of the thermal conductivity of the CCl₄ clathrate of Dianin's compound is taken after Klemens¹⁷³

$$\tau_U^{-1} = B \omega^2 T e^{-\frac{\theta_D}{\alpha T}} \quad (7.16)$$

where B and α are empirical parameters. Sometimes, in order to take into account the relative role of Umklapp and Normal processes, the preexponential temperature dependence takes the form, T^η , with η ranging from 1 to 8 (*e.g.* Berman and Brock assume quadratic dependence,¹⁷⁴ Callaway and von Baeyer assume cubic¹⁷⁵).

Uncertainty in the determination of the Umklapp scattering rate may also arise from the assumed isotropy of a crystal. Anisotropy may cause extra collisions with different frequency dependencies.

The boundary scattering rate, τ_B^{-1} , is given by^{176,177}

$$\tau_B^{-1} = \frac{v}{1.18 \bar{d}} \quad (7.17)$$

where \bar{d} is the diameter of the sample.

The general form of the resonant scattering rate, τ_S^{-1} , is given by^{171,178}

$$\tau_S^{-1} = GD \frac{\omega_0^2 \omega^2}{(\omega_0^2 - \omega^2)^2} \quad (7.18)$$

where G is the concentration of the scatterers (*i.e.* the number of scatterers per unit volume), D is related to the strength of the optic-acoustic coupling and ω_0 is the optical vibrational frequency involved in the resonant scattering.

This model assumes two different contributions to resonant scattering in the

CCl₄ clathrate of Dianin's compound. One stems from the motion of the methyl groups of the host lattice, and the other is from motions of the CCl₄ guest molecule. (These concentrations vary with temperature according to the thermal expansion,⁹⁹ but the small temperature variation of G had no noticeable effect on the resulting fit. At $T = 200$ K, G is 7.8×10^{27} m⁻³ for the methyl groups and 0.4×10^{27} m⁻³ for the CCl₄ molecules.) The dependence of the motion of the methyl groups on the included guest is the basis for treating these scatterers as free parameters in the fit.¹⁷²

The experimental data was least-squares fitted within the described model. The resulting fit is shown, along with the experimental data, in Figure 7.7. The values of B and α extracted from the fit are 1.40×10^{-19} s K⁻¹ and 1.55, respectively. The values of ω_0 and D for the methyl groups are 4.57×10^{11} s⁻¹ and 1.40×10^{-13} m³ s⁻¹, respectively; ω_0 and D for the carbon tetrachloride molecule are 1.65×10^{12} s⁻¹ and 1.40×10^{-13} m³ s⁻¹, respectively.

The values of resonant frequencies should not be taken too literally, as thermal conductivity data do not yield high-resolution spectroscopic information concerning vibrations in solids, especially in complex structures like Dianin's compounds or hydrates.

The physical picture of heat transport that takes into account contributions from only two resonant scatterers (the host lattice and the guest molecule) might be a reasonable simplification of the real processes in Dianin-CCl₄. The larger the value of D , the more effective the resonant coupling between the optic and the acoustic modes is, which leads to reduced thermal conductivity. The clathrand yields the same

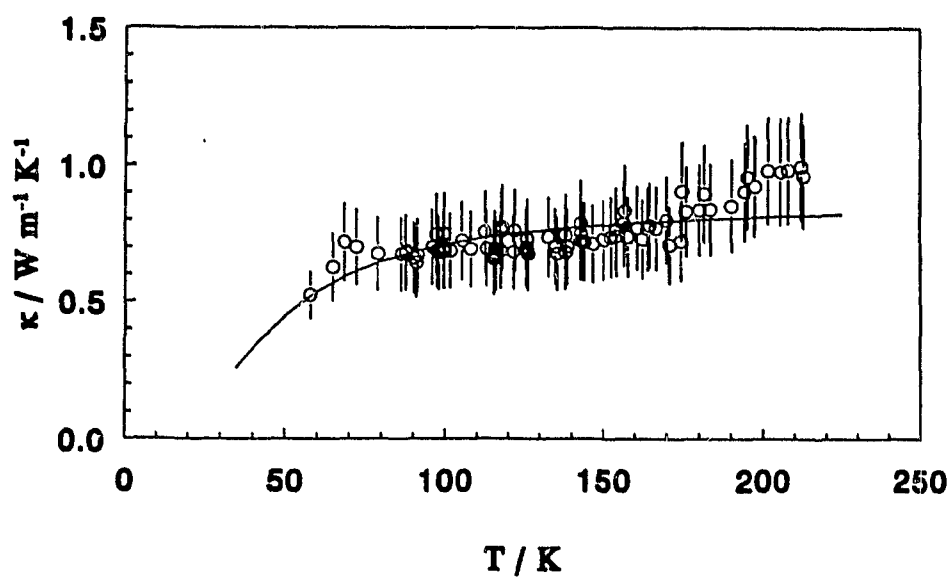


Figure 7.7 The experimental thermal conductivity of the CCl_4 clathrate of Dianin's compound (\circ and error bars) and the least-squares fit to the resonant-scattering model ($-$), as described in the text.

value of the resonant coupling constant ($D = 1.4 \times 10^{-13} \text{ m}^3 \text{ s}^{-1}$)⁸⁶ as Dianin- CCl_4 , and the resonant coupling parameters for the methyl groups and the guest in the ethanol clathrate are larger (both are $1.6 \times 10^{-13} \text{ m}^3 \text{ s}^{-1}$).⁸⁶ These findings are consistent with the experimental observation of similar thermal conductivities for Dianin- CCl_4 and the clathrand, and lower values for Dianin- $\text{C}_2\text{H}_5\text{OH}$.⁸⁶

7.4.1.6 ROLE OF THE GUEST

This investigation appears to allow the first comparison of thermal conductivity of an inclusion compound with guests of significantly different molecular masses and shapes, fitting the cages in different ways. In the Dianin system, ethanol guests have a significant effect on the thermal conductivity⁸⁶ (reducing κ by about a factor of 2), whereas we have now found that CCl_4 guests leave the thermal conductivity virtually unchanged from the clathrand.

Since the Dianin system is one of the most often studied lattice inclusion assemblies, much is known about its physical properties. This allows more detailed consideration of factors that results in the unusual thermal conductivity effects.

Several aspects of the system show little dependence on the presence and type of guest: the gross features of the host lattice structure are independent of the presence of guests;^{11,99} lattice dynamics of the Dianin host lattice are insensitive to the presence and type of guest;¹⁷⁹ the velocity of sound is the virtually the same (within 3%) for the clathrand and Dianin- $\text{C}_2\text{H}_5\text{OH}$.⁵⁶ These facts indicate that the role of the guest in thermal conductivity in this system is not likely related to matters

concerning the host lattice *per se*.

Attention is turned now to guest species. The most striking difference between Dianin- CCl_4 and Dianin- $\text{C}_2\text{H}_5\text{OH}$ is the degree of dynamical disorder of the guest species.

In Dianin- CCl_4 , the guest is lodged in the cage, with its three-fold axis coincident with the three-fold axis of the host lattice, and with the axial Cl at the midpoint of the hour-glass-shaped cage (see Figure 3.3). NQR studies show only weak guest-host interactions in Dianin- CCl_4 .¹⁸⁰ An analysis of the heat capacity of Dianin- CCl_4 shows the guest molecule to behave much as CCl_4 in its ordered bulk solid state.⁵⁵ From analysis of the crystallographic data (thermal motion analysis), CCl_4 is found⁹⁹ to have librational frequencies of 40 cm^{-1} and 27 cm^{-1} , which compare well with the determinations of 47 cm^{-1} and 37 cm^{-1} from NQR studies.¹⁸⁰ Calculations¹⁸¹ based on atom-atom potential for Dianin- CCl_4 reveal a barrier to reorientation of the CCl_4 molecule of 22 kJ mol^{-1} , which is too high to allow the guest molecule to reorient freely in the cage. Therefore, the picture of the CCl_4 guest is a molecule trapped in the cavity, undergoing librations (mean squared amplitudes of libration of 10.7° with respect to the *c*-axis, and 7.2° with respect to the *a*- and *b*-axes at room temperature).⁹⁹

On the other hand, the ethanol molecules in Dianin- $\text{C}_2\text{H}_5\text{OH}$ are considerably freer to move in the cage. One indication of this comes from analysis of the heat capacity: ethanol guests experience degrees of freedom comparable to liquid ethanol.⁵⁵ A detailed single-crystal ^2H NMR study of Dianin- $\text{C}_2\text{H}_5\text{OH}$ has shown that

at temperatures as low as 60 K the ethanol molecules have rotational and translational degrees of freedom, and even at $T = 70$ K the two ethanol molecules can exchange places in their cage.¹⁸²

This picture — CCl_4 molecules held in their cage, and ethanol molecules free to move in their cage — is entirely consistent with the thermal conductivity results and the resonance scattering model. CCl_4 molecules are much less able to absorb the energy of the heat-carrying acoustic phonons, and the thermal conductivity of Dianin- CCl_4 is much like that of the host lattice, whereas the heat-carrying acoustic modes can interact with localized modes associated with motion of the ethanol molecules in Dianin- $\text{C}_2\text{H}_5\text{OH}$, decreasing the thermal conductivity. This picture is reinforced by the values of the resonance coupling constant from the fits to the experimental data.

7.4.2 THE CBr_4 CLATHRATE OF HPTB

7.4.2.1 EXPERIMENTAL FINDINGS

The temperature profile of the thermal conductivity of the CBr_4 clathrate of HPTB is shown in Figure 7.8. The data are presented in Table 7.2. The κ values are similar to that of the tetrahydrofuran clathrate hydrate.⁸¹ The temperature derivative of the thermal conductivity, as in other clathrates (*vide supra*), is positive in the temperature range of this experiment (30 K to 150 K).

In light of the previously described findings for Dianin- CCl_4 , HPTB- CBr_4 shows temperature evolution of κ more characteristic of glassy materials than for *most* crystalline solids where *most* here refers to systems that have been investigated.

7.4.2.2 GLASSY-LIKE BEHAVIOUR

Employing equation (7.12), the scaled thermal conductivity of this system falls into the same pattern that is characteristic for glassy materials (see Figure 7.5). Here the following values were used in this expression. The Debye temperature was assumed to be 135 K which is the average value for θ_D between 30 K and 90 K derived from the heat capacity data with $n=54$ (Section 6.4.5). θ_D ranges between 120 K and 155 K for temperatures from 30 K to 90 K; above 90 K, θ_D steeply decreases (shown in Figure 6.11). Since the measurements of κ are from 30 K to 150 K the above assumption seems to be reasonable. The average velocity of sound was assumed to be 1410 m/s (derived from the elastic constants; Section 6.4.5).

The mean free path as a function of temperature calculated from equation (1.1)

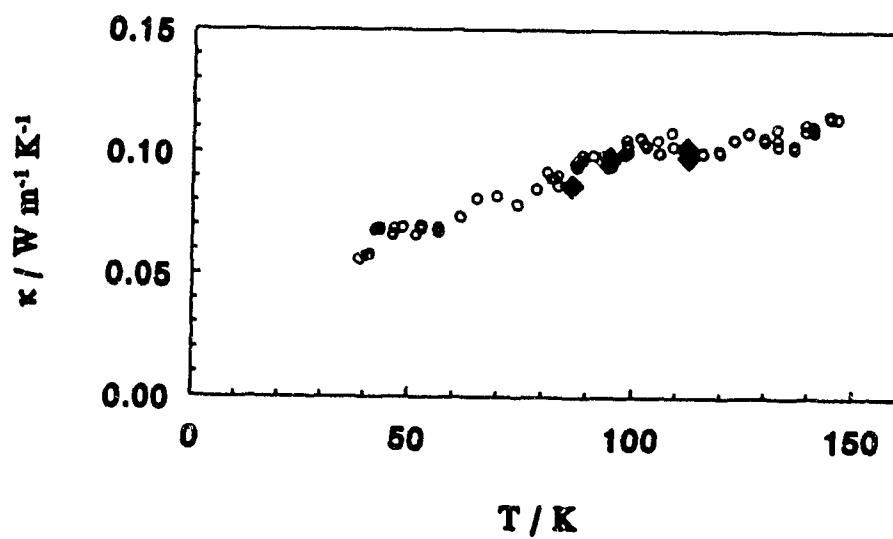


Figure 7.8 The experimental thermal conductivity of the CBr_4 clathrate of HPTB. (\blacklozenge denotes points taken for another crystal for which measurements were interrupted; the cross-sectional area of this crystal was 25.83 mm^2 , the distance between the thermocouple junctions was 3.5 mm).

Table 7.2 The thermal conductivity of the CBr_4 clathrate of HPTB.

T	κ	T	κ	T	κ
[K]	[W K ⁻¹ m ⁻¹]	[K]	[W K ⁻¹ m ⁻¹]	[K]	[W K ⁻¹ m ⁻¹]
38.66	0.0559	87.39	0.0956	101.72	0.1059
40.10	0.0574	87.54	0.0946	102.43	0.1039
41.11	0.0580	87.74	0.0941	102.70	0.1031
42.24	0.0679	87.90	0.0967	102.93	0.1026
42.50	0.0686	88.07	0.0963	103.09	0.1030
43.26	0.0685	88.28	0.0957	105.49	0.1053
43.37	0.0689	88.94	0.0990	105.69	0.1003
43.49	0.0681	88.98	0.0969	105.84	0.1002
46.34	0.0664	89.03	0.0971	106.07	0.1000
46.54	0.0660	89.09	0.0972	108.72	0.1087
46.66	0.0686	91.12	0.0989	109.01	0.1030
48.42	0.0689	91.21	0.0988	109.21	0.1027
48.62	0.0692	91.31	0.0989	112.26	0.1019
51.68	0.0662	93.37	0.0988	112.52	0.0985
52.49	0.0698	93.80	0.0972	112.66	0.0983
52.66	0.0684	94.08	0.0968	115.76	0.1004
52.83	0.0698	94.36	0.0972	115.91	0.0998
56.39	0.0682	94.67	0.0968	119.47	0.1013
56.54	0.0691	94.99	0.0978	119.60	0.1006
56.74	0.0673	95.09	0.0959	119.72	0.1005
61.53	0.0734	95.25	0.0946	122.91	0.1058
65.32	0.0810	95.38	0.0950	123.00	0.1058
69.82	0.0820	97.92	0.1003	123.10	0.1055
74.34	0.0787	98.11	0.0993	126.11	0.1087
78.67	0.0850	98.42	0.0995	126.23	0.1082
80.95	0.0920	98.58	0.1054	129.74	0.1065
81.89	0.0895	98.72	0.0999	129.84	0.1051
82.75	0.0893	98.73	0.1035	129.94	0.1053
83.52	0.0907	98.86	0.1030	132.60	0.1103
83.67	0.0864	98.98	0.1004	132.75	0.1057
86.67	0.0865	101.60	0.1063	132.88	0.1032

cont.

Table 7.2 continued...

T	κ
[K]	[W K ⁻¹ m ⁻¹]
136.62	0.1034
136.74	0.1022
139.24	0.1118
139.35	0.1094
140.92	0.1111
140.99	0.1098
141.13	0.1089
144.56	0.1158
144.69	0.1148
144.78	0.1155
146.22	0.1146
146.37	0.1148

is shown in Figure 7.9. It is quite constant at a value of 3 Å, which is of the order of the average separation between guests and host molecules along the *c*-axis. It increases slightly below 50 K. It is similar in character to that of the ethanol clathrate of Dianin's compound and indicates the similarity to the glassy-like behavior. One has to realize that this low value of the mean free path is unrealistic for Debye crystals (continuum-wave theory) for which the minimum path should be about 6 Å (the minimum path from atomistic point of view).⁶⁵ The low value of *l* for HPTB-CBr₄ is caused by the crudeness of the dominant-phonon approximation (*i.e.* equation (1.1)).

7.4.2.3 SLACK'S MINIMUM THERMAL CONDUCTIVITY

The Slack minimum thermal conductivity, $\kappa_{Smin\infty}$, hypothetically near the melting point (*vide supra*) is given by¹⁶⁷

$$\kappa_{Smin\infty} = \frac{3k_B v^2}{2n\Omega v_A} \quad (7.19)$$

where Ω is the average volume per atom, v_A is the acoustic phonon cut-off frequency ($v_A = k_B \theta_D / (n^{1/3} \hbar)$; n is the number of atoms in the unit cell). This simplified model does not include contributions from the optic modes (due to the absence of necessary information in this case). This yields $\kappa_{Smin\infty} = 0.015 \text{ W m}^{-1} \text{ K}^{-1}$ which is about 10 times less than the experimentally determined values. It indicates that the phonon-phonon scattering is at less than maximum possible effectiveness.

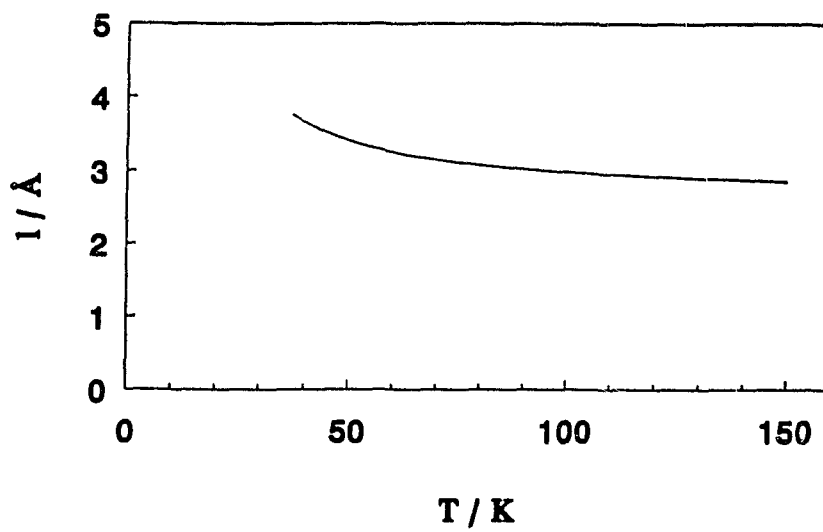


Figure 7.9 The mean free path of phonons in the CBr_4 clathrate of HPTB.

7.4.2.4 EINSTEIN MODEL

Einstein tried to explain the thermal conductivity of crystalline solids by concept of a random walk of localized (Einstein) oscillators.⁶⁸ It was an extension of his model of the heat capacity. This model failed to give a reasonable correspondence to experimental findings due to presumed randomness which does not occur in crystals. However this model seems to yield reasonable explanation if employed for the modelling of thermal conductivity of amorphous materials and highly disordered crystals.⁶⁸ Since the thermal conductivity of HPTB-CBr₄ seems to bear glassy-like features, the Einstein model was applied here. It is given by⁶⁸

$$\kappa_{Eins} = \frac{k_B^2 n_d^{1/3}}{\hbar \pi} \theta_E \frac{x^2 e^{-x}}{(e^x - 1)^2} \quad (7.20)$$

where θ_E is the Einstein temperature evaluated from the isochoric heat capacity of the compound with the assumption of 54 sites per unit cell (as in the calculation of Debye temperature) and $\theta_E=65$ K; n_d is the number density of sites in the solid ($n_d=54$ per unit cell) and $x=\theta_E/T$. The volume thermal expansion was employed to yield the temperature dependence of κ_{Eins} . The resultant curve is shown in Figure 7.10.

Despite its crudeness, the Einstein model gives surprisingly good correspondence with the experimental data.

7.4.2.5 CAHILL-POHL MODEL

Cahill and Pohl⁶⁸ extended the Einstein concept (*vide supra*). The temperature

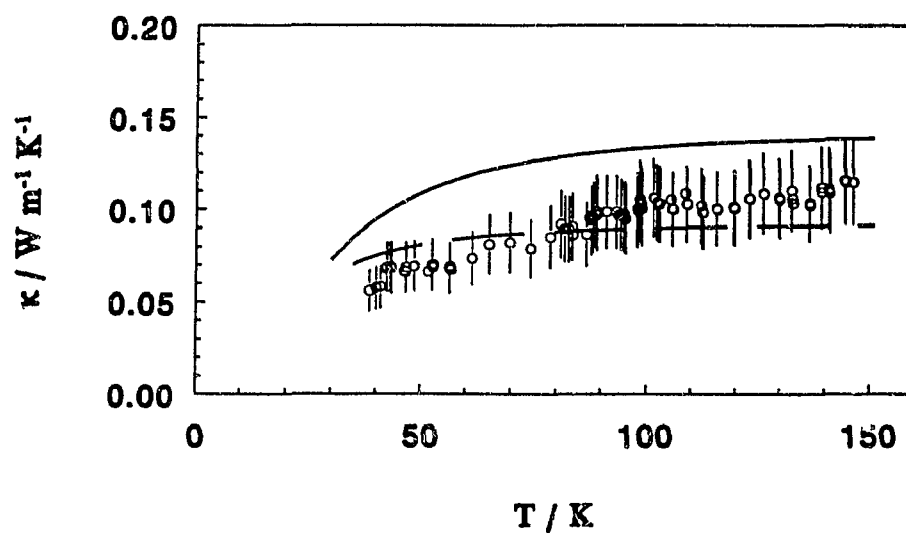


Figure 7.10 The experimental thermal conductivity of the CBr_4 clathrate of HPTB (\circ and error bars) and the Einstein (- -), and Cahill-Pohl model (-).

evolution of the thermal conductivity in their model is given by equation (7.13). The plot of κ_{CP} as a function of the temperature is shown in Figure 7.10. Once again the correspondence to the experimental values is surprisingly good. Although experimental values of κ are lower in the temperature range of measurement, they tend to approach κ_{CP} at higher temperatures.

Yet *in toto* the Einstein approach yields a better estimation of the thermal conductivity than the Cahill-Pohl model which can be regarded as its refined version. This indicates, most likely, that these two approaches do not lead to a correct answer as to why such a highly effective thermal resistivity mechanism governs heat flux in this system.

Another drawback of models based on minimum thermal conductivity is the classical picture of the phenomenon. If the phonon wave vector \underline{k} is to have a well-defined value then the spatial extent of the wave-packet cannot be as small as the interatomic separations,⁹² which is one of the basic assumption of these models.

7.4.2.6 RESONANT SCATTERING MODEL

Previously presented arguments concerning the resonant scattering model for the thermal conductivity of clathrates apply also to the HPTB-CBr₄ assembly. Prospective candidates for resonant scatterers are the phenyl rings and the guest molecules. However the infrared frequencies of phenyl rings range¹⁸³ from 420 cm⁻¹ to 1625 cm⁻¹ and since the phonons responsible for the heat flux fall into the energy window⁶⁸ *ca.* 10 cm⁻¹ to 120 cm⁻¹, the phenyl rings seem to be excluded. Remaining

candidates are the CBr_4 guest molecules. This view is based on common structural and dynamical features among clathrates, and crystallographic results which demonstrate that the CBr_4 molecules in HPTB- CBr_4 experience translational as well as librational motion (Section 3.3.2). It is most likely that these vibrations can give rise to localized modes. This is also supported by the heat capacity results. The single-molecule molar heat capacity exceeds the bulk molar heat capacity of the CBr_4 molecule by about R between 30 and 120 K (see Figure 6.6). This can be brought about by vibrational rattling or libration of the guest molecule in the clathrate cavity. The magnitude of the excess heat capacity would correspond to a frequency that coincides with the energy range of phonons that conduct heat.

The previously described formalism was applied to fit the experimental thermal conductivity, κ , of the CBr_4 clathrate of HPTB to equation (7.15) with the overall scattering rate $\tau^{-1} = \tau_U^{-1} + \tau_B^{-1} + \tau_S^{-1}$. The experimental parameters used in the fit were as follows: the radius of the sample was 2.11 mm, the density of scatterers was assumed to be two per cage; the volume thermal expansion also was used (Section 5.3). On the basis of the heat capacity results (Section 6.4.5) the Debye temperature used in the fit was 135 K. The average sound velocity derived from the elastic constants, *i.e.* $v = 1410 \text{ m s}^{-1}$, was used in the fitting procedure. The resultant fit is shown in Figure 7.11. The values of the fitted parameters are: $B = 9.39 \times 10^{-20} \text{ s K}^{-1}$, $D = 1.17 \times 10^{-14} \text{ m}^3 \text{ s}^{-1}$, $\alpha = 2.89$ and $\omega_0 = 6.88 \times 10^{12} \text{ s}^{-1}$. As was explained previously the resonant frequency should not be taken *verbatim*. Yet the magnitude of the fitted parameter, ω_0 , appears to reflect an average frequency of the guest vibration. This

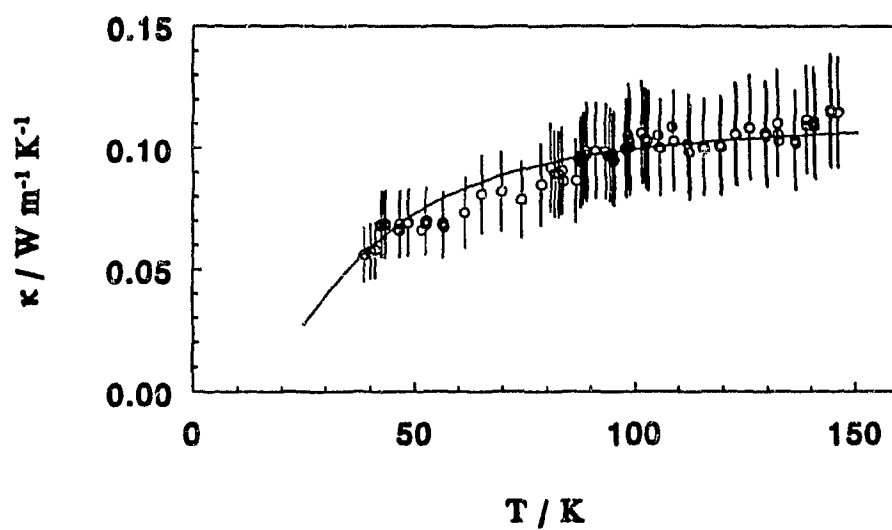


Figure 7.11 The experimental thermal conductivity of the CBr_4 clathrate of HPTB (\circ and error bars) and the least-square fit to the resonant-scattering model (—).

model quite precisely describes the temperature evolution of the thermal conductivity of HPTB-CBr₄ system. It also exhibits a slight positive temperature derivative of the thermal conductivity. The coupling constant, D , is of the order $10^{-14} \text{ m}^3 \text{ s}^{-1}$. For comparison, the coupling constants for Dianin's systems⁸⁶ were of the order $10^{-13} \text{ m}^3 \text{ s}^{-1}$ and for tetrahydrofuran clathrate hydrate⁸² were of the order $10^{-15} \text{ m}^3 \text{ s}^{-1}$. Since these systems cannot be compared directly due to differences in their structural makeup and concomitant lattice dynamics (*e.g.* hydrogen bonding, which is absent in HPTB-CBr₄ plays an important role in THF clathrate hydrate and Dianin's systems), the values of D only indicate similar type of matching.

In the case of HPTB-CBr₄ the major role in the thermal resistivity mechanism seems to be played by the guest species. Their motion appears to be responsible for lowering the thermal conductivity coefficient to values characteristic for glassy materials. The dynamics of the crystal lattice, as probed by the Brillouin scattering (Cauchy ratios), showed the angular and/or torsional nature of the crystal interaction (*vide supra*; Section 4.4.2). This most likely implies that translational-rotational coupling is a premise of the resonant scattering model. Moreover, it is believed that constraints of the harmonic approximation, fulfilled quite well for most of translational vibrations, are not satisfied to the same degree by rotational vibrations.¹⁸⁴ Enhanced anharmonicity is the obvious culprit of such an effective thermal resistivity mechanism. Experiments as well as computations corroborate this point of view for other materials (*e.g.* mixed crystals^{165,185}). On the other hand, the vibrational rattling of the guest molecules in the cavities appears also to be responsible for localized

vibrations coupled to acoustic modes of the host lattice as in the case of the clathrate hydrates with atomic guests.⁸⁵

7.4.3 CONCLUSIONS

The thermal conductivities of clathrate systems have been the subject of several studies since its unusual behaviour was first reported in 1979.⁷⁶ A number of approaches were applied to understand this *anomalous* crystalline thermal behaviour. Different aspects of either structural or dynamical features of clathrates were emphasized in those interpretations, ranging from an atomic level of consideration (as in the case of hydrates where tunneling states caused by the proton disorder were erroneously purported to be the source of the thermal resistance mechanism⁸⁴) to loosely defined hopping process of heat transporting excitations¹⁸⁶ perhaps similar in nature to the presented Einstein or Cahill-Pohl models, or to the recent attempts to explain the high temperature thermal conductivity of glassy materials.⁷¹ Subsequent experimental investigations of different clathrates revealed weak points of these explanations.⁸⁰

On the other hand, the resonant scattering model successfully explains the thermal conductivity of the investigated materials. It must be stressed that the model itself is general in nature and presents the most comprehensive treatment of the problem. It does not rely on the particular properties of chosen systems, which was the main flaw of other models, but instead approaches the thermal conductivity of clathrates from a very general point of view. The question is rather what these systems have in common that manifests itself as an attenuation of the thermal conductivity. It also takes into consideration other solid state systems that present similar thermal behaviour but have little resemblance to clathrates. At the same time

the resonant scattering model allows for a thorough explanation of the thermal conductivity.

The thermal conductivity of Dianin- CCl_4 has been found to be almost the same as for the host lattice without guests, in contrast with results for Dianin- $\text{C}_2\text{H}_5\text{OH}$ where the presence of the guests has been found to increase thermal resistance (decrease thermal conductivity).⁸⁶ The source of the extra thermal resistance in Dianin- $\text{C}_2\text{H}_5\text{OH}$ appears to be motions of the ethanol guest molecules in the cages, which can interact with the heat-carrying acoustic modes. This model is consistent with the observed high thermal resistance in clathrate hydrates, as guests freely move in the symmetrical hydrate cages. In contrast, the guest molecules are not able to move so freely in Dianin- CCl_4 , and this source of thermal resistance is not active; as a result, the thermal conductivity of Dianin- CCl_4 is much the same as that of the host lattice.

The origin of the highly effective thermal resistance mechanism in HPTB- CBr_4 was identified with the motion of the guest species. It is similar to that of the hydrates. Unfortunately, attempts to grow single crystals of HPTB of sufficient size to carry out single crystal thermal conductivity measurements were unsuccessful. Therefore the comparison of the thermal conductivity to that of the host compound, as had been done for the hydrates, or the direct examination of the thermal conductivity of the isomorphous host compound as in the case of the Dianin clathrand, was not performed. The only feasible test seems to be future determination of the thermal conductivity of HPTB powder samples.

This study proves that molecular architecture and ensuing dynamics can control thermal conductivity. These principles can underlie thermal properties of a wide variety of materials. Glass-like behaviour of thermal conductivity of these crystalline materials is ascribed to molecular motion. The ultimate test of every theory is an experiment. This study shows that the low-frequency motion of molecular moieties can significantly affect thermal properties. The physical picture of the enhanced thermal resistivity mechanism is rather independent of the particular solid state system. It would be salutary to examine crystals with molecular motion that gives rise to acoustic-optical coupling. For example tetracyanoethylene¹⁸⁷ or s-traizine¹⁸⁸ seem to be excellent candidates. Although the reason that these materials have been studied to date is quite different (to investigate their phase transitions) they display features of the lattice dynamics required for resonance scattering, *i.e.* translational-rotational coupling. The continuation of the investigation of Dianin's compound and/or its analogues should also be very instructive due to the plethora of guests these compounds can trap and thus the variety of behaviour these species can experience in the host framework. As the present investigation shows, the type of guest dynamics is important in determining thermal properties. Another lattice inclusion compound which would be of interest is tri-o-thymotide¹⁸⁹ (TOT for short). The TOT molecule is flexible and it is known for its ability to enclathrate a large number of chemical species (about 100 so far).¹⁸⁹ This material can crystallize either as a channel inclusion compound or as a clathrate. This would allow one to carry out quite an instructive comparable study of the thermal properties.

CHAPTER 8

SUMMARY

It can be said that motions of chemical species in molecular crystals underlie many properties of these materials. Investigations of lattice dynamics can be divided into techniques utilizing observations of microscopic quantities, such as different spectroscopies, and more classical methods based on observations of macroscopic quantities. The latter approach was mainly employed in this study, *i.e.* calorimetry and thermal conductivity determination. Measurements of the heat capacities and the thermal conductivity coefficients as functions of temperature, as well as other experiments carried out here, were indirect in the sense that the character of motions of the chemical species was inferred from the experimental findings.

This study showed that lattice dynamics are highly anharmonic in the investigated systems. The most dramatic manifestation of this is the very low and "glass-like" thermal conductivities measured here. The heat capacity data and the resonant-scattering model of thermal conductivity provide insight into understanding of the motions of either molecular moieties (methyl groups of Dianin's molecule in Dianin-CCl₄) or whole molecules (CCl₄ in Dianin-CCl₄ and CBr₄ in HPTB-CBr₄). Localized optic modes due to motions of these molecular units seem to be responsible for the highly effective thermal-resistant mechanism in these materials. Since there appears to be an interaction between the guest and host molecules, this model of

thermal conductivity also indirectly lends support to the view of mechanical stability of clathrates in which guest molecules play a crucial role.

Another aspect of the anharmonic interactions is the thermal expansion. The enhanced thermal expansion of clathrate hydrates and the clathrates of Dianin's compound with respect to the crystal structures of the host compounds can be explained by the augmented internal phonon pressure on the walls of the crystal. The absence of this phenomenon for the HPTB systems was ascribed to the differences in the structural and energetic makeup of these systems.

Despite the same crystallographic structure and the similarity between the HPTB molecule and the Dianin's supramolecule, the fact that HPTB yields clathrates is rather fortuitous since the topology of the HPTB clathrates and the structural matrix of Dianin's system is different. This conclusion is supported by stability information for HPTBⁿ clathrates.

This study also showed that the molecular architecture and the ensuing dynamics of the crystal lattice appear to have a significant effect on thermal conductivity. The pendant-like methyl groups of Dianin's molecule and the mobile guest molecules seem to experience motions which give rise to localized modes. The physical picture of the heat-resistant mechanism, given by the resonant-scattering model, is that of spatially well-defined centres of localized optic modes impeding the flow of acoustic phonons *i.e* a three-dimensional matrix of localized optic vibrations damping the acoustic waves. The energies of the optic and acoustic modes have to be similar in order for this process to take place.

Thermal properties and vibrational spectroscopy of the investigated systems also indicate that the lattice dynamics of the investigated clathrates do not fully conform to the external vibration formalism which employs a conceptual partitioning of vibrations into internal and external modes. This assumption does not hold for these systems since these modes are not energetically well-separated. The coupling between these modes can significantly affect phonon dispersion relations in comparison with the theoretical treatment of lattice motions in the spirit of the formal theory of the dynamics of external modes in complex crystals in the harmonic approximation. This corollary can be projected on other structures consisting of relatively flexible molecular clusters where ranges of crystal and valence field forces might be in a propinquity. This also issues a caveat for the use of the rigid molecule approximation. It also can be viewed in the wider context of all problems set by lattice dynamics including phonon-assisted solid-state reactions where the crystal energetics and nature of motions of chemical species in solid structures seem to play a crucial role in governing their chemical functioning, or modelling behaviour of systems of great industrial interest such as drugs where mechanical stability is one of the prominent features.

APPENDIX

Table A1 Heat capacity of CBr_4 as determined in the experiment.

T	C	T	C	T	C
[K]	[J K ⁻¹ mol ⁻¹]	[K]	[J K ⁻¹ mol ⁻¹]	[K]	[J K ⁻¹ mol ⁻¹]
32.55	44.068	94.04	81.566	123.73	90.062
34.38	47.064	94.46	82.513	126.19	91.216
36.59	48.553	97.27	82.736	126.98	91.503
39.70	51.546	97.64	82.549	127.23	92.815
41.12	53.726	97.74	83.071	128.13	92.569
45.53	53.630	98.61	83.357	131.81	91.875
45.54	55.352	101.67	85.191	131.84	93.071
49.46	57.945	102.41	84.446	132.02	92.272
50.46	58.957	103.37	84.267	132.03	92.634
53.26	59.951	106.26	85.587	132.58	92.791
54.36	61.901	106.56	86.035	136.39	93.346
57.31	63.644	107.22	86.310	136.76	93.576
59.30	63.690	107.50	87.075	137.04	93.719
61.94	65.393	108.23	85.950	137.09	93.306
64.70	66.448	110.86	87.378	137.83	93.348
67.10	68.404	111.53	87.546	141.51	94.854
69.46	69.366	112.10	87.783	141.69	93.866
72.45	69.985	112.34	87.931	141.72	94.722
74.46	72.469	113.11	87.572	141.82	94.595
77.63	74.154	115.32	88.358	142.15	94.213
78.84	74.840	115.38	88.142	143.56	95.577
82.54	77.263	117.04	88.903	146.01	96.827
83.36	76.860	117.18	88.868	146.71	96.505
87.70	79.070	118.03	88.239	146.84	95.764
88.22	78.842	119.32	89.374	147.05	96.546
88.68	79.496	119.42	89.076	147.26	96.683
88.90	78.499	120.39	89.839	148.62	98.274
90.79	80.153	121.99	89.611	150.51	96.896
92.91	81.550	122.05	89.885	151.74	97.371
93.15	81.324	123.36	90.696	151.90	96.810

cont.

Table A1 continued...

T	C	T	C	T	C
[K]	[J K ⁻¹ mol ⁻¹]	[K]	[J K ⁻¹ mol ⁻¹]	[K]	[J K ⁻¹ mol ⁻¹]
152.44	97.697	188.05	104.982	223.88	114.307
153.10	98.206	190.45	104.807	224.55	112.434
155.03	97.278	193.10	106.883	225.08	113.117
156.82	98.291	193.27	105.143	225.42	113.678
156.98	97.719	193.39	105.601	228.41	113.465
157.63	99.016	195.26	105.828	229.08	114.552
157.84	98.675	195.57	105.833	229.31	113.331
159.61	97.787	198.14	107.065	232.31	113.541
161.92	98.371	198.58	106.670	232.74	113.940
162.09	98.751	198.79	106.746	233.12	115.385
162.19	99.764	199.88	106.041	233.45	113.923
163.08	99.133	200.06	107.086	234.30	115.961
164.19	98.635	203.23	107.989	234.41	114.653
166.81	100.236	203.91	107.343	235.61	115.382
167.08	100.123	204.16	108.425	236.42	114.358
167.24	100.675	204.17	107.972	236.87	114.323
168.14	100.493	204.88	107.938	237.54	117.053
168.74	100.380	208.36	110.117	237.61	114.886
171.47	101.822	208.38	110.404	237.75	116.826
172.28	100.816	209.29	109.030	239.13	114.816
172.41	100.879	209.63	110.656	239.52	116.241
173.15	101.789	209.63	108.906	239.56	115.844
173.25	101.585	212.56	110.859	240.77	116.848
176.15	101.064	213.53	111.380	241.72	116.768
177.49	101.904	214.36	110.754	241.90	116.686
177.60	101.914	214.67	110.925	242.43	117.113
177.75	102.825	215.13	111.342	242.82	115.705
178.10	102.711	216.72	112.543	244.69	116.553
180.87	103.178	218.68	111.803	245.80	116.470
182.73	103.270	219.04	112.885	248.17	115.931
182.80	102.401	220.06	112.120	249.76	117.441
185.64	104.602	220.54	112.940	249.78	118.007
186.76	104.571	220.87	113.202	249.92	118.213
188.02	103.654	223.76	112.749	250.21	118.919

cont.

Table A1 continued...

T	C	T	C	T	C
[K]	[J K ⁻¹ mol ⁻¹]	[K]	[J K ⁻¹ mol ⁻¹]	[K]	[J K ⁻¹ mol ⁻¹]
251.17	118.060	270.73	120.367	302.20	131.660
251.74	118.406	270.88	121.866	303.62	134.460
252.99	119.589	271.15	122.685	305.72	134.942
253.48	119.173	271.72	124.671		
254.09	119.086	272.52	123.364		
254.90	120.204	275.06	123.262		
255.20	120.573	275.71	122.119		
255.47	119.357	276.07	125.911		
255.59	120.511	276.36	125.288		
256.37	120.185	276.56	124.623		
258.05	118.596	276.75	126.575		
258.57	120.686	276.86	122.344		
260.07	119.445	277.45	125.148		
260.28	119.649	277.59	126.777		
260.36	121.695	280.03	125.341		
260.48	121.290	280.90	124.210		
260.57	119.650	281.28	124.652		
261.47	121.055	281.70	127.466		
261.50	122.305	281.82	126.104		
262.22	120.664	282.77	124.788		
262.78	120.668	283.51	125.319		
264.06	121.095	283.72	126.452		
264.41	120.359	284.89	128.542		
265.17	122.617	285.21	127.071		
265.44	123.254	286.81	129.439		
265.63	120.792	287.05	129.441		
265.64	121.561	288.88	129.632		
265.70	122.585	289.94	128.537		
266.31	122.855	291.66	128.126		
266.62	123.706	292.50	128.701		
266.99	120.219	292.53	129.854		
267.47	122.974	293.76	130.008		
267.64	122.267	296.07	131.108		
270.05	121.593	296.75	133.123		

Table A2 Heat capacity of HPTB as determined in the experiment.

T	C	T	C	T	C
[K]	[J K ⁻¹ mol ⁻¹]	[K]	[J K ⁻¹ mol ⁻¹]	[K]	[J K ⁻¹ mol ⁻¹]
31.84	106.918	109.16	333.201	174.76	476.058
35.26	122.495	111.81	341.920	174.76	476.058
39.05	140.357	113.56	345.704	175.22	481.428
42.92	142.656	117.40	352.909	176.63	479.852
46.69	171.251	118.41	353.207	179.07	485.669
50.25	178.969	121.19	358.842	181.27	493.305
52.07	180.404	123.32	362.772	184.53	503.245
53.73	184.404	124.39	364.350	188.51	510.487
57.27	199.394	125.06	365.929	191.76	520.319
60.98	206.086	126.72	369.298	192.53	523.823
64.54	212.394	128.27	375.110	194.47	530.028
65.95	222.071	131.43	381.172	196.39	532.170
68.18	223.750	131.74	379.084	197.47	536.570
70.04	233.488	133.95	385.063	199.03	537.766
72.54	241.968	137.03	392.667	203.04	543.988
73.77	243.688	138.44	395.515	206.33	557.253
77.04	255.098	138.51	397.042	206.56	555.528
77.71	259.395	141.22	404.059	208.87	561.654
81.71	266.988	145.17	411.521	213.52	573.681
85.70	276.343	148.48	417.306	213.62	576.461
85.84	278.228	151.90	427.382	214.90	577.917
86.53	280.889	152.69	428.757	217.09	586.872
89.73	284.374	155.81	437.708	217.64	587.231
90.81	286.447	158.66	442.878	219.39	590.534
91.93	291.087	159.78	443.008	220.45	592.198
92.75	296.351	162.94	452.701	224.98	605.510
93.77	296.047	165.43	456.625	227.65	614.239
96.53	305.541	166.32	461.179	228.24	612.712
98.19	308.807	170.10	470.159	229.87	616.004
100.33	316.153	172.23	472.667	232.31	622.688
103.49	321.800	174.52	478.328	234.32	625.988
105.52	328.463	174.52	478.328	235.56	630.757

cont.

Table A2 continued...

T	C
[K]	[J K ⁻¹ mol ⁻¹]
236.48	634.882
239.64	642.384
241.84	647.509
243.44	648.117
244.85	654.284
246.96	656.513
248.69	659.941
250.17	666.407
252.37	672.033
255.04	678.063
259.84	684.420
262.76	690.570
266.11	696.490
268.56	702.789
272.14	707.866
273.99	714.060
275.11	715.385
277.59	723.147
279.35	730.722
282.69	738.859
285.54	747.508
286.11	748.190
290.25	759.694
293.44	766.660
295.76	772.924
299.35	779.932
303.40	790.390
307.47	798.176
310.36	810.561
310.97	810.272
312.29	815.461

Table A3 Heat capacity of HPTB-CBr₄ as determined in the experiment.

T	C	T	C	T	C
[K]	[J K ⁻¹ mol ⁻¹]	[K]	[J K ⁻¹ mol ⁻¹]	[K]	[J K ⁻¹ mol ⁻¹]
31.47	224.800	85.76	460.430	148.42	622.747
31.66	221.065	90.94	465.111	149.31	623.808
33.71	234.144	91.06	464.035	150.89	628.727
34.98	235.809	91.17	464.751	152.13	635.289
36.46	246.023	93.57	475.270	155.79	641.271
39.28	269.276	96.30	480.912	155.92	636.808
40.18	271.288	97.49	484.734	158.22	647.202
44.11	281.917	98.27	490.280	158.23	639.712
44.93	283.806	100.62	495.811	158.31	650.746
46.94	317.897	101.50	497.179	162.10	651.700
47.81	307.878	105.10	509.269	162.63	655.630
49.54	312.446	106.71	515.115	163.19	656.524
51.21	350.523	107.70	516.190	164.52	670.023
52.00	344.115	110.27	523.205	164.92	659.412
54.44	350.160	111.93	525.948	167.85	673.892
54.63	338.658	112.21	523.516	170.75	679.649
57.43	354.366	114.80	537.789	173.03	679.125
61.28	371.154	116.69	539.984	175.91	687.508
61.46	378.259	117.13	541.270	176.96	697.833
64.35	373.115	119.35	546.125	178.16	700.921
65.22	382.738	121.93	554.134	178.42	696.999
67.28	380.967	122.36	553.644	178.44	701.925
69.02	397.805	123.16	553.347	180.48	704.487
70.23	386.599	126.54	569.539	182.59	707.232
72.64	406.399	129.11	571.953	183.23	712.002
73.48	411.929	129.64	573.122	183.74	713.236
76.14	424.928	133.01	581.336	185.74	720.687
77.01	426.252	136.16	596.736	187.97	729.768
79.56	441.096	136.34	592.657	189.31	726.757
80.56	428.395	141.09	606.081	189.51	729.697
82.59	454.369	142.73	608.532	193.35	735.965
84.84	447.833	143.60	612.971	195.48	751.798

cont.

Table A3 continued...

T	C	T	C
[K]	[J K ⁻¹ mol ⁻¹]	[K]	[J K ⁻¹ mol ⁻¹]
195.78	826.655	246.74	750.758
196.05	816.998	247.62	752.067
201.00	828.521	250.60	759.829
203.04	836.222	250.75	771.755
203.62	837.578	253.43	774.314
206.80	833.799	257.29	781.792
208.70	852.271	257.60	800.347
209.68	853.614	260.11	796.956
210.31	854.013	263.93	797.368
210.63	843.477	264.46	803.491
213.43	854.973	266.81	804.376
216.43	864.254	270.60	814.318
216.48	874.599	273.45	814.063
217.03	879.487	277.20	818.658
218.26	876.298	280.09	819.378
220.06	875.446	283.19	998.186
223.33	888.979	286.72	1030.25
224.22	885.798		
225.91	901.186		
226.75	904.856		
230.17	899.355		
230.47	916.929		
232.02	932.456		
233.43	926.838		
233.56	933.533		
237.03	950.506		
237.19	956.059		
239.85	959.992		
240.10	963.429		
241.16	967.809		
243.89	983.064		
243.92	986.684		

Table A4 The smoothed values of C_V for CBr_4 .

T / K	$C_V / \text{J K}^{-1} \text{mol}^{-1}$	T / K	$C_V / \text{J K}^{-1} \text{mol}^{-1}$
30.0	42.15	175.0	96.66
35.0	46.19	180.0	97.50
40.0	49.98	185.0	98.33
45.0	53.52	190.0	99.17
50.0	56.85	195.0	100.01
55.0	59.95	200.0	100.86
60.0	62.85	205.0	101.65
65.0	65.57	210.0	102.45
70.0	68.10	215.0	103.24
75.0	70.46	220.0	104.03
80.0	72.66	225.0	104.82
85.0	74.72	230.0	105.61
90.0	76.64	235.0	106.38
95.0	78.44	240.0	107.13
100.0	80.11	245.0	107.87
105.0	81.68	250.0	108.57
110.0	83.14	255.0	109.23
115.0	84.52	260.0	109.84
120.0	85.81	265.0	110.38
125.0	87.03	270.0	110.85
130.0	88.19	275.0	111.21
135.0	89.28	280.0	111.46
140.0	90.32	285.0	111.55
145.0	91.31		
150.0	92.27		
155.0	93.19		
160.0	94.08		
165.0	94.96		
170.0	95.81		

Table A5 The smoothed values of C_v for HPTB-CBr₄.

T / K	C_v / J K ⁻¹ mol ⁻¹	T / K	C_v / J K ⁻¹ mol ⁻¹
30.0	217.24	175.0	687.42
35.0	244.88	180.0	700.35
40.0	270.91	185.0	713.40
45.0	295.42	190.0	726.60
50.0	318.55	195.0	739.92
55.0	340.39	200.0	753.39
60.0	361.05	205.0	766.98
65.0	380.63	210.0	780.69
70.0	399.22	215.0	794.51
75.0	416.92	220.0	808.42
80.0	433.80	225.0	822.40
85.0	449.96	230.0	836.43
90.0	465.47	235.0	850.48
95.0	480.41	240.0	864.52
100.0	494.84	245.0	878.51
105.0	508.83	250.0	892.43
110.0	522.46	255.0	906.21
115.0	535.76	260.0	919.83
120.0	548.81	265.0	933.22
125.0	561.65	270.0	946.34
130.0	574.34	275.0	959.11
135.0	586.90	280.0	971.49
140.0	599.40	285.0	983.38
145.0	611.85	290.0	994.73
150.0	624.30	295.0	1005.44
155.0	636.78	300.0	1015.42
160.0	649.31	305.0	1024.59
165.0	661.91	310.0	1032.85
170.0	674.61		

Table A6 Positional parameters and B(eq) of nonhydrogen atoms for HPTB.

Atom	x / a	y / b	z / c	B(eq)
S(1)	0.0007(1)	0.2287(1)	0.7025(1)	3.3(1)
S(2)	0.3147(1)	0.0336(1)	0.8470(1)	3.3(1)
S(3)	-0.3078(1)	0.1872(1)	0.8520(1)	3.3(1)
C(1)	0.4377(2)	-0.1526(2)	0.8510(2)	2.8(3)
C(2)	0.5912(3)	-0.1881(3)	0.8582(3)	4.8(3)
C(3)	0.6976(3)	-0.3240(3)	0.8445(4)	5.9(3)
C(4)	0.6519(3)	-0.4259(3)	0.8285(3)	5.0(3)
C(5)	0.4988(3)	-0.3932(3)	0.8274(3)	4.8(3)
C(6)	0.3903(3)	-0.2552(3)	0.8667(3)	3.8(2)
C(7)	0.0932(2)	0.3461(2)	0.7013(2)	3.1(2)
C(8)	0.1648(3)	0.4055(3)	0.5773(3)	4.1(2)
C(9)	0.2256(3)	0.5110(4)	0.5626(4)	5.8(3)
C(10)	0.2193(4)	0.5559(4)	0.6703(5)	6.5(4)
C(11)	0.1521(4)	0.4955(4)	0.7940(4)	5.9(4)
C(12)	0.0875(3)	0.3907(3)	0.8105(3)	4.4(3)
C(13)	-0.2795(2)	0.1163(2)	0.7162(2)	2.6(2)
C(14)	-0.1532(3)	-0.0039(3)	0.6899(2)	3.3(2)
C(15)	-0.1520(3)	-0.0539(3)	0.5847(3)	4.0(3)
C(16)	-0.2743(3)	0.0132(3)	0.5080(3)	4.6(3)
C(17)	-0.3996(3)	0.1327(3)	0.5339(3)	4.6(3)
C(18)	-0.4028(3)	0.1849(3)	0.6373(2)	3.5(2)
C(19)	0.1403(2)	0.0148(2)	0.9339(2)	2.4(2)
C(20)	0.0039(2)	0.1022(2)	0.8693(2)	2.4(2)
C(21)	-0.1356(2)	0.0848(2)	0.9332(2)	2.3(2)

Table A7 Positional parameters and B(eq) of nonhydrogen atoms for HPTB-CBr₄.

Atom	x / a	y / b	z / c	B(eq)
Br(1)	0.5461(1)	0.3439(1)	0.0350(1)	7.35(9)
Br(2)	0.6667	0.3333	-0.0866(2)	11.5(3)
S(1)	0.1101(2)	0.8545(2)	0.0031(1)	1.8(1)
C(1)	0.0541(7)	0.7721(7)	0.0718(5)	1.5(4)
C(2)	0.0598(9)	0.6793(8)	0.0736(6)	3.3(5)
C(3)	0.027(1)	0.6143(8)	0.1289(6)	4.3(6)
C(4)	-0.013(1)	0.641(1)	0.1797(6)	4.2(6)
C(5)	0.0226(8)	0.731(1)	0.1796(5)	3.3(5)
C(6)	0.0138(8)	0.7979(8)	0.1263(5)	2.6(5)
C(7)	0.0459(7)	0.9333(7)	0.0002(5)	1.5(2)
C(8)	0.6667	0.3333	0.006(1)	4(2)

REFERENCES

1. Lehn, J.-M. *Pure & Appl. Chem.* 1978, **50**, 871.
2. Lehn, J.-M. *Angew. Chem. Int. Ed. Engl.* 1988, **27**, 89.
3. Destro, R.; Gavezzotti, A. "Studies in Physical and Theoretical Chemistry" vol. **69**, p.161; Ed. Pierrot, M.; Elsevier, Amsterdam, 1990.
4. Davies, J. E. D.; Kemula, W.; Powell, H. M.; Smith, N. O. *J. Incl. Phenom.* 1983, **1**, 3.
5. Weber, E.; Josel, H. -P. *J. Incl. Phenom.* 1983, **1**, 79.
6. Powell, H. M. "Inclusion Compounds" vol. **1**, p. 1; Eds. Atwood, J. L.; Davies, J. E. D.; MacNicol, D. D.; Academic Press, London, 1984.
7. Weber, E. "Topics in Current Chemistry" vol. **140**, p. 1; Ed. Weber, E.; Springer-Verlag, Berlin, 1987.
8. Whitesides, G. M.; Mathias, J. P.; Seto, C. T. *Science* 1991, **254**, 1312.
9. Rebek, J. "Topics in Current Chemistry" vol. **149**, p. 189; Ed. Weber, E.; Springer-Verlag, Berlin, 1988.
10. Kitaigorodsky, A. I. "Molecular Crystals and Molecules"; Academic Press, New York, 1973.
11. MacNicol, D. D; McKendrick, J. J.; Wilson, D. R. *Chem. Soc. Rev.* 1978, **7**, 61.
12. Powell, H. M. *J. Chem. Soc.* 1948, 61.
13. van der Waals, J.H. *Trans. Faraday Soc.* 1956, **52**, 184.
14. van der Waals, J. H. "Advances in Chemical Physics" vol. **II**, p. 1; Ed. Prigigone, I.; Interscience Publishers, New York, 1959.
15. Belosludov, V. R.; Lavrentiev, M. Yu.; Dyadin, A. Yu. *J. Incl. Phenom.* 1991, **10**, 399.
16. Rodger, P. M. *Mol. Simulation* 1990, **5**, 315.
17. Rodger, P. M. *J. Phys. Chem.* 1990, **94**, 6080.

18. Lynden-Bell, R. M. *Mol. Phys.* 1993, **79**, 313.
19. Palin, D. E.; Powell, H. M. *J. Chem. Soc.* 1947, 208.
20. von Stackelberg, M. *Naturwissenschaften* 1949, **36**, 327.
21. Davies, J. E. D. *J. Mol. Structure* 1981, **75**, 1.
22. Breck, D. W. "Zeolite Molecular Sieves"; John Wiley, New York, 1974.
23. Gmelin, L. "Gmelins Handbuch der Anorg. Chem." 1960, 9, No. **B2**, 1102.
24. Davy, H. *Phil. Trans. Roy. Soc.* 1811, **101**, 30.
25. Faraday, M. *Quart. J. Sci. Lit. Arts* 1823, **15**, 71.
26. Wöhler, F. *Justus Liebigs Ann. Chem.* 1849, **69**, 297.
27. Mylius, F. *Ber. Bunsenges Phys. Chem.* 1886, **19**, 999.
28. Thomas, J. M.; Harris, K. D. M. "Studies in Organic Chemistry" vol. **32**, p. 179; Ed. Desiraju, G. R.; Elsevier, Amsterdam, 1987.
29. Davies, J. E. D. "Inclusion Compounds" vol. **3**, p. 37; Eds. Atwood, J. L.; Davies, J. E. D.; MacNicol, D. D.; Academic Press, London, 1984.
30. Tsoucaris, G. "Studies in Organic Chemistry" vol. **32**, p. 207; Ed. Desiraju, G. R.; Elsevier, Amsterdam, 1987.
31. Arad-Yellin, R.; Green, B. S.; Knossow, M.; Tsoucaris, G. "Inclusion Compounds" vol. **3**, p. 263; Eds. Atwood, J. L.; Davies, J. E. D.; MacNicol, D. D.; Academic Press, London, 1984.
32. Worsh, D.; Vogtle F. "Topics in Current Chemistry" vol. **140**, p. 21; Ed. Weber, E.; Springer-Verlag, Berlin, 1987.
33. Szejtli, J. "Inclusion Compounds", vol. **3**, p. 331; Eds. Atwood, J. L.; Davies, J. E. D.; MacNicol, D. D.; Academic Press, London, 1984.
34. Tam W.; Eaton, D. F.; Calabrese, J. C.; Williams, I.D.; Wang, Y.; Anderson, A. *Chem. Mater.* 1989, **1**, 128.
35. Barrer, R. M.; Stuart, W. I. *Proc. Roy. Soc. (London)* 1957, **A243**, 172.
36. Miller, S. L. "Physics and Chemistry of Ice", p. 42, Eds. Whalley, E.; Jones, S. J.; Gold, L. W.; Royal Society of Canada, Ottawa, 1972.

37. Pearson, C. F.; Halleck, P. M.; McGuire, P. L.; Hermes, R.; Mathews, M. *J. Phys. Chem.* 1983, **87**, 4180.
38. Jeffrey, G. A. "Inclusion Compounds", vol. 1, p.135, Eds. Atwood, J. L.; Davies, J. E. D.; MacNicol, D. D.; Academic Press, London, 1984.
39. Ripmeester, J. A.; Ratcliffe, C. I. *NRC Report No. C1181-89S*, August 1989.
40. Holder, G. D.; Kamath, V. A.; Godbole, S. P. *Ann. Rev. Energy* 1984, **9**, 427.
41. Nisbet, E. *Nature* 1990, **347**, 23.
42. MacNicol, D. D. "Inclusion Compounds" vol. 2, p. 1; Eds. Atwood, J. L.; Davies, J. E. D.; MacNicol, D. D.; Academic Press, London, 1984.
43. MacNicol, D. D. "Inclusion Compounds" vol. 2, p. 123; Eds. Atwood, J. L.; Davies, J. E. D.; MacNicol, D. D.; Academic Press, London, 1984.
44. Goldberg, I. "Topics in Current Chemistry" vol. 149, p. 1; Ed. Weber, E.; Springer-Verlag, Berlin, 1988.
45. Blackman, M. "Encyclopedia of Physics" vol. VII, part 1, p. 325; Ed. Klugge, S.; Springer-Verlag, Berlin, 1955.
46. Westrum, E. F. "Physics and Chemistry of the Organic Solid State" vol. 1, p. 1; Eds. Fox, D.; Labes, M. M.; Weissberger, A.; Interscience Publishers, New York, 1963.
47. Westrum, E. F. *J. Thermal Analysis* 1978, **14**, 5.
48. Pohl, R. O. "Topics in Current Physics" vol. 24, p. 27; Ed. Phillips, W. A.; Springer-Verlag, Berlin, 1981.
49. White, M. A. "Comprehensive Supramolecular Chemistry" Vol. 8, to be published; Ed. Ripmeester, J. A.; Pergamon Press, 1995.
50. Gmelin, E. *Thermochemica Acta* 1979, **29**, 1.
51. Chihara, H. *Ber. Bunsenges. Phys. Chem.* 1983, **87**, 188.
52. Parsonage, N. G.; Staveley, L. A. K. "Inclusion Compounds", vol. 3, p. 1; Eds. Atwood, J. L.; Davies, J. E. D.; MacNicol, D. D.; Academic Press, London, 1984.
53. Comper, J.; Quesnel, A.; Fyfe, C.; Boyd, R.K. *Can. J. Chem.* 1983, **61**, 92.
54. White, M. A.; MacLean, M. T. *J. Phys. Chem.* 1984, **89**, 1380.
55. White, M. A.; Zakrzewski, M. *J. Incl. Phenom.* 1990, **8**, 215.

56. Zakrzewski, M.; White, M. A. *J. Phys.:Condens. Matter* 199, **3**, 6703.
57. Tse, J. S.; Klein, M. L.; McDonald, I. R. *J. Phys. Chem.* 1983, **87**, 4198.
58. Krishnan, R. S.; Srinivasan, R.; Devanarayanan, S. "Thermal Expansion of Crystals"; Pergamon Press Ltd., Oxford, 1979.
59. Wallace, D. C. "Thermodynamics of Crystals"; John Wiley & Sons, Inc., New York, 1972.
60. Barron, T. H.; Berg, W. T.; Morrison, J. A. *Proc. R. Soc. London, Ser. A* 1957, **242**, 478.
61. Leadbetter, A. J. *Proc. R. Soc. London, Ser. A* 1965, **287**, 403.
62. Berman, R. "Thermal Conductivity in Solids"; Clarendon Press, Oxford, 1976.
63. Kittel, C. *Phys. Rev.* 1949, **75**, 972.
64. Zeller, R. C.; Pohl, R. O. *Phys. Rev. B* 1971, **4**, 2029.
65. Anderson, A. C. "Topics in Current Physics" vol. **24**, p. 65; Ed. Phillips, W. A.; Springer-Verlag, Berlin, 1981.
66. Debye, P. "Vortraege über die Kinetische Theorie der Materie und der Electizitaet" p. 17; Tübner: Berlin, 1914.
67. Freeman, J. J; Anderson, A. C. *Phys. Rev. B* 1986, **34**, 5684.
68. Cahill, D. G.; Pohl, R. O. *Ann. Rev. Phys. Chem.* 1988, **39**, 93.
69. Gil, L.; Ramos, M. A.; Bringer, A.; Buchenau, U. *Phys. Rev. Lett.* 1993, **70**, 182.
70. Sheng, P.; Zhou, H. *Science* 1991, **253**, 539.
71. Orbach, R. J. *J.Non-Cryst. Solids* 1993, **164**, 2.
72. Feldman, J. L.; Kluge, M. D.; Allen, P.B.; Wooten, F. *Phys. Rev. B.* 1993, **48**, 12589.
73. De Yoreo, J. J.; Pohl, R. O.; Burns, G. *Phys. Rev. B* 1985, **32**, 5780.
74. Yadon, L. N.; Nicholls, C. I.; Haase, D. G. *Phys. Rev. B* 1989, **40**, 5215.
75. Ackerman, D. A.; Moy, D.; Potter, R. C.; Anderson, A.C. *Phys. Rev. B* 1981, **8**, 3886.

76. Stoll, R. D.; Bryan, G. M. *J. Geophys. Res.* 1979, **84**, 1629.
77. Ross, R. G.; Andersson, P.; Bäckström, G. *Nature (London)* 1981, **290**, 322.
78. Tse, J. S.; McKinnon, W.R.; Marchi, M. *J. Phys. Chem.* 1987, **91**, 4188.
79. Marchi, M.; Mountain, R. D. *J. Chem. Phys.* 1987, **86**, 6454.
80. Tse, J. S. *Annals of the New York Academy of Sciences* 1994, **715**, 187.
81. White, M. A. *J. Phys. (Les Ulis, Fr.)* 1987, **C1**, 565.
82. Tse, J. S.; White, M. A. *J. Phys. Chem.* 1988, **92**, 5006.
83. Andersson, P.; Ross, R. G. *J. Phys. C.: Solid State Physics* 1983, **16**, 1423.
84. Ahmad, N.; Phillips, W. A. *Solid State Commun.* 1987, **63**, 167.
85. Handa, Y. P.; Cook, J. G. *J. Phys. Chem.* 1987, **91**, 6327.
86. Zakrzewski, M.; White, M. A. *Phys. Rev. B* 1992, **45**, 2809.
87. Ross, R. G. *J. Incl. Phenom.* 1990, **8**, 227.
88. MacNicol, D. D.; Wilson, D. R. *J.C.S. Comm.* 1976, 494.
89. Hardy, A. D.; MacNicol, D. D.; Wilson, D.R. *J. Chem. Soc. (Perkin Trans. II)* 1979, 1011.
90. Chandler, D. "Introduction to Modern Statistical Mechanics"; Oxford University Press, New York, 1987.
91. Born, M.; Huang, K. "Dynamical Theory of Crystal Lattices"; Oxford University Press, London, 1954.
92. Ashcroft, N. M.; Mermin, N. D. "Solid State Physics"; Holt, Reinhart and Winston, New York, 1976.
93. Brüesch, P. "Phonons: Theory and Experiments I"; Springer-Verlag Berlin, 1982.
94. Srivastava, G. P. "The Physics of Phonons"; Adam Hilger Bristol, 1990.
95. Ludwig, W. "Recent Developments in Lattice Theory"; Springer-Verlag, Berlin, 1967.
96. Venkataraman, G.; Sahni, V. C. *Phys. Rev. B.* 1970, **42**, 409.
97. Powles, J. G. *Berichte der Bunsen-Gesellschaft für Physikalische Chemie* 1976, **80**, 259.

98. Rao, K. R.; Chaplot, S. L. "Phonons in Condensed Matter Physics", p. 3; Eds. Singh, R. K.; Sanyal, S. P.; John Wiley & Sons, New York, 1990.
99. Abriel, W.; du Bois, A.; Zakrzewski, M.; White, M. A. *Can. J. Chem.* 1990, **68**, 1352.
100. Baker, W.; Floyd, A. J.; McOmie, J. F. W.; Pope, G.; Weaving, A. S.; Wilde, J. H. *J. Chem. Soc.* 1956, 2010.
101. Imashiro, F. *J. Am. Chem. Soc.* 1993, **115**, 2231.
102. MacNicol, D. D.; Mallinson, P. R.; Murphy, A.; Sym, G. *J. Tetrahedron Letters* 1982, **23**, 4131.
103. Millier, B.; Van Oort, M.; White, M. A. *J. Chem. Ed.* 1988, **62**, 64.
104. Crystallographic measurements done by Prof. T. S. Cameron and P. Bakshi; The material in this section has been submitted to *Can. J. Chem.* 1994; Michalski, D.; White, M. A.; Bakshi, P.; Cameron, T. S.; Swainson, I.
105. CHEM-X, Chemical Design Ltd., Oxford, England, 1990.
106. Schomaker, V.; Trueblood, K. N. *Acta Cryst.* 1968, **B24**, 63.
107. Moore, M.; Baert, F.; Lefebvre, J. *Acta Cryst. B* 1977, **33**, 3681.
108. Gilmore, C. J.; MacNicol, D. D.; Mallinson, P. R.; Murphy, A. *J. Incl. Phenom.* 1984, **1**, 295.
109. Cohen, S.; Powers, R.; Rudman, R. *Acta Cryst.* 1979, **B34**, 1670.
110. This part of the thesis has already been published. Michalski, D.; Mróz, B.; Kiefte, H.; White, M. A.; Clouter, M. J. *J. Phys. Chem.* 1993, **97**, 12949.
111. Nye, J. F. "Physical Properties of Crystals"; Oxford University Press, Oxford, 1985.
112. Cummins, H. Z.; Schoen, P. E.; Arecchi, F. T. "Laser Handbook" Vol. 2, p. 1029; Ed. Schultz-Dubois, E. O.; North-Holland, Amsterdam, 1972.
113. Vacher, R.; Boyer, L. *Phys. Rev. B* 1972, **6**, 639.
114. Dil, J. G. *Rep. Prog. Phys.* 1982, **45**, 285.
115. Brose, H.-K. "Elcon- A Computer Program for Fitting Elastic Constants to Phonon Velocities", Department of Chemistry, Wayne State University, Detroit, 1989.
116. James, F.; Roos, M. *Computer Physics Commun.* 1975, **3**, 343.

117. James, F. "MINUIT - Reference Manual" 1992, CERN, Geneva, Switzerland.
118. Ahmad, S. F.; Kiefte, H.; Clouter, M. J.; Whitmore, M. D. *Phys. Rev. B* 1982, **23**, 4131.
119. Zakrzewski, M.; Mróz, B.; Kiefte, H.; White, M. A.; Clouter, M. J. *J. Phys. Chem.* 1991, **95**, 1783.
120. Kiefte, H.; Clouter, M. J.; Gagnon, R. E. *J. Phys. Chem.* 1985, **89**, 3103.
121. Schmicker, D.; van Smaalen, S.; Haas, C.; Harris, K. D. M. *Phys. Rev. B* 1994, **49**, 11572.
122. Zuk, J.; Kiefte, H.; Clouter, M. J. *J. Chem. Phys.* 1991, **95**, 1950.
123. Zuk, J.; Kiefte, H.; Clouter, M. J. *J. Chem. Phys.* 1990, **92**, 917.
124. Zuk, J.; Brake, D.; Kiefte, H.; Clouter, M. J. *J. Chem. Phys.* 1989, **91**, 5285.
125. Dye, R. C.; Eckhardt, C. J. *J. Chem. Phys.* 1989, **90**, 2090.
126. Tse, J. S.; Klein, M. L.; McDonald, I. R. *J. Chem. Phys.* 1984, **81**, 6146.
127. Yoshihara, A.; Bernstein, E. R. *J. Chem. Phys.* 1982, **77**, 5319.
128. Watchman, J. B.; Tefft, W. E.; Lam, D.G., Jr.; Stinchfield, R. P. *J. Natl. Bur. Std.* 1960, **64A**, 213.
129. Gammon, P. H.; Kiefte, H.; Clouter, M. J. *J. Phys. Chem.* 1983, **87**, 4025.
130. Askarpour, V.; Kiefte, H.; Clouter, M. J. *Can. J. Chem.* 1988, **66**, 541.
131. Barron, T. H.; Collins, J. G.; White, G. K. *Advances in Physics* 1980, **29**, 609.
132. Choy, C. L.; Wong, S. P.; Young, K. *Phys. Rev. B.* 1984, **29**, 1741.
133. Schauer, A. *Can. J. Phys.* 1964, **42**, 1857.
134. Larson, A. C.; Von Dreele, R. B. "GSAS-General Structure Analysis System", Los Alamos National Laboratory, 1990.
135. Zakrzewski, M.; White, M. A.; Abriel, W. *J. Phys. Chem.* 1990, **94**, 2203.
136. Ceccaldi, D.; Ghelfenstein, M.; Szwarc, H. *J. Phys. C.: Solid State Phys.* 1975, **8**, 417.
137. Tse, J. S. *J. Physique Coll.* 1987, **48**, C1 543.

138. Kuchnev, V. I.; Tolkachev, A. M.; Manzhelii, V.G. *Sov. Phys. Solid State* 1975, **17**, 399.
139. Marshall, J. G.; Staveley, A. K.; Hart, K. R. *Trans. Faraday Soc.* 1956, **52**, 19.
140. More, M.; Lefebvre, J.; Fouret, R. *Acta Cryst. B* 1977, **33**, 3862.
141. Coulon, G.; Descamps, M. *J. Phys. C: Solid St. Phys.* 1980, **14**, 2847.
142. Dove, M. T. *J. Phys. C.: Solid State Phys.* 1986, **19**, 3325.
143. Dove, M. T.; Lynden-Bell, R. M. *J. Phys. C.: Solid State Phys.* 1986, **19**, 3343.
144. Barron, T. H. K.; Gibbons, T. G.; Mun, R. W. *J. Phys. C: Solid State Phys.* 1971, **4**, 2805.
145. Zallen, R. *Phys. Rev. B* 1974, **9**, 4485.
146. Chandrasekharan, V.; Farbre, D.; Thiery, M. M.; Uzan, E.; Donkersloot, M. C. A.; Walmsley, S. H. *Chem. Phys. Letters* 1974, **26**, 284.
147. Van Oort, M. J. M.; White, M.A. *Rev. Sci. Instrum.* 1987, **58**, 1239.
148. Durieux, M.; Astrov, D. N.; Kemp, W. R. G.; Swenson, C. A. *Metrologia* 1979, **15**, 57.
149. International practical temperature Scale of 1968, *Metrologia* 1969, **5**, 35.
150. Goldberg, R. N.; Weir, R. D. *Pure & Appl. Chem.* 1992, **10**, 1545.
151. Van Oort, M. J. M. Ph.D. Thesis, Dalhousie University, 1987.
152. Parsonage, N. G.; Staveley, L. A. K. *Mol. Phys.* 1959, **2**, 212.
153. Tse, W. S.; Liang, N. T.; Lin, W. W.; Chiang, P. Y. *Chem. Phys. Lett.* 1985, **119**, 67.
154. Spectrum was made available courtesy of Bruker.
155. Engeln, I. *Polym. Sci. Polym. Phys. Edn.* 1980, **18**, 2227.
156. Gavezzotti, A.; Simonetta, M. *Chemical Reviews* 1982, **82**, 1.
157. Choy, C. L.; Hunt, R. G.; Salinger, G. L. *J. Chem. Phys.* 1970, **52**, 3629.
158. Stephens, R. B.; Cieloszyk, G. S.; Salinger, G. L. *Physics Letters* 1972, **38A**, 215.

159. Atake, T.; Chihara, H. *J. Chem. Thermodynamics* 1971, **3**, 51.
160. Ohta, T.; Yamamuro, O.; Matsuo, T. unpublished work.
161. Callaway, J. *Phys. Rev.* 1959, **113**, 10546.
162. Touloukian, Y. S.; Powell, R. W.; Ho, C. Y.; Klemens, P. G. "Thermophysical Properties of Matter" Vol. 2, p. 13a; IFI/Plenum, New York, 1970.
163. Slack, G. A. *Phys. Rev.* 1957, **105**, 832.
164. Rosenbaum, R. L. *Rev. Scien. Instrum.* 1968, **39**, 890.
165. Pohl, R.O.; De Yoreo, J.J.; Meissner, M.; Knaak, W. "Physics of Disordered Materials", p. 529; Eds. Adler, D.; Fritzsche, H.; Ovshinsky, S.R.; Plenum Press, New York, 1985.
166. Lou, L. F. *Solid State Commun.* 1976, **19**, 335.
167. Slack, G. "Solid State Physics" Vol. 34, p. 1; Eds. Ehrenreich, H.; Seitz, F.; Turnbull, D.; Academic Press, New York, 1979.
168. Cahill, D. G.; Watson, S. K.; Pohl, R. O. *Phys. Rev. B.* 1992, **46**, 6131.
169. Wybourne, M. N.; Kiff, B. J.; Batchelder, D. N. *Phys. Rev. Letters* 1984, **53**, 580.
170. Sears, V. F.; Powell, B. M.; Tse, J. S.; Ratcliffe, C. I.; Handa, Y. P. *Physica B* 1992, **180&181**, 658.
171. Seward, W. D.; Narayanamurti, V. *Phys. Rev* 1966, **148**, 463.
172. Ripmeester, J.A. *J. Inc. Phenom.* 1983, **1**, 87.
173. Klemens, P. G. "Solid State Physics" Vol. 8, p. 1; Eds. Seitz, F.; Turnbull, D.; Academic Press, New York, 1958.
174. Berman, R.; Brock, J. C. F. *Proc. Roy. Soc. A* 1965, **289**, 46.
175. Callaway, J.; von Baeyer, H. C. *Phys. Rev.* 1960, **120**, 1149.
176. Casimir, H. B. G. *Physica* 1938, **5**, 495.
177. Carruthers, P. *Rev. Mod. Phys.* 1962, **33**, 92.
178. Pohl, R.O. *Phys. Rev. Letters* 1962, **8**, 481.
179. White, M. A.; Powell, B. M.; Sears, V. F. *Mol. Cryst. Liq. Cryst.* 1992, **211**, 177.

180. Pang, L.; Lucken, E. A. C.; Bernadelli, G. *J. Am. Chem. Soc.* 1990, **112**, 8754.
181. Pang, L.; Whitehead, M. A. *J. Molecular Structure (Theochem)* 1992, **89**, 143.
182. Bernhard, T.; Zimmermann, H.; Haeberlen, U. *Molec. Phys.* 1992, **77**, 1123.
183. Lambert, J. B.; Shurvell, H. F.; Lightner, D. A.; Cooks, R. G. "Introduction to Organic Spectroscopy"; Macmillan Publishing Company, New York, 1987.
184. Luty, T.; van der Avoird, A.; Berns, R. M. *J. Chem. Phys.* 1980, **73**, 5305.
185. Bauernfeind, W.; Keller, J.; Schröder *J. de Physique C* 1981, **6**, C1-247.
186. Dharma-wardana, M. W. C. *J. Phys. Chem.* 1983, **87**, 4185.
187. Chaplot, S. L.; Mierzejewski, A.; Lefebvre, J.; Pawley, G. S.; Luty, T. *Journal de Physique Colloque C6*, 1981, **42**, C6-584.
188. Luty, T.; van der Avoird, A. *Chem. Phys.* 1984, **83**, 133.
189. Gerdil, R. in "Molecular Inclusion and Molecular Recognition - Clathrates I", p. 71; Ed. Weber, E.; Springer-Verlag, Berlin, 1987.